UNIVERSITY OF CALIFORNIA, SAN DIEGO

Taylor Glacier as an archive of ancient ice for large-volume samples: Chronology, gases, dust, and climate

A dissertation submitted in partial satisfaction of the
requirements for the degree
Doctor of Philosophy

in

Earth Sciences

by

Daniel Baggenstos

Committee in charge:

Jeffrey P. Severinghaus, Chair
Helen A. Fricker
Ralph F. Keeling
Dan Lubin
Mark H. Thiemens

2015

The dissertation of Daniel Baggenstos is approved, and it is acceptable in quality and form for publication on microfilm and electronically:

_____

_____

_____

_____

_____
Chair

University of California, San Diego

2015

TABLE OF CONTENTS

LIST OF FIGURES

LIST OF TABLES

ACKNOWLEDGEMENTS

First of all, I would like to thank my advisor Jeff Severinghaus. I could not have wished for a better mentor. His enthusiasm for science is immense, and I feel privileged to have had the opportunity to spend several months in the field with him. Maybe the most important thing he taught me was that it is ok and worthwhile to follow your instinct and see where it takes you, even if it looks hopeless at first.

None of this work would have been possible without the people who participated in the four field seasons on Taylor Glacier. Thomas Bauska, Ed Brook, Christo Buizert, Michael Dyonisius, Xavier Fain, Joshua Goetz, Ben Hmiel, Michael Jayred, Kate Koons, Tanner Kuhl, Robb Kulin, James Lee, Chandra Llewellyn, Logan Mitchell, Avery Palardy, Vasilii Petrenko, Paul Rose, Bija Sass, Hinrich Schaefer, Adrian Schilt, Jeff Severinghaus and Martha Story were all part of the field crew and essential to making each season a success. A special thanks goes to Thomas Bauska who spent a lot of time thinking about stratigraphy on Taylor Glacier.

A big thanks also to the whole science support community in McMurdo, Antarctica. They provided truly outstanding support in every possible way. Camping equipment, carpentry needs, parts for repair, etc.; whenever we needed something we could count on assistance from the science support team.

I owe a lot to my collaborators in the ice core community. Various people in Ed Brook's lab at Oregon State have contributed methane measurements that are presented in various chapters in this thesis. The dust and water isotope measurements from Joe McConnell's lab at the Desert Research Institute are the foundation of chapter 3. The dust size measurements made by Benjamin Grente and Jean-Robert Petit in Grenoble are a very valuable addition to my thesis.

The camaraderie of the members of the Severinghaus lab means a lot to me. Vas and Anais were a constant source of encouragement and motivation. I've benefited enormously from them freely sharing their knowledge. Ross was always there when I needed help in the lab. Kenji taught me how to run the noble gas isotope method developed by Melissa.

I have many fond memories of my classmates Kaushik, Xue, and Guangming. They were in large part responsible for making the dreaded first year interesting and fun.

My family has always been nothing but encouraging and supportive over the years. I am looking forward to seeing them more regularly soon.

Finally, I would like to thank Janine for a lot of wonderful moments. Without her support this thesis would never have been written.

Chapter 2, in part, is currently being prepared for submission of the material. Baggenstos, D., T.K. Bauska, J.P. Severinghaus, E.J. Brook, H. Schaefer, V.V. Petrenko, J.E. Lee, and C. Buizert. The dissertation author was the primary investigator and author of this material.

Chapter 3, in part, is currently being prepared for submission of the material. Baggenstos, D., J.P. Severinghaus, J.R. McConnell, M. Sigl, O. Maselli, J.-R. Petit, and B. Grente. The dissertation author was the primary investigator and author of this material.

VITA

2015	Doctor of Philosophy in Earth Sciences, University of California, San Diego
2007-2015	Graduate Student Researcher, University of California, San Diego
2007	Master of Science in Earth Sciences, ETH Zürich, Switzerland

PUBLICATIONS

McConnell J.R., et al., Accelerated deglaciation linked to ozone depletion from volcanic eruptions 17.8k years so, submitted to *Science*.

WAIS Divide Project Members, Precise interpolar phasing of abrupt climate change during the last ice age, *Nature*, in press.

Mitchell L.E., et al., Observing and modeling the influence of layering on bubble trappig in polar firn, *Journal of Geophysical Research - Atmospheres*, in press.

Buizert C., et al., The WAIS Divide deep ice core WD2014 chronology - Part 1: Methane synchronization (68-31 ka BP) and the gas age-ice age difference, *Climate of the Past*, 11, 153-173, 2015.

Schilt A., et al., Isotopic constraints on marine and terrestrial N_2O emissions during the last deglaciation, *Nature*, 516, 2014.

Buizert C., et al., Radiometric Kr-81 dating identifies 120,000-year-old ice at Taylor Glacier, Antarctica, *Proceedings of the National Academy of Sciences of the United States of America*, 111, 6876-6881, 2014.

Petrenko V.V., et al., High-precision C-14 measurements demonstrate production of in situ cosmogenic (CH4)-C-14 and rapid loss of in situ cosmogenic (CO)-C-14 in shallow Greenland firn, *Earth and Planetary Sciences Letters*, 365, 190-197, 2013.

Arnold T., et al., Nitrogen trifluoride global emissions estimated from updated atmospheric measurements, *Proceedings of the National Academy of Sciences of the United States of America*, 110, 2029-2034, 2013.

Weigel A.P., D. Baggenstos, M.A. Liniger, F. Vitard, and C. Appenzeller, Probabilistic verification of monthly temperature forecasts, *Monthly Weather Review*, 136, 5162-5182, 2008.

Baggenstos D., Probabilistic verification of operational monthly temperature forecasts, Master Thesis, ETH Zürich, 2007.

ABSTRACT OF THE DISSERTATION

Taylor Glacier as an archive of ancient ice for large-volume samples: Chronology, gases, dust, and climate

by

Daniel Baggenstos

Doctor of Philosophy in Earth Sciences

University of California, San Diego, 2015

Professor Jeffrey P. Severinghaus, Chair

The aim of this dissertation is twofold, to develop a new ice sheet margin site on Taylor Glacier as a paleo-climate archive, and to resolve the controversy of the Taylor Dome chronology. The motivation for the former is that ice from deep ice core drilling projects is a precious commodity because only a finite amount of it is available from each core. This precludes measurements of trace constituents that need large sample sizes.

Ice margin sites can provide an ice archive that complements the deep drilling efforts. We present a suite of gas measurements from Taylor Glacier, Antarctica, that allow us to date the outcropping ice. We find that ice from the last glacial cycle is exposed at the glacier surface over tens of kilometers. Every

climatic interval of the last 125,000 years has been identified, from the penultimate interglacial to the Holocene, laying the foundation for future work. The age of the ice generally increases as one moves down-glacier, but at most locations the across flow age gradient is at least a magnitude larger. We have developed a high resolution age model for an across flow transect covering 50,000 to 8,000 years ago, that offers the chance to study the Last Glacial Maximum and the deglaciation in detail. We also describe and interpret large scale folding observed in the stratigraphy that can provide information on the deformation history.

The second focus of this dissertation is to revisit the Taylor Dome chronology, which is at the center of a controversial finding suggesting a direct link of Taylor Dome climate and changes happening in the North Atlantic during the deglaciation. We use measurements of calcium and H_2O isotopes in a true horizontal ice core from Taylor Glacier to show unambiguously that the Taylor Dome area temperature history is synchronous with the warming observed in other Antarctic ice cores, and not with North Atlantic records. We also find that the accumulation rate during the Last Glacial Maximum was extremely low, the overestimation of which led to the error in the original time scale. There is evidence from noble gas isotopic composition that a substantial convective zone formed during the same period. We present a new Taylor Dome time scale to replace the now obsolete original Taylor Dome chronology.

Chapter 1

Introduction

Ice cores have become one of the cornerstones of modern paleoclimatology. They contain an abundance of information about past climates, including proxies for temperature (Jouzel et al. (1997); Severinghaus and Brook (1999)) and trapped bubbles of ancient air allowing the reconstruction of past greenhouse gas concentrations (Petit et al. (1999); Schilt et al. (2010)), as well as a multitude of other parameters. One shortcoming of traditional ice core drilling is that only a limited amount of ice is recovered from every drilling site. This prevents measurements of trace components that need large sample sizes, but also inhibits testing of new measurements and constrains the possibilities in general. Entry of young investigators into the field is hampered by a lack of available samples on which to make novel measurements. Furthermore, traditional ice coring is expensive and logistically challenging, requiring the formation of large multi-institution or multinational research cooperatives that are not suited to accomplish a research goal in a quick and efficient fashion.

The old ice found in the central regions of the great ice sheets can also be retrieved from certain locations on the ice sheet margin (Reeh et al. (1991)). Several different types of ice margin sites can be identified (Bintanja (1999); Sinisalo and Moore (2010); Petrenko (2013)). The land-based Greenland ice margin sites are areas within the ablation zone where ice flow stagnates, typically because of topographical blockage. Ablation is dominated by melting during the summer months. In Antarctica, so-called blue ice areas are commonly observed close to mountain

ranges and nunataks, where high winds and a topographical rain shadow combine to inhibit snow accumulation, which exposes bare blue ice at the surface. Here, sublimation is the dominant process with little to no melting depending on the site. A special type of blue ice area is found in the Dry Valleys of McMurdo in the form of valley glaciers. Strong katabatic winds descending from the polar plateau cause a negative net mass balance. Sublimation is the primary mass-loss process, with 2/3 of the mass loss occurring in summer (Bliss et al. (2011)). Taylor Glacer is one of those valley glaciers, being fed by ice that is deposited on the ice sheet, on the northern flank of Taylor Dome.

The concept of a horizontal ice core is based on the notion that ice buried in the accumulation zone surfaces again in the ablation zone. If a continuous record can be identified, this marginal ice may be a valuable source for easily accessible large volume samples for paleoclimate studies. However, the ice at margin sites has arrived there on a long trajectory through the depths of the ice sheet, and has typically been deformed along the way. The deformation itself is of interest for studies of ice dynamics, but from a climate archive perspective it presents a complication. To be useful for climate studies, it is necessary to understand the age distribution on the ice surface. Accurate and reliable dating is the foundation of every paleoclimate archive.

Different approaches have been applied to date the outcropping ice at margin sites. The earliest attempts to date blue ice areas were based on meteorite ages (Cassidy et al. (1992)). The main drawback, apart from the fact that meteorite dating is not very precise, is that the meteorite can stay at the surface for a long time while the ice continues to ablate, especially in blue ice areas. Therefore there is no clear link between the meteorite age and the age of the ice. A dating method based on measuring ^{14}C concentration in air trapped in the ice was developed by van Roijen et al. (1994), however, in situ production of ^{14}C in the ice matrix (Lal et al. (1990)) and the large sample volumes required for the analysis make this method sub-optimal for high resolution dating. Jenk et al. (2007) have been able to measure ^{14}C of micro-particles extracted from ice core samples which allows them to establish ice ages with a precision of 2-10 % in the last 500 years. This

method holds great promise for dating Holocene ice with good precision. When volcanic ash or tephra layers can be found in blue ice areas, they can be radioisotopically dated and offer robust age markers (Dunbar et al. (2008)). Boudinage can complicate the interpolation from the measured layer to the sampling site, and depending on how many volcanic layers can be found there is significant uncertainty in the interpolation between age markers. Ice flow modeling has been used at some very old sites (several 100,000 years old) but it is generally not precise enough to be used on its own (Grinsted et al. (2003)). However, in conjunction with other dating methods it can be a very useful tool. The ratios of heavy to light isotopes of oxygen and hydrogen in ice and snow (δ^{18}O and δD) provide a simple method to determine whether samples at a given site were deposited during a glacial or an interglacial period (Sinisalo et al. (2007)). Furthermore, if a sequence of stable H_2O isotope values can be matched to a well-dated record because of synchronous climate changes at the two sites, the chronology from the well-dated site can be adopted (Custer (2006); Moore et al. (2006); Aciego et al. (2007)). If available, supraglacial moraine structures, radar isochrones, and layer counting can provide useful additional information about the surface age pattern of the blue ice area. Finally, the relative concentration and isotopic composition of time-varying but globally well-mixed gases trapped in the ice can be correlated to any well-dated deep ice core for which the same gas measurements are available (Bender et al. (1994); Sowers and Bender (1995)). This method has been successfully applied at a Greenland ice margin site (Petrenko et al. (2006); Schaefer et al. (2009)), and may be the most useful strategraphic proxy because the dating can be performed continuously and the matching to deep ice cores is robust if globally well-mixed gases are used.

In Chapter 2, we apply the gas composition matching method by using a combination of oxygen isotopes of O_2 and methane concentrations to establish ages for the ice that is exposed on the surface of Taylor Glacier. We also discuss the age pattern as the surface expression of the stratigraphy, and implications for the deformation history.

Chapter 3 describes what we can learn from Taylor Glacier about the past

climate of the region. It clears up a long-standing mystery regarding the Taylor Dome climate history and its chronology.

In Chapter 4, we present more measurements of gas composition from additional locations on the glacier, strengthening and expanding the results from Chapter 1.

Chapter 5 describes an effort to use inert gas isotopes as tracers of kinetic fractionation during the Last Glacial Maximum, a time of extremely low accumulation in the Taylor Dome area and a time of lower-than-expected diffusive column thickness inferred from δ^{15}N.

References

Aciego, S. M., Cuffey, K. M., Kavanaugh, J. L., Morse, D. L., and Severinghaus, J. P.: Pleistocene ice and paleo-strain rates at Taylor Glacier, Antarctica, Quaternary Research, 68, 303–313, doi:10.1016/j.yqres.2007.07.013, 2007.

Bender, M., Sowers, T., Dickson, M. L., Orchardo, J., Grootes, P., Mayewski, P. A., and Meese, D. A.: Climate Correlations Between Greenland And Antarctica During The Past 100,000 Years, Nature, 372, 663–666, doi:10.1038/372663a0, 1994.

Bintanja, R.: On the glaciological, meteorological, and climatological significance of Antarctic blue ice areas, Reviews of Geophysics, 37, 337–359, doi:10.1029/1999RG900007, 1999.

Bliss, A. K., Cuffey, K. M., and Kavanaugh, J. L.: Sublimation and surface energy budget of Taylor Glacier, Antarctica, Journal of Glaciology, 57, 684–696, doi:10.3189/002214311797409767, 2011.

Cassidy, W., Harvey, R., Schutt, J., Delisle, G., and Yanai, K.: The meteorite collection sites of Antarctica, Meteoritics, 27, 490–525, doi:10.1111/j.1945-5100.1992.tb01073.x, 1992.

Custer, S.: Eemian records of $\delta^{18}O_{atm}$ and CH_4 correlated to the Vostok EGT4 timescale from the Moulton blue ice field, West Antarctica, BSc thesis, Pennsylvania State University, 46 pp. Available at: www.geosc.psu.edu/undergrads/documents/documents/StantonCusterthesis.pdf, 2006.

Dunbar, N. W., McIntosh, W. C., and Esser, R. P.: Physical setting and tephrochronology of the summit caldera ice record at Mount Moulton, West Antarctica, Geological Society of America Bulletin, 120, 796–812, doi:10.1130/B26140.1, 2008.

Grinsted, A., Moore, J., Spikes, V. B., and Sinisalo, A.: Dating Antarctic blue ice areas using a novel ice flow model, Geophysical Research Letters, 30, doi:10.1029/2003GL017957, 2003.

Jenk, T., Szidat, S., Schwikowski, M., Gäggeler, H., Wacker, L., Synal, H.-A., and Saurer, M.: Microgram level radiocarbon (^{14}C) determination on carbonaceous particles in ice, Nuclear Instruments and Methods in Physics Research Section B: Beam Interactions with Materials and Atoms, 259, 518–525, doi:10.1016/j.nimb.2007.01.196, accelerator Mass Spectrometry Proceedings of the Tenth International Conference on Accelerator Mass Spectrometry, 2007.

Jouzel, J., Alley, R., Cuffey, K., Dansgaard, W., Grootes, P., Hoffmann, G.,

Johnsen, S., Koster, R., Peel, D., Shuman, C., Stievenard, M., Stuiver, M., and White, J.: Validity of the temperature reconstruction from water isotopes in ice cores, Journal of Geophysical Research: Oceans, 102, 26 471–26 487, doi: 10.1029/97JC01283, 1997.

Lal, D., Jull, A. J. T., Donahue, D., Burtner, D., and Nishiizumi, K.: Polar ice ablation rates measured using in situ cosmogenic ^{14}C, Nature, 346, 350–352, doi:10.1038/346350a0, 1990.

Moore, J. C., Nishio, F., Fujita, S., Narita, H., Pasteur, E., Grinsted, A., Sinisalo, A., and Maeno, N.: Interpreting ancient ice in a shallow ice core from the South Yamato (Antarctica) blue ice area using flow modeling and compositional matching to deep ice cores, Journal of Geophysical Research: Atmospheres, 111, D16 302, doi:10.1029/2005JD006343, 2006.

Petit, J. R., Jouzel, J., Raynaud, D., Barkov, N. I., Barnola, J.-M., Basile, I., Bender, M., Chappellaz, J., Davis, M., Delaygue, G., Delmotte, M., Kotlyakov, V. M., Legrand, M., Lipenkov, V. Y., Lorius, C., PEpin, L., Ritz, C., Saltzman, E., and Stievenard, M.: Climate and atmospheric history of the past 420,000 years from the Vostok ice core, Antarctica, Nature, 399, 429–436, doi:10.1038/ 20859, 1999.

Petrenko, V.: Encyclopedia of Quaternary Science, 2nd ed., chap. Ice Core Records: Ice Margin Sites, pp. 416–430, Elsevier, 2013.

Petrenko, V., Severinghaus, J., Brook, E., Reeh, N., and Schaefer, H.: Gas records from the West Greenland ice margin covering the Last Glacial Termination: a horizontal ice core, Quaternary Science Reviews, 25, 865–875, doi:10.1016/j. quascirev.2005.09.005, 2006.

Reeh, N., Oerter, H., Letréguilly, A., Miller, H., and Hubberten, H.-W.: A new, detailed ice-age oxygen-18 record from the ice-sheet margin in central West Greenland, Global and Planetary Change, 4, 373–383, doi:10.1016/0921-8181(91) 90003-F, 1991.

Schaefer, H., Petrenko, V., Brook, E., Severinghaus, J., Reeh, N., Melton, J., and Mitchell, L.: Ice stratigraphy at the Pakitsoq ice margin, West Greenland, derived from gas records, Journal of Glaciology, 55, 411–421, doi:10.3189/ 002214309788816704, 2009.

Schilt, A., Baumgartner, M., Schwander, J., Buiron, D., Capron, E., Chappellaz, J., Loulergue, L., Schüpbach, S., Spahni, R., Fischer, H., and Stocker, T. F.: Atmospheric nitrous oxide during the last 140,000 years, Earth and Planetary Science Letters, 300, 33–43, doi:10.1016/j.epsl.2010.09.027, 2010.

Severinghaus, J. P. and Brook, E. J.: Abrupt Climate Change at the End of the

Last Glacial Period Inferred from Trapped Air in Polar Ice, Science, 286, 930–934, doi:10.1126/science.286.5441.930, 1999.

Sinisalo, A. and Moore, J. C.: Antarctic blue ice areas - towards extracting palaeoclimate information, Antarctic Science, 22, 99–115, doi:10.1017/S0954102009990691, 2010.

Sinisalo, A., Grinsted, A., Moore, J. C., Meijer, H. A. J., Martma, T., and Van De Wal, R. S. W.: Inferences from stable water isotopes on the Holocene evolution of Scharffenbergbotnen blue-ice area, East Antarctica, Journal of Glaciology, 53, 427–434, doi:10.3189/002214307783258495, 2007.

Sowers, T. and Bender, M.: Climate Records Covering The Last Deglaciation, Science, 269, 210–214, doi:10.1126/science.269.5221.210, 1995.

van Roijen, J., Bintanja, R., van der Borg, K., van den Broeke, M., de Jong, A., and Oerlemans, J.: Dry extraction of $^{14}CO_2$ and ^{14}CO from Antarctic ice, Nuclear Instruments and Methods in Physics Research Section B: Beam Interactions with Materials and Atoms, 92, 331–334, doi:10.1016/0168-583X(94)96029-1, 1994.

Chapter 2

Atmospheric gas records from Taylor Glacier, Antarctica, reveal ancient ice covering the entire last glacial cycle

Abstract

Old ice for paleo-environmental studies, traditionally accessed through deep core drilling in the central regions of the large ice sheets, can also be retrieved at the surface from ice sheet margins. The nearly unlimited amount of ice available at these sites satisfies a need in the community for studies of trace components requiring large sample volumes. For margin sites to be useful as ancient ice archives, the ice stratigraphy needs to be understood and age models need to be established. We present measurements of trapped gases in ice from Taylor Glacier, Antarctica, to date the ice and assess the completeness of the chrono-stratigraphy. Using $\delta^{18}O$ of O_2 and methane concentration, we unambiguously identify ice from the last glacial cycle, covering every climate interval from the early Holocene to the penultimate interglacial. A high resolution transect reveals the deglaciation and the Last Glacial Maximum (LGM) in detail. We observe large scale deformation of the ice

in the form of folding, but individual stratigraphic layers do not appear to have undergone irregular thinning. Rather, it appears that a block of ice containing the entire LGM-deglaciation sequence has been transported from the interior of the ice sheet to the surface of Taylor Glacier relatively undisturbed. We present an age model that builds the foundation for future gas studies on Taylor Glacier. A comparison with the Taylor Dome ice core confirms that Taylor Glacier is better suited for paleo-climate reconstructions of the LGM due to higher accumulation rates.

2.1 Introduction

Ice cores from Greenland and Antarctica have provided high resolution climate information over the past eight glacial cycles. Many important climate parameters such as temperature, precipitation and greenhouse gas concentrations have been reconstructed using ice core measurements, providing a long-term perspective on modern climate change and a testing ground for climate models. However, ice cores suffer from severe limits on the volume of ice available, precluding measurements that require large sample volumes. Blue ice areas, where ancient ice is brought to the surface by ice flow, and especially continental ice margins have been recognized as an inexpensive, useful archive of paleo-climate information, which is not encumbered by sample size restrictions (Sinisalo and Moore (2010), Petrenko (2013)).

In a steady state regime, the mass balance surplus on top of the Antarctic ice sheet is compensated for by ice flow towards its margins and eventually ice loss, mostly through calving into the ocean. However, in some places, ablation due to strong sublimation and low ice velocities combine to remove the young ice and expose old ice at the surface. The conditions needed for such outcropping of ancient ice are typically orographical rain shadows and/or flow stagnation because of obstacles such as nunataks or mountain ranges. A detailed review of blue ice areas and their specific meteorological and glaciological settings can be found in Bintanja (1999).

Historically, blue ice areas have been of interest mainly as meteorite traps (Whillans and Cassidy (1983)), but in the last decade, some blue ice sites have been investigated for paleo-climatic information. In Antarctica, this includes sites at Scharffenbergbotnen (Sinisalo et al. (2007)), Allan Hills (Spaulding et al. (2013)), Mount Moulton (Custer (2006); Korotkikh et al. (2011)), Yamato Mountain (Moore et al. (2006)), and Taylor Glacier (Aciego et al. (2007)). Depending on the initial accumulation rate and the ice dynamics at a specific site, such records can span anywhere from a few thousand years at Yamato Mountain to a few hundred thousand years at Allan Hills.

The main challenge in blue ice settings is age control. Traditional ice coring on domes or ridges is primarily a 1-D problem with ages increasing monotonically with depth. Similarly, at ice margins, one can expect the oldest ice at the very edge of the ice sheet and increasingly younger ages as one approaches the snow/ice transition. In principle, a monotonic undisturbed sequence of layers can be found on the margin just as it was deposited on top of the ice sheet (Reeh et al. (1991)). However, deformation along the flow path from the ice sheet interior to the margin, typically close to the bed, can lead to non-uniform thinning, folding, and faulting of the stratigraphic layers, complicating the dating and interpretation of the strata. Most previous work has relied on radiometrically dated ash layers (Dunbar et al. (2008)) or stable water isotopes (Aciego et al. (2007), Spaulding et al. (2013)) to establish ages for the outcropping ice. In this study, we use gases trapped in bubbles in the ice to date the ice and study the deformation it has acquired on its travel path.

The near surface environment, which can alter the composition of the trapped gases through contamination with modern air, poses another challenge specific to ice margin sites. Most blue ice surfaces in Antarctica are riddled with a mosaic of thermal contraction cracks, formed by winter cooling, which provide a pathway for modern air to invade several meters deep into the ice (Popp (2008)).

The ablation zone of Taylor Glacier (TG) is an ideal site for this study for the following reasons: (1) It has been studied by glaciologists extensively (Robinson (1984), Kavanaugh and Cuffey (2009), Kavanaugh et al. (2009a), Kavanaugh et al.

(2009b)), and therefore the flow field, sublimation rates and other glaciologically important parameters are well know; (2) a deep ice core was drilled near the deposition site for Taylor Glacier ice on Taylor Dome (TD) in 1993/1994, a mere 200 km upstream of Taylor Glacier, providing a point of reference and comparison (Morse et al. (2007), Steig et al. (2000)); (3) it is a climatologically interesting area because of a controversial study by Steig et al. (1998) that attributed a Greenland-style deglacial warming to Taylor Dome; (4) it is reasonably close to McMurdo station with long periods of stable weather, making it a logistically simple field operation; and (5) previous work by Aciego et al. (2007) has shown that tens of kilometers of Pleistocene ice are exposed at the surface.

Stable water isotopes, as used by Aciego et al. (2007) to determine a pre-Holocene age for most of the Taylor Glacier ablation zone, are a robust dating tool, able to identify rapid transitions and long term changes in the climate under which the ice was formed, but they do not provide unique age markers. Taking advantage of the trapped gas content in glacial ice allows for a more precise dating of the ice, due to the fact that many gases are globally well-mixed and therefore must be the same in all trapped air sections (Bender et al. (1994)). Changes in the concentration and isotopic composition of globally well-mixed trace gases are continuously being recorded in trapped gas bubbles as new ice forms. If a reference record for such gases from a well-dated deep ice core is available, it is possible to match an undated record to it and to uniquely identify the age of the ice using a suitable combination of gases (Blunier et al. (2007)). In this study we use methane concentrations and molecular oxygen (O_2) isotopic composition and match them to the same tracers measured in a well-dated deep ice core (WAIS Divide). Methane and oxygen are ideally suited for this purpose because their average atmospheric lifetimes are very different: $\sim$1,000 years for oxygen, but only 10 years for methane. Methane concentrations react very quickly to changes in methane sources and sinks, leading to large and fast variations, which provide precise age matching tie points. Oxygen isotopic content varies more slowly but contributes uniquely-identifying information to the synchronization, especially at times when methane has many similar-sized fast variations or none at all. It is the combination of the two gases

that makes it a powerful dating tool. This method has been used to synchronize deep ice cores (Malaize et al. (1994), Capron et al. (2010)) and was also successfully used at the Pakitsoq ice margin in West Greenland to date a sequence of layers covering the last deglaciation (Petrenko et al. (2006), Schaefer et al. (2009)).

In this paper we present records of atmospheric composition from ancient ice outcropping in the ablation zone of Taylor Glacier. The aim is to date the ice and assess the completeness of the chronostratigraphy. At this site virtually unlimited amounts of old ice can be collected at the surface, allowing for the study of new proxies that have hitherto been precluded by sample size restrictions (Buizert et al. (2014)), and increasing the precision of established measurements that are hindered by small sample volumes. Section 2 offers a description of the sampling strategy and the laboratory analyses. In section 3 we show that the trapped gas records are well preserved and contain a wealth of paleo-climate information. We describe two sampling transects that contain the deglaciation to Marine Isotope Stage 3 (MIS 3) and possibly older ice. We discuss the stratigraphic layering and the observed folding. Finally, we present a high resolution age model for a newly established record and highlight the differences of Taylor Glacier and Taylor Dome in the characteristics of their firn columns during the deglaciation.

2.2 Study area and methods

The Taylor Glacier ablation zone has been described in detail by Aciego et al. (2007) and Kavanaugh and Cuffey (2009): In short, ice flows from the northern flank of Taylor Dome through the Transantarctic Mountains into Taylor Valley (Figure 2.1). Ice velocities are on the order of 10 m/yr in the center, and decrease towards the lateral margins where the glacier is frozen to the ground. Sublimation is 10-30 cm/yr over most of the ablation zone, with higher rates close to the terminus (Bliss et al. (2011)). The ice surface is nearly horizontal and mostly free of major crevasses. The large difference of summer and winter temperatures causes thermal contraction cracks that cover the entire surface of the glacier. Most of these cracks are confined to the surface, with a few reaching 4 m depth, and none

were observed having propagated deeper than 6 m. There are numerous cryoconite holes with wind-blown sediment on the surface. The air bubbles in the ice are typically elongated, a testament to their deformation history (Alley and Fitzpatrick (1999)).

Ice samples were collected during the 2009/10, 2010/11, 2011/12, and 2013/14 field seasons for analysis of oxygen and nitrogen isotopic composition and methane concentration. We present data from two sampling lines, one that parallels the flow direction, and one that lies perpendicular to it (Figure 2.2). On the along flow line, 98 samples were collected over 20 km following the hypothetical center flow line (hereafter called the along-flow profile). The sampling resolution increases from 1 sample per 500 m at the upstream end to 1 sample per 100 m close to the terminus. On the perpendicular line, 300 samples were collected spanning 700 m in distance, in varying spatial resolution (from 1 m to 10 m), and approximately perpendicular to the along-flow profile (hereafter called the across-flow transect). All samples originate from 4.5 m to 5 m depth and were carefully examined to be free of fractures that still exist at this depth. The methane and $\delta^{18}O_{atm}$ data from the along flow profile are already published in Buizert et al. (2014), but they are not discussed there in detail, which is why we will be elaborating on these measurements here. In addition, three cores were drilled to 12 m depth in different locations to examine if the near surface environment has an effect on the gas composition. These cores were sub-sampled in high depth resolution for a total of 65 samples. Again, we took great care to avoid fractures in these samples. However, in the shallowest $\sim$2 m the fractures are too pervasive to sample only clean ice, such that most shallow samples do incorporate some fractures.

Locations for the along flow profile and deep core samples were recorded via GPS, while locations on the across flow transect were established with measuring tape and a limited number of GPS positions for reference because the across flow sampling spacing (1 m in some sections) is smaller than the accuracy of our GPS unit (5 m). Bamboo poles left in the across flow transect allow us to revisit the same sampling line for several years. Ice samples from the same location but drilled in different years show excellent reproducibility. All drilling was done with a PICO

shallow coring drill assisted with a Sidewinder electric power head provided by Ice Drilling Design and Operations (IDDO). After drilling and logging, the ice samples were stored for up to two weeks on site in an ice cave at approximately -10°C in the 2009/10 season and in regular chest freezers at -24°C in the following seasons, before being transferred to McMurdo Station.

We decided to tie the Taylor Glacier gas records to the WAIS Divide ice core (WDC). The WDC is described in detail elsewhere (WAIS Divide Project Members (2013)); for our purposes it is an ideal reference core because of its high quality gas records (Marcott et al. (2014)) and precise dating (Buizert et al. (2015)).

The analytical method for measuring $\delta^{18}O_{atm}$ and $\delta^{15}N$ at Scripps Institution of Oceanography (SIO) has been described by Petrenko et al. (2006). The raw data were corrected for pressure imbalance and chemical slope (for $\delta^{18}O$, $\delta^{15}N$, and $\delta Ar/N_2$) using established analytical corrections, and the results were normalized to air collected off the Scripps Pier. Following Bender et al. (1994) and Sowers and Bender (1995), we apply the gravitational correction to $\delta^{18}O$ using measured $\delta^{15}N$: $\delta^{18}O_{gravcorr} = \delta^{18}O_{measured} - 2 \cdot \delta^{15}N_{measured}$. For all Taylor Glacier samples, a gas loss correction was applied as described by Severinghaus et al. (2009): Observed anomalies in $\delta O_2/N_2$ and $\delta Ar/N_2$ are used to correct $\delta^{18}O_{gravcorr}$ for inferred gas loss in this way: $\delta^{18}O_{atm} = \delta^{18}O_{gravcorr} + a \cdot [\delta O_2/N_{2gravcorr} + c] + b \cdot \delta Ar/N_{2gravcorr}$. a and b are empirical coefficients determined by a multivariate regression of pair differences of $\delta^{18}O_{gravcorr}$ with respect to pair differences of $\delta O_2/N_{2gravcorr}$ and $\delta Ar/N_{2gravcorr}$. c is also an empirical coefficient used to offset $\delta O_2/N_{2gravcorr}$ in such a way as to set the average value of $\delta^{18}O_{atm}$ in the last 2000 years to zero. We do not have any samples from Taylor Glacier for the last two millennia, and therefore cannot tune c in this way. To facilitate synchronization to the WDC $\delta^{18}O_{atm}$ record, we pick c such as to get identical values for both records at distinct features, e.g. extrema or plateaus. For the 400 Taylor Glacier samples measured in duplicates, a and b turned out to be 0.0119 and -0.0155, reasonably close to Severinghaus et al. (2009)'s coefficients of 0.0136 and -0.0130, suggesting that the same gas loss mechanism is at work. This gas loss correction was not applied to the WAIS Divide samples since the empirical gas loss relation is unlikely to be true for

gas in a clathrate state as are all WAIS Divide samples older than 10 ka. However, the WAIS Divide samples exhibit much less gas loss in general due to very good temperature control during drilling, transport, and storage (Souney et al. (2014)), such that the quality of the data is essentially the same as gas loss corrected Taylor Glacier data.

For Taylor Glacier, a total of 725 samples from 352 separate locations or depths were analyzed on a Finnigan MAT Delta V mass spectrometer, mostly in duplicates. Of those 725 samples 12 were rejected for objective reasons such as incomplete transfer of the gas or other manual errors. An additional 7 samples were rejected due to poor agreement with replicates from the same location/depth. The remaining 706 samples have a pooled standard deviation of 0.005 ‰ for δ^{15}N and 0.011 ‰ for $\delta^{18}O_{atm}$, which is identical to the analytical precision achieved by Severinghaus et al. (2009). For WAIS Divide, 169 samples from 147 depths were analyzed on the same instrument. The 21 duplicate samples have a pooled standard deviation of 0.010 ‰ for $\delta^{18}O_{atm}$ and 0.003 ‰ for δ^{15}N.

Methane concentrations were measured in the field and in the lab at OSU. The analytical methods for the field measurements are described by Petrenko et al. (2006) and Schaefer et al. (2006). The initial field measurements were corroborated by lab measurements, using the analytical method described by Mitchell et al. (2011). Corrections for solubility, blank size, and gravitational enrichment are applied.

2.3 Results and discussion

2.3.1 Reliability of the gas records

Figure 2.3 shows three high-resolution depth profiles of $\delta^{18}O_{atm}$ and methane concentration at different locations on the glacier. Overall, the methane profiles show more variability than the $\delta^{18}O_{atm}$ profiles. This is not surprising given the higher short term variability of the underlying methane record, and the fact that methane as a trace gas is easier to contaminate than molecular oxygen as a major component of the air mixture. From 0 m to 4 m depth, clear and significant anoma-

lies are apparent in the methane profiles. The $\delta^{18}O_{atm}$ profiles show such anomalies only in core D3. Since we observe essentially three different patterns (methane decreasing with $\delta^{18}O_{atm}$ also decreasing, methane decreasing with $\delta^{18}O_{atm}$ stable, methane increasing with $\delta^{18}O_{atm}$ stable) it is difficult to determine the exact processes responsible for this, but it is likely due to a combination of entrainment of modern air through cracks and biological activity in cryoconite holes and in cracks (Stibal et al. (2012)). Below 4 m there is no sign of contamination of any kind (the drop in methane values from 580 ppb to 470 ppb in core D3 is a paleo-atmospheric signal, as explained below, and not an artifact). This means that samples from deeper than 4 m are representative of the gas composition at the time the air was trapped in the ice. We can then use these data to assign ages to the different locations by comparing the gas values to other ice cores. If we assume these samples are from the last glacial cycle (a reasonable hypothesis given that these sites are 10+ km upstream from a site that has been dated to 125 ka BP (before present = before 1950 AD) by Buizert et al. (2014)), the gas data suggest a unique age for core D1 and D3, and two possible ages for D2 (compare to Figure 2.4): For core D1, the combination of methane just under 400 ppb and $\delta^{18}O_{atm}$ of 0.95 ‰ is only possible in the Last Glacial Maximum (LGM), at ∼20 ka BP. For D2, characterized by $\delta^{18}O_{atm}$ of 0.4 ‰ and 450 ppb methane concentration, either an age of 35 to 45 ka BP or around 90 ka BP would satisfy the constraints provided by the two gases. In this case it is not possible to uniquely identify the age based on a single data point, but additional data from nearby would likely allow us to exclude one of the two options. For D3, a $\delta^{18}O_{atm}$ of 1.1 ‰ is enough to uniquely identify the age as 15 ka BP. This is exactly the time of the Oldest Dryas - Bølling transition with a large increase in methane, which explains the large shift in the D3 methane profile. The fact that methane decreases from 580 ppb to 470 ppb with depth then must mean that at this site the ice gets younger with depth. For D1 and D2, the constant methane and $\delta^{18}O_{atm}$ values with depth suggests that at these locations the ice has the same age with depth, i.e. the ice stratigraphy is close to or vertical.

2.3.2 Along-flow profile covers entire glacial cycle

The along flow transect covers 25 km of the ablation zone of Taylor Glacier, closely following the central flow line. As expected from first principles, the ice gets older with decreasing distance to the terminus (Figure 2.4): From 28 km to 24 km, methane concentrations of 650-750 ppb are a clear indicator for Holocene ages of these samples. In addition, increasing $\delta^{18}O_{atm}$ in the glacier flow direction shows that the ice is getting older in that direction. From 23 km to 19 km, the gas records go through the reverse deglacial sequence: Younger Dryas (460 ppb methane, 0.6 ‰ $\delta^{18}O_{atm}$), Bølling/Allerød (650 ppb methane, 0.6-1.1 ‰ $\delta^{18}O_{atm}$), and Oldest Dryas (350-450 ppb methane, 1.1-1.0 ‰ $\delta^{18}O_{atm}$). The following section, 19 km to 13 km, is characterized by $\delta^{18}O_{atm}$ of 0.4-0.2 ‰ and variable methane concentrations, the combination of which is indicative of MIS 3, which spans 30 to 60 ka BP. Continuing further downstream, it is not possible any more to align the Taylor Glacier along flow record with a deep ice core record simply by stretching and squeezing it, because MIS 4 ($\delta^{18}O_{atm}$ of 0.7 ‰) is missing entirely. Still, $\delta^{18}O_{atm}$ alternating between 0.5 ‰ and -0.1 ‰, as seen from 13 km to 7 km, is consistent with MIS 5a - 5d. Finally, the very low $\delta^{18}O_{atm}$ values of -0.4 ‰ close to the glacier terminus are a clear indication of interglacial origin, in this case most likely Eemian ($\sim$125 ka BP). The Eemian age of this part of the glacier has already been independently confirmed by Buizert et al. (2014) using Kr-81 dating.

This transect confirms that there are large amounts of Pleistocene-age ice outcropping on Taylor Glacier, in agreement with Aciego et al. (2007). The Oldest Dryas and LGM layers are significantly more compressed than one would expect looking at the Siple Dome or WAIS Divide record. However, it is consistent with the Taylor Dome record, that also has an anomalously thin LGM layer because of low accumulation rates (Steig et al. (2000), Morse et al. (2007)). Hyper-arid conditions in the Taylor Dome region were probably the result of a change in atmospheric circulation, with moisture bearing storms coming from the North, rather than from the South as today, because of the advance of the Ross ice shelf far into the Ross sea (Morse et al. (1998)).

Even though the samples from the Aciego et al. (2007) study are not from

the exact same locations, it is still instructive to compare their age/distance relation with the one from our along flow profile (Figure 2.5): For kilometer 28 to 20, the two age models are in good agreement with each other. Downstream of kilometer 16, our ages are consistently older than Aciego et al. (2007)'s ages, with the discrepancy increasing with decreasing distance to the terminus. The most plausible explanation for this age discrepancy is that there is substantial across flow age variability, and Aciego et al. (2007) sampled along a line that is slightly offset from our sampling profile. The fact that the stratigraphy gets more and more compressed towards the terminus, as expected from a simple model but also evident in the age/distance relationship, can then explain why the age discrepancy increases moving downglacier.

2.3.3 Across-flow transect reveals deglaciation in high resolution

The same deglacial sequence identified in the along-flow profile is also found in the across flow transect, albeit with a complicating twist. Instead of one $\delta^{18}O_{atm}$ maximum, at the Oldest Dryas/Bølling transition, as in deep ice cores, there are three, along with an additional Bølling/Allerød interval, characterized by elevated methane values (Figure 2.4). This can be explained by a large z-fold structure, which leads to a tripling of a limb of the fold. The folding is discussed in detail below. The youngest ice in this transect is of Early Holocene age, while the oldest ice is approximately 60,000 years old based on $\delta^{18}O_{atm}$ of 0.2 ‰. Further it is noteworthy that the whole sequence from the early Holocene well into MIS 3 is compressed into a few hundred meters, whereas it takes almost 15 km in the along flow direction to cover that same time span. The most logical explanation for this observation is that the strike of the outcropping layers, or isochrons, is parallel to the flow direction. Another way of saying the same thing would be that the largest change of age with distance is perpendicular to the glacier flow. This interpretation is strongly supported by satellite imagery, airborne imagery, and observations on the ground, all of which show individual layers of different shades of blue colors that run parallel to the flow direction (Figure 2.6). The color of the ice varies

from almost white blue to red-ish blue due to different amounts of dust in the ice, representing different climate states, and thus chronostratigraphic layers, and not flow artifacts.

This age distribution is a somewhat surprising result, since it is not predicted by basic theory, which says that age pattern should be tied to the flow field in a straightforward way. Without knowing the full 3-D structure of the stratigraphy of the glacier it is difficult to reconstruct the ice dynamics and deformation history that led to the observed age pattern. However, we can hypothesize about the processes that could arrange the stratigraphy in the along flow direction. One possibility is that large velocity gradients in the flow field cause longitudinal shearing, which will eventually orient all in-glacial structures, no matter what orientation, parallel to the flow direction. The Taylor Glacier ablation zone is narrow enough that the surface velocity is dependent on the distance to the margin for most of the area. Only in a narrow central band is true plug flow behaviour observed (Kavanaugh and Cuffey (2009)). However, even close to the equilibrium line, 60 km from the terminus, where the ice from the polar plateau enters Taylor Valley, one can find such along flow oriented features. At this point the glacier is much wider which reduces the influence of lateral shearing, but it is still possible that large velocity gradients exist because of bottom topography. Another explanation for the unusual pattern of stratigraphy and flow holds that layers deposited horizontally on the plateau could rotate by 90 degrees upon entering a glacial trough or valley which would produce outcropping stratigraphy that parallels the flow direction. In the end, the combination of bottom topography, accumulation history, surface flow and flow at depth is too complex for us to reconstruct the entire deformation history which produced the surface stratigraphy that we can observe today. Finally, the across flow stratigraphy can explain how Aciego et al. (2007)'s and our along flow sampling line can have dramatically different ages despite their proximity.

2.3.4 Large scale folding

The most obvious stratigraphic feature is the layer representing ice deposited in the LGM, with a characteristic red-ish color due to high dust concentra-

tions in the ice matrix. In the across flow transect, this 'dusty band' is encountered in two locations, from -110 m to -160 m, and around 0 m (Figure 2.6a). The gas signature in both locations is the same, confirming that we are looking at a single layer, that must somehow be connected. Indeed, a short distance downstream the two limbs connect in a large folded structure. The fold is easily visible on airborne and satellite imagery (Google Maps (2015)). It is a z-fold, composed of a synform/antiform pair, with the axial planes approximately vertical and parallel to the flow direction. The north-western limb is visible at the surface for the first time at the across flow transect, and continues to emerge in the downglacier direction at a shallow angle. The syncline (south-western part of the z-fold, with young layers in the center of the fold) also emerges at the same shallow angle, and disappears from the surface a few kilometers downstream, exposing the older layers underneath it.

We managed to estimate the dipping angle of the layers at a few spots in the transect by drilling vertical profiles and comparing the data to the surface sequence (not shown). For the 'young' side, the layer dip is 70° to 80°, but decreases as expected with increasing proximity to the fold axis. On the 'old' side, the layer dip away from the fold is approximately 90°, i.e. vertical. We used all this information to draw a sketch of the fold geometry (Figure 2.6b). It shows the multiplication of a single limb in undisturbed stratigraphy into three limbs in the folded part as seen in our gas data: The upright limb of the syncline, the overturned limb that is part of the syncline and anticline, and the upright limb of the anticline.

Folding and deformation of any kind is very much expected in a fluid medium like glacial ice. Folds can easily form in a variety of settings, as long as there are velocity gradients which induce shearing (Jacobson (2001)) or layers of differing rigidity. Indeed one can find folds in many parts of Taylor Glacier, ranging in scale from one meter to hundreds of meters, typically in the form of z-folds. It is not clear where these folds form, with previous research showing that some folds originate upstream of the region of streaming flow in a West Antarctic ice stream (Jacobel et al. (1993)). In structural geology, z-folds are usually viewed as minor folds in the limbs of larger synform or antiform structures (Bell (1981),

Hudleston and Treagus (2010)). In this case, this interpretation would imply a large syncline with the layers folded up symmetrically to fit the u-shaped valley.

2.3.5 An age model based on gas synchronization

The across flow transect is the preferred sampling line for the deglaciation, LGM, and MIS 3 time periods, because it is oriented perpendicular to the stratigraphic layers which is the ideal sampling setup. The along flow profile runs almost parallel to the strata, which can easily lead to sampling artifacts. We developed a high resolution age model for the across flow transect using our gas data and a dynamic programming algorithm developed by Lisiecki and Lisiecki (2002) to correlate the paleo-climate records. We use sharp methane transitions and inflections in the CO_2 record (Bauska (2013)) as fixed tie points (Table 2.1) and let the computer algorithm wiggle match the $\delta^{18}O_{atm}$ in between the tie points. The algorithm minimizes the difference between two data series while observing fixed tie points and discouraging large accumulation rate changes, which is equivalent to saying that the resulting distance/age curve be smooth. To assess the uncertainty in our age estimates, we apply a Monte Carlo randomization scheme by running the model 5,000 times while resampling the $\delta^{18}O_{atm}$ input data subject to its analytical error. The resulting uncertainty is a lower bound of the total uncertainty, since the model uses certain constraints on the age/distance relationship which we are not randomizing. Still, we believe that the resulting uncertainty is a reasonably good estimate as long as the sampling resolution is high. Because of the fold in the stratigraphy, we create two separate age models, one each for the 'old' (-80 m to -300 m) and 'young' (30 m to 260 m) side of the fold. The two age models overlap by approximately 2,000 years. Figure 2.7 shows the resulting distance/age relationship as well as the age uncertainties. The distance/age curve looks surprisingly similar to depth/age curves from deep ice cores (Figure 2.7) with older layers being more compressed than younger ones which is equivalent to a flattening in the depth/age curve. Non-uniform thinning, which has been described as a consequence of deformation at the West Greenland ice margin (Petrenko et al. (2006)), does not seem to have significantly affected this sequence of layers. The

uncertainties in our age model are relatively small (less than 500 years) in the 'young' section, thanks to methane transition tie points and a rapidly changing $\delta^{18}O_{atm}$. In the 'old' section, age uncertainties are substantially larger because of few methane tie points, long periods of no change in $\delta^{18}O_{atm}$ and low sampling resolution for the oldest part.

2.3.6 Taylor Glacier vs. Taylor Dome

After placing the Taylor Glacier across flow profile on a time scale, we can compare it to deep ice cores, with Taylor Dome being the most logical and interesting choice due to its proximity to the Taylor Glacier deposition site. $\delta^{15}N$ of N_2 of air trapped in ice is enriched compared to atmospheric values due to gravity driven diffusive un-mixing in the firn column (Craig et al. (1988), Sowers et al. (1989)). The enrichment is nearly linearly related to the thickness of the diffusive column, and is therefore used as a proxy for firn thickness, although it is also affected by firn temperature gradients (Severinghaus et al. (1998)) and potentially a convective zone (Kawamura et al. (2006)). Comparing $\delta^{15}N$ from Taylor Dome gas records and Taylor Glacier gas records highlights interesting differences (Figure 2.7): During the LGM ($\sim$20 ka BP), gravitational enrichment as seen in $\delta^{15}N$ almost ceases ($\delta^{15}N \approx 0$) at Taylor Dome, suggesting a very thin firn and possibly deep air convection, both of which are only possible with an extremely low accumulation rate. Taylor Glacier $\delta^{15}N$ is also low but never falls below 0.07 ‰, indicating a thicker, more 'healthy' firn during this climate period, most likely due to a higher accumulation rate. In addition, the layer thickness of the dusty band, representing the LGM, at Taylor Glacier is $\sim$50 m, whereas it is only $\sim$10 m thick in the Taylor Dome ice core, using measured dissolved calcium concentration as a proxy for dust (Steig et al. (2000)). Since the layer dip is nearly vertical on the old side of the fold, the distance measured on the surface is equal to the true layer thickness. It is likely that the LGM layer in Taylor Dome has been subjected to more thinning than the layers that are exposed on Taylor Glacier, but the difference is not enough to explain the five-fold difference in observed thicknesses. This conclusion is in agreement with radar profiles (Morse

et al. (1998)) that show that the LGM layer is significantly thicker on the northern flank of Taylor Dome than where the deep ice core was drilled, because of a change in storm trajectories. This view is further strengthened by more recent work from Morse et al. (2007) that confirms that the accumulation rate during the LGM at Taylor Dome was even lower than previously estimated. All of the above makes Taylor Glacier more suitable for paleo-climate reconstructions of the LGM than the original deep ice core.

2.4 Conclusions

Taylor Glacier is the first ice margin site in Antarctica where paleo-atmospheric gas records from the last glacial cycle have been explored in detail. The gases are well preserved below 4 m depth and contain unaltered climate information. The combination of $\delta^{18}O_{atm}$ and methane concentration allows for unambiguous identification of different climatic intervals in the ice through comparison to deep ice core records. Using this approach, a complete sequence of ice ranging from 8 to 55 ka BP has been identified. Certain parts of the ablation zone are folded, however, this has not been an obstacle to obtaining good quality gas records.

Our age model builds the foundation for future work on the across flow transect. Studies that have been limited by availability of ancient ice may become feasible. Taylor Glacier could become an easy to access archive of ancient air (and ice), which complements traditional deep ice coring efforts. Furthermore, a comparison to Taylor Dome shows that Taylor Glacier is better suited for paleo-climate reconstructions of the LGM than the Taylor Dome ice core because the ice was deposited at higher accumulation rates. Finally, the age of the ice at the Taylor Glacier terminus is of interest to biologists studying the microbial community in Lake Bonney, a perennially frozen lake formed by Taylor Glacier outflow (Fountain et al. (1999)). We have shown that the very oldest ice at the terminus is potentially quite a lot older (125+ ka BP) than previously estimated.

Understanding the stratigraphy in the lower part of the ablation zone is still work in progress. We are expecting more deformation in this very old ice

because the ice has travelled close to the bedrock. Unfortunately remote sensing analysis of large scale structures in the stratigraphy is hampered by a network of melt channels that obscure the stratigraphic signature of the ice. The three dimensional stratigraphic pattern identified in this study presents a powerful tool to glaciologist studying ice dynamics and deformation processes. It also presents a challenge to explain the mechanics that led to the observed stratigraphy. Future work on the across flow transect could include increasing the sampling resolution to 1 m for the oldest part, and additional depth profiles that would constrain the layer dip in more places.

2.4.1 Acknowledgements

We thank Kurt Cuffey for helpful discussions on glaciology and flying tents. The US Antarctic Program provided outstanding logistical support. IDDO (Ice Drilling Design and Operations) provided the drilling systems. The Polar Geospatial Center (PGC) provided satellite imagery. We thank Paul Rose for bringing his magic to our field camp. Xavier Fain, Tanner Kuhl, Robb Kulin, Logan Mitchell, and Adrian Schilt all helped with sampling in the field. We thank Ross Beaudette for laboratory assistance. This work is supported through NSF Grants #0839031 and #1246148.

This chapter, in part, is currently being prepared for submission of the material. Baggenstos, D., T.K. Bauska, J.P. Severinghaus, E.J. Brook, C. Buizert, H. Schaefer, V.V. Petrenko, and J.E. Lee. The dissertation author was the primary investigator and author of this material.

Table 2.1: Fixed tie points used in the gas age model synchronizing Taylor Glacier to WAIS Divide. Note that two tie points (at 2207.5 m and 2259.5 m WAIS Divide depth) are overlapping, i.e. are used both for the 'old' and the 'young' side of the transect. WAIS Divide is on the WD2014 age scale (Buizert et al. (2015)).

Gas age [yrs BP]	WAIS Divide depth [m]	TG across flow distance [m]	Type of tie point
8,123	1,620.0	220	CH4 minimum
11,451	1,972.0	100	CH4 maximum and CO2 inflection
11,548	1,983.4	98	CH4 transition midpoint
12,092	2,035.0	86	CO2 transition midpoint
12,583	2,079.5	78	CH4 minimum
12,757	2,095.5	71	CH4 transition midpoint
13,991	2,207.5	40	CH4 minimum
13,991	2,207.5	-82	CH4 minimum
14,577	2,259.5	29	CH4 transition midpoint
14,577	2,259.5	-90	CH4 transition midpoint
16,027	2,368.0	-108	CO2 peak
16,098	2,372.0	-111	CH4 peak
16,640	2,399.5	-115	CO2 transition midpoint
17,418	2,432.0	-119	CO2 inflection point
35,653	2,959.1	-173	CH4 transition
38,391	3,021.6	-183.5	CH4 transition
41,654	3,094.4	-194.5	CH4 transition
43,543	3,130.4	-200	CH4 transition

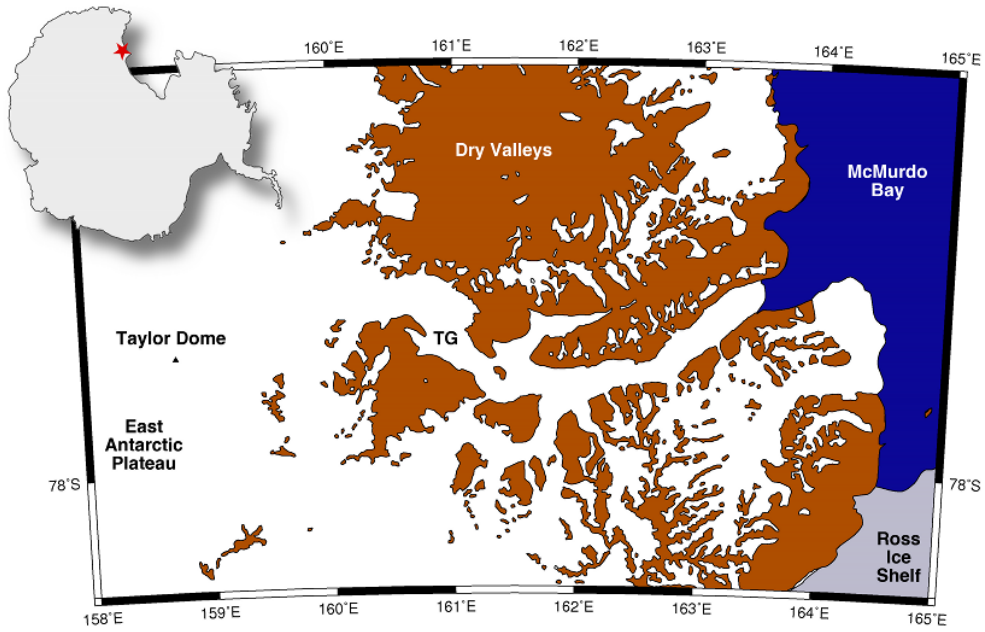

Figure 2.1: Map of the study region in the southern McMurdo Dry Valleys, with Taylor Glacier in the center. The McMurdo Dry Valleys are a series of snow-free valleys within Victoria Land. The region is one of the world's most extreme deserts. Ice flowing into Taylor Valley originates on the northern flank of Taylor Dome, on the polar plateau.

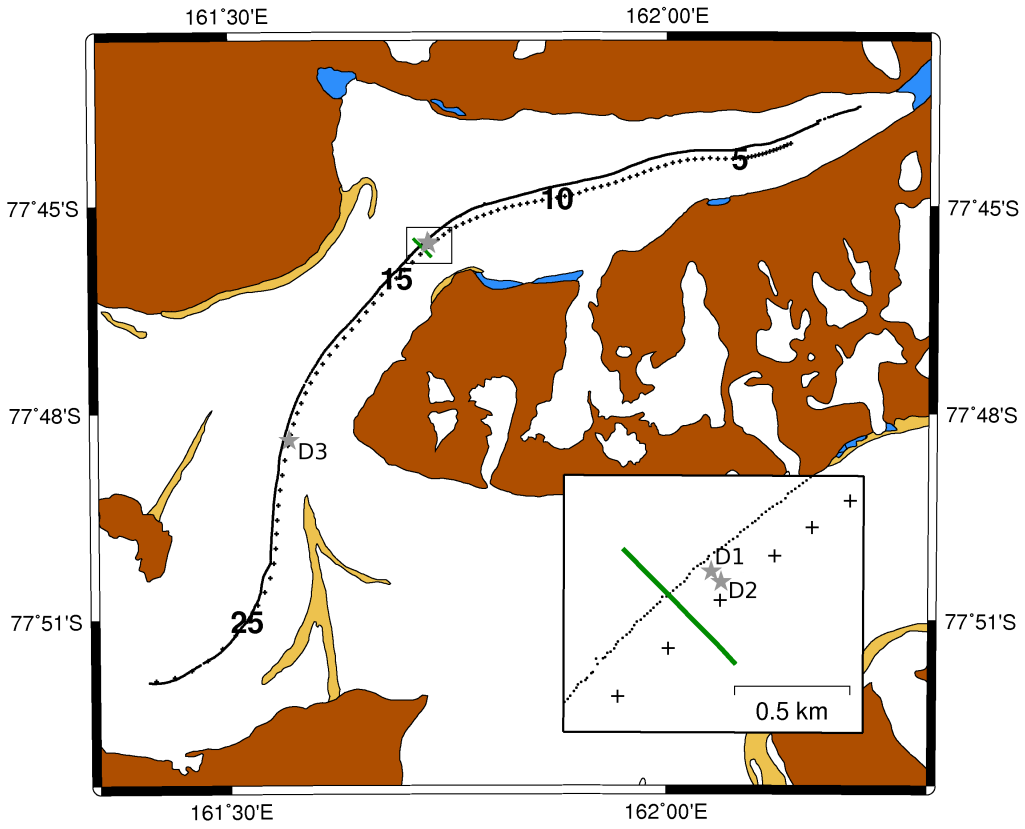

Figure 2.2: Overview of the Taylor Glacier ablation zone including the sampling lines. Aciego et al. (2007)'s samples (·) and our along flow profile samples (+) are shown. Each symbol represents one sample. The solid green line represents the across flow transect. Gray stars indicate the positions of the three deep cores. Numbers on the profile denote approximate distance from the glacier terminus in km. The insert shows a blown-up version of the across flow transect. Ice flow is from the SW to the NE. Taylor Glacier receives a small amount of ice from the Ferrar Glacier (lower right), with a faint but distinct suture separating the two ice masses.

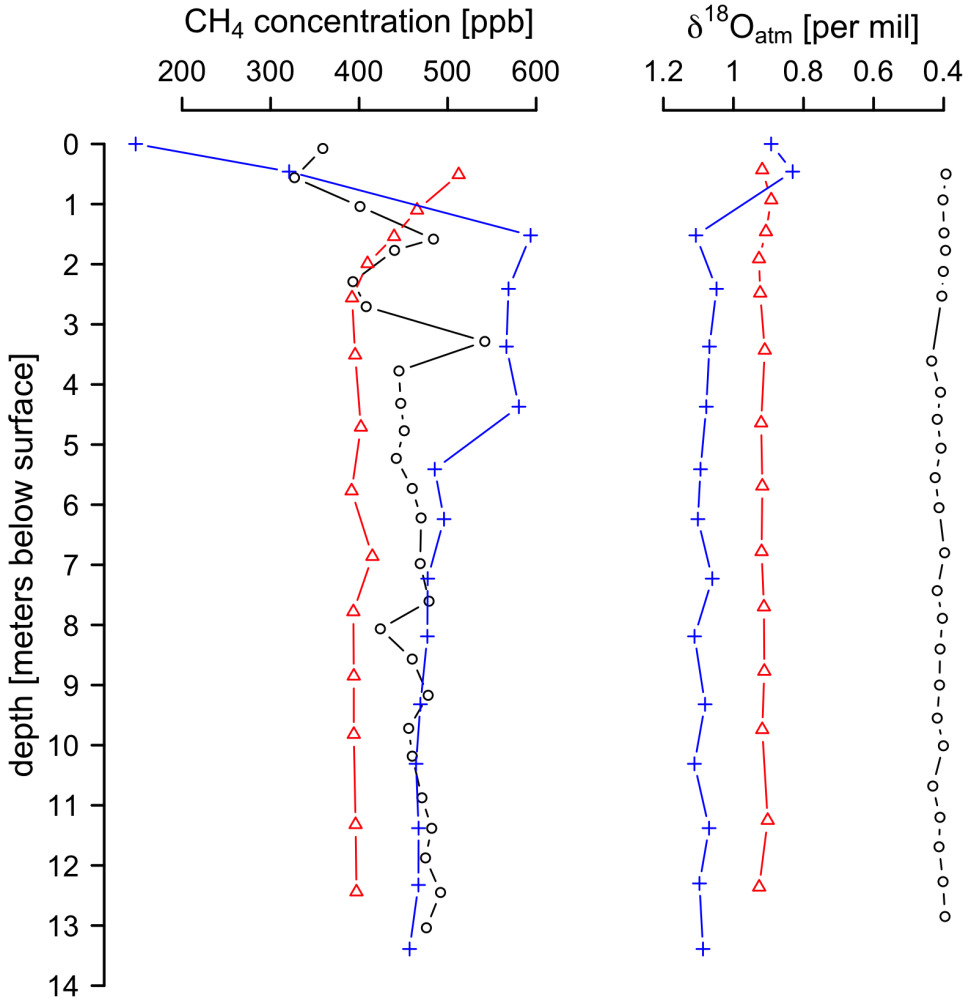

Figure 2.3: Depth profiles of methane and $\delta^{18}O_{atm}$ at the deep core sites D1 ($\triangle$), D2 ($\circ$), and D3 ($+$). The analytical uncertainty based on replicate analyses is smaller than the size of the symbols in the plot for both methane (1-σ of 5 ppb) and $\delta^{18}O_{atm}$ (1-σ of 0.01 ‰)

Figure 2.4: Results from the along flow profile and the across flow transect and reference records from traditional deep ice cores. $\delta^{18}O_{atm}$ (blue) and methane (red) records from deep ice cores (Siple Dome, WAIS Divide, EDML) and from Taylor Glacier (across flow, along flow). Siple Dome data is published in Severinghaus et al. (2009) ($\delta^{18}O_{atm}$) and Brook et al. (2005) (methane), and shown on a time scale that has been methane synchronized to GISP2. WAIS Divide methane data has been published by (Buizert et al. (2015)). High resolution Taylor Glacier across flow methane data covering the deglaciation is from Bauska (2013). EDML data is from Schilt et al. (2010) (methane) and Capron et al. (2010) ($\delta^{18}O_{atm}$). For TG across flow, the 0 m point is somewhat arbitrary. The intersection point of the two TG sampling lines is at -240 m on the across flow scale, and at 13.5 km on the along flow scale. Gray bars highlight well known climate periods: Last Glacial Maximum (LGM), Oldest Dryas (OD), Bølling/Allerød (B/A), and Younger Dryas (YD).

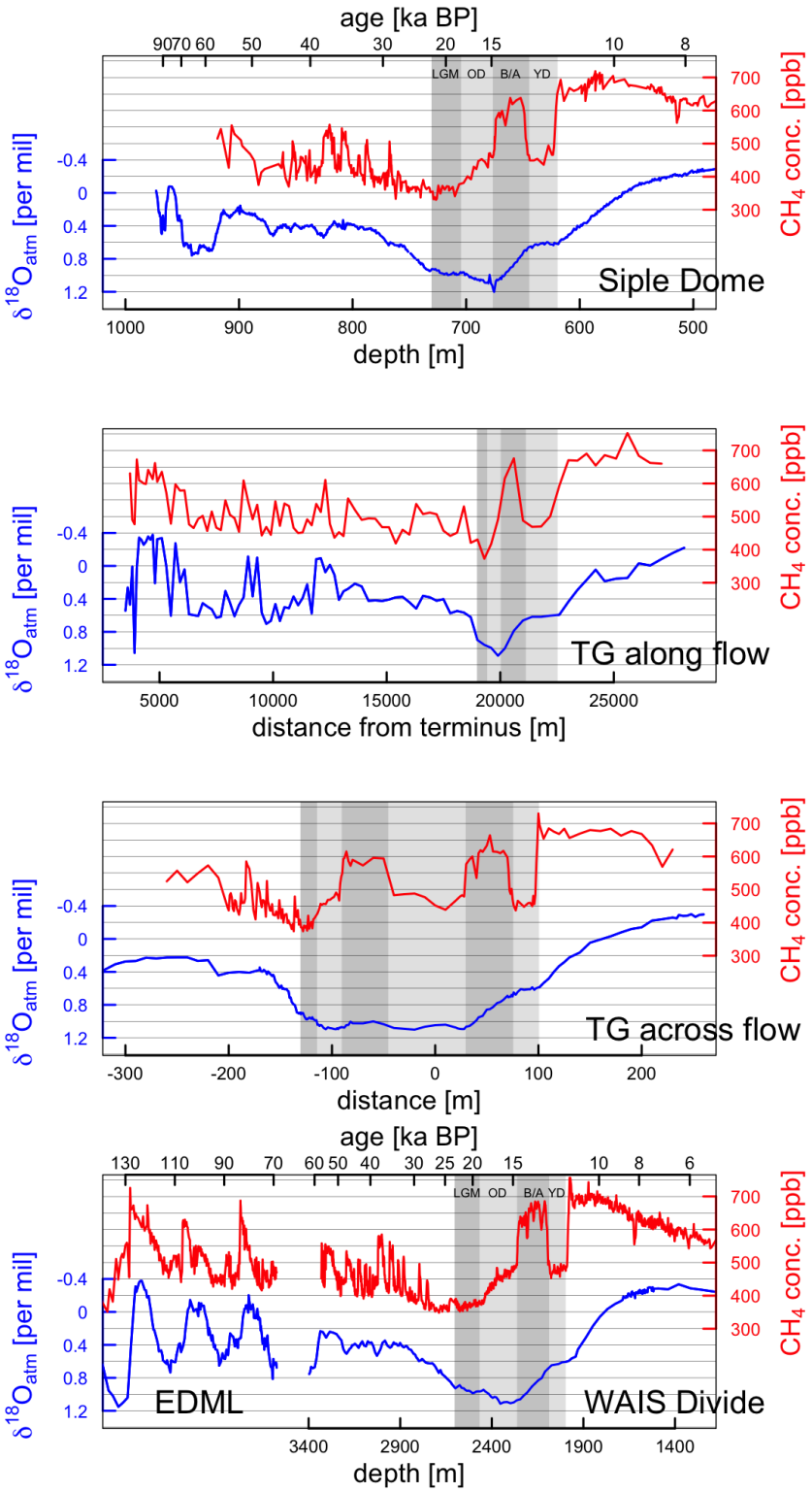
age [ka BP]
LGM
OD
B/A
YD
Siple Dome
depth [m]
TG along flow
distance from terminus [m]
TG across flow
distance [m]
EDML
WAIS Divide
δ18Oatm [per mil]
CH4 conc. [ppb]

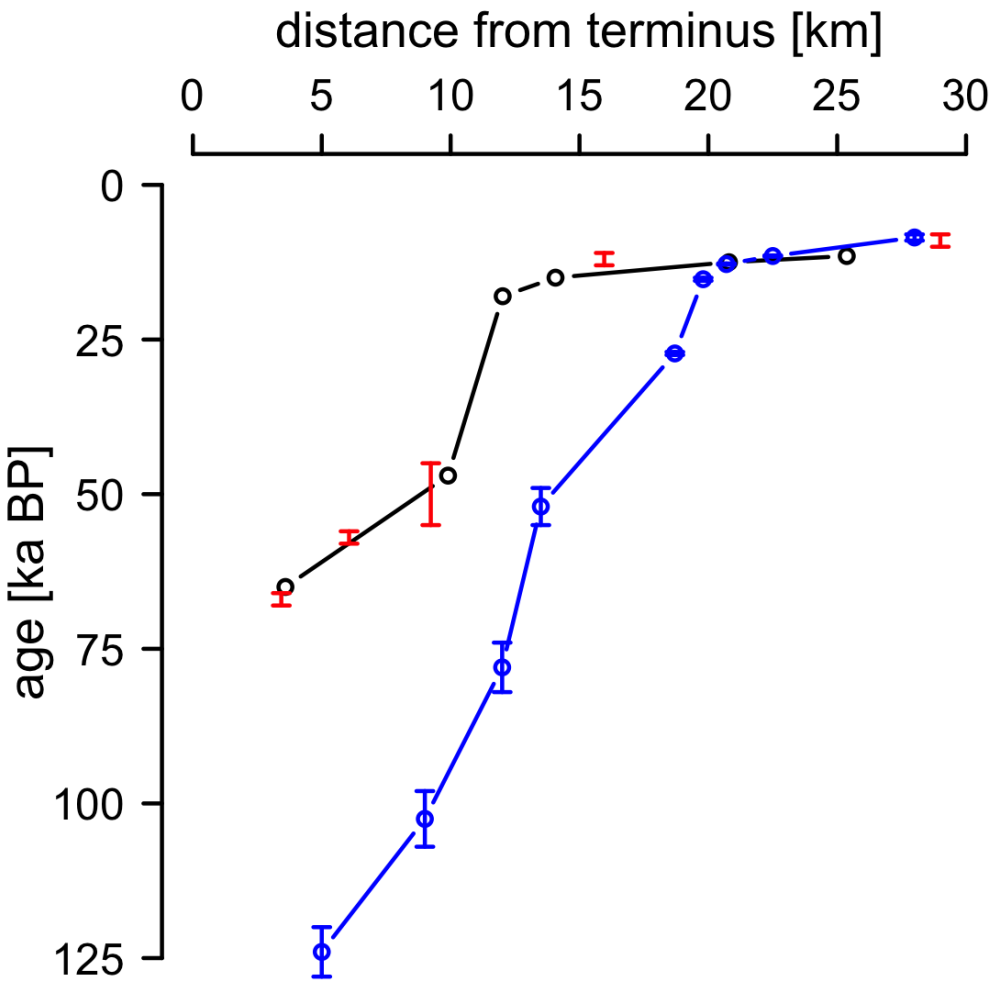

Figure 2.5: Distance age estimates for the Taylor Glacier ablation zone. (Black) Aciego et al. (2007)'s age model based on matching δD to Taylor Dome and supported by five $\delta^{18}O_{atm}$ age estimates (red, from their Figure 5). 1 km was added to Aciego et al. (2007)'s distance scale to account for the fact that their sampling line ended approximately 1 km from the glacier terminus. (Blue) Our along flow profile age model, based on $\delta^{18}O_{atm}$ and methane concentration. Note that the sampling locations were not identical in both studies and therefore the results are not directly comparable.

Figure 2.6: Folding visible in aerial photography and a cross-sectional sketch. A: Photo of the across flow transect sampling area showing two limbs of the dusty band. Color settings were adjusted to enhance the color differences. The solid black line marks the approximate boundary of the dusty band. The dashed black line marks the across glacier transect. The camp is visible in the upper right. Glacier flow is from top to bottom and indicated by arrows. For scale, the south-eastern limb of the dusty band, on the left in the photo, is ∼60 m wide. Photo by Ed Brook. B: Sketch of the z-fold, showing its surface expression and a cross section.

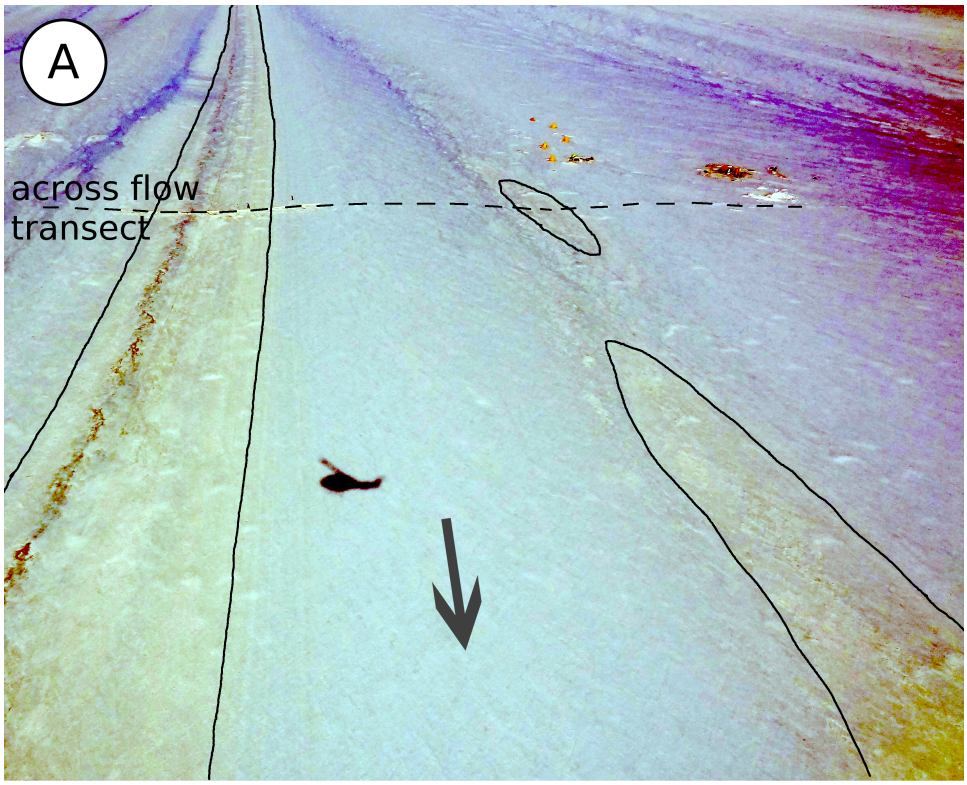
A
across flow
transect

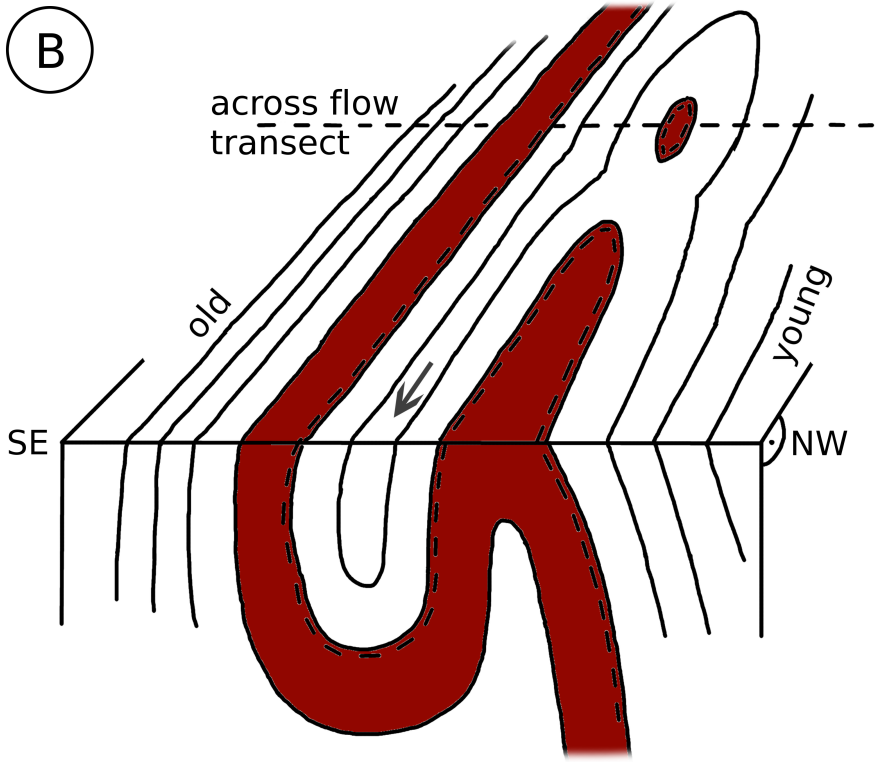
B
across flow
transect
old
young
SE
NW

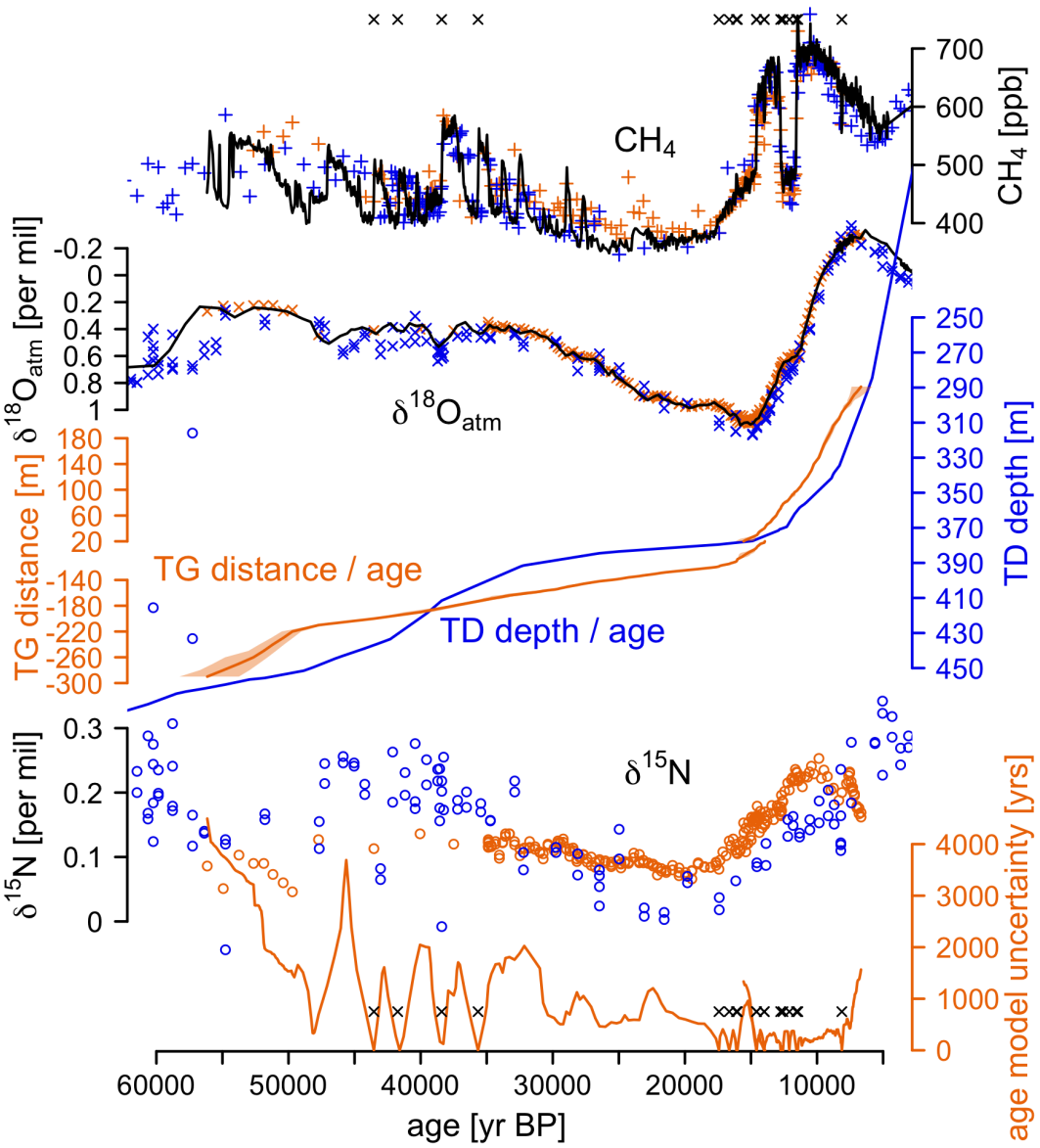

Figure 2.7: Gas records from Taylor Glacier, Taylor Dome, and WAIS Divide from 50 ka to 10 ka BP. Gas records from WAIS Divide (black), Taylor Dome (blue), and Taylor Glacier (orange, this study and Bauska (2013)) as well as Taylor Dome depth/age curve and Taylor Glacier distance/age and uncertainty estimates are shown. WAIS data are from this study ($\delta^{18}O_{atm}$) and Buizert et al. (2015) (methane), and plotted on the WD2014 time scale. Taylor Dome data are from Brook et al. (2000) and Ahn and Brook (2007) (methane), Steig et al. (1998) and Sucher (1997) ($\delta^{18}O_{atm}$ and $\delta^{15}N$), all shown on a time scale that was methane synchronized to GISP2 (Brook et al. (2000), Ahn and Brook (2007)). Black crosses on the top and bottom of the plot show fixed tie points used in the synchronization.

References

Aciego, S. M., Cuffey, K. M., Kavanaugh, J. L., Morse, D. L., and Severinghaus, J. P.: Pleistocene ice and paleo-strain rates at Taylor Glacier, Antarctica, Quaternary Research, 68, 303–313, doi:10.1016/j.yqres.2007.07.013, 2007.

Ahn, J. and Brook, E. J.: Atmospheric CO_2 and climate from 65 to 30 ka B.P., Geophysical Research Letters, 34, L10 703, doi:10.1029/2007GL029551, 2007.

Alley, R. B. and Fitzpatrick, J. J.: Conditions for bubble elongation in cold ice-sheet ice, Journal of Glaciology, 45, 147–154, URL http://pubs.er.usgs.gov/publication/70022129, 1999.

Bauska, T. K.: Carbon cycle variability during the last millennium and last deglaciation, Ph.D. thesis, Oregon State University, URL http://hdl.handle.net/1957/44146, 2013.

Bell, A.: Vergence: an evaluation, Journal of Structural Geology, 3, 197–202, doi:10.1016/0191-8141(81)90015-8, 1981.

Bender, M., Sowers, T., Dickson, M. L., Orchardo, J., Grootes, P., Mayewski, P. A., and Meese, D. A.: Climate Correlations Between Greenland And Antarctica During The Past 100,000 Years, Nature, 372, 663–666, doi:10.1038/372663a0, 1994.

Bintanja, R.: On the glaciological, meteorological, and climatological significance of Antarctic blue ice areas, Reviews of Geophysics, 37, 337–359, doi:10.1029/1999RG900007, 1999.

Bliss, A. K., Cuffey, K. M., and Kavanaugh, J. L.: Sublimation and surface energy budget of Taylor Glacier, Antarctica, Journal of Glaciology, 57, 684–696, doi:10.3189/002214311797409767, 2011.

Blunier, T., Spahni, R., Barnola, J.-M., Chappellaz, J., Loulergue, L., and Schwander, J.: Synchronization of ice core records via atmospheric gases, Climate of the Past, 3, 325–330, doi:10.5194/cp-3-325-2007, 2007.

Brook, E. J., Harder, S., Severinghaus, J., Steig, E. J., and Sucher, C. M.: On the origin and timing of rapid changes in atmospheric methane during the last glacial period, Global Biogeochemical Cycles, 14, 559–572, doi:10.1029/1999GB001182, 2000.

Brook, E. J., White, J. W. C., Schilla, A. S. M., Bender, M. L., Barnett, B., Severinghaus, J. P., Taylor, K. C., Alley, R. B., and Steig, E. J.: Timing of millennial-scale climate change at Siple Dome, West Antarctica, during the last glacial period, Quaternary Science Reviews, 24, 1333–1343, doi:

10.1016/j.quascirev.2005.02.002, 2005.

Buizert, C., Baggenstos, D., Jiang, W., Purtschert, R., Petrenko, V. V., Lu, Z.-T., Müller, P., Kuhl, T., Lee, J., Severinghaus, J. P., and Brook, E. J.: Radiometric ^{81}Kr dating identifies 120,000-year-old ice at Taylor Glacier, Antarctica, Proceedings of the National Academy of Sciences, 111, 6876–6881, doi: 10.1073/pnas.1320329111, 2014.

Buizert, C., Cuffey, K. M., Severinghaus, J. P., Baggenstos, D., Fudge, T. J., Steig, E. J., Markle, B. R., Winstrup, M., Rhodes, R. H., Brook, E. J., Sowers, T. A., Clow, G. D., Cheng, H., Edwards, R. L., Sigl, M., McConnell, J. R., and Taylor, K. C.: The WAIS Divide deep ice core WD2014 chronology - Part 1: Methane synchronization (68-31 ka BP) and the gas age-ice age difference, Climate of the Past, 11, 153–173, doi:10.5194/cp-11-153-2015, 2015.

Capron, E., Landais, A., Lemieux-Dudon, B., Schilt, A., Masson-Delmotte, V., Buiron, D., Chappellaz, J., Dahl-Jensen, D., Johnsen, S., Leuenberger, M., Loulergue, L., and Oerter, H.: Synchronising EDML and NorthGRIP ice cores using δ^{18}O of atmospheric oxygen ($\delta^{18}O_{atm}$) and CH_4 measurements over MIS5 (80–123 kyr), Quaternary Science Reviews, 29, 222–234, doi:10.1016/j.quascirev. 2009.07.014, climate of the Last Million Years: New Insights from EPICA and Other Records, 2010.

Craig, H., Horibe, Y., and Sowers, T.: Gravitational Separation Of Gases And Isotopes In Polar Ice Caps, Science, 242, 1675–1678, doi:10.1126/science.242. 4886.1675, 1988.

Custer, S.: Eemian records of $\delta^{18}O_{atm}$ and CH_4 correlated to the Vostok EGT4 timescale from the Moulton blue ice field, West Antarctica, BSc thesis, Pennsylvania State University, 46 pp. Available at: www.geosc.psu.edu/undergrads/documents/documents/StantonCusterthesis.pdf, 2006.

Dunbar, N. W., McIntosh, W. C., and Esser, R. P.: Physical setting and tephrochronology of the summit caldera ice record at Mount Moulton, West Antarctica, Geological Society of America Bulletin, 120, 796–812, doi:10.1130/ B26140.1, 2008.

Fountain, A., Lyons, W., Burkins, M., Dana, G., Doran, P., Lewis, K., McKnight, D., Moorhead, D., Parsons, A., Priscu, J., Wall, D., Wharton, R., and Virginia, R.: Physical controls on the Taylor Valley ecosystem, Antarctica, Bioscience, 49, 961–971, URL http://www.jstor.org/stable/10.1525/bisi.1999.49.12.961, 1999.

Google Maps: Taylor Glacier [Satellite imagery], Retrieved from http://goo.gl/2qwnqC, 2015.

Hudleston, P. J. and Treagus, S. H.: Information from folds: a review, Journal of Structural Geology, 32, 2042–2071, doi:10.1016/j.jsg.2010.08.011, Structural Diagenesis, 2010.

Jacobel, R., Gades, A., Gottschling, D., Hodge, S., and Wright, D.: Interpretation of radar-detected internal layer folding in West Antarctic ice streams, Journal of Glaciology, 39, 528–537, 1993.

Jacobson, H. P.: Folding of stratigraphic layers in ice domes, Thesis (Ph. D.), University of Washington, URL http://hdl.handle.net/1773/6837, 2001.

Kavanaugh, J. L. and Cuffey, K. M.: Dynamics and mass balance of Taylor Glacier, Antarctica: 2. Force balance and longitudinal coupling, Journal Of Geophysical Research: Earth Surface, 114, F04 011, doi:10.1029/2009JF001329, 2009.

Kavanaugh, J. L., Cuffey, K. M., Morse, D. L., Bliss, A. K., and Aciego, S. M.: Dynamics and mass balance of Taylor Glacier, Antarctica: 3. State of mass balance, Journal Of Geophysical Research: Earth Surface, 114, F04 012, doi: 10.1029/2009JF001331, 2009a.

Kavanaugh, J. L., Cuffey, K. M., Morse, D. L., Conway, H., and Rignot, E.: Dynamics and mass balance of Taylor Glacier, Antarctica: 1. Geometry and surface velocities, Journal Of Geophysical Research: Earth Surface, 114, F04 010, doi:10.1029/2009JF001309, 2009b.

Kawamura, K., Severinghaus, J. P., Ishidoya, S., Sugawara, S., Hashida, G., Motoyama, H., Fujii, Y., Aoki, S., and Nakazawa, T.: Convective mixing of air in firn at four polar sites, Earth and Planetary Science Letters, 244, 672–682, doi:10.1016/j.epsl.2006.02.017, 2006.

Korotkikh, E. V., Mayewski, P. A., Handley, M. J., Sneed, S. B., Introne, D. S., Kurbatov, A. V., Dunbar, N. W., and McIntosh, W. C.: The last interglacial as represented in the glaciochemical record from Mount Moulton Blue Ice Area, West Antarctica, Quaternary Science Reviews, 30, 1940–1947, doi:10.1016/j.quascirev.2011.04.020, 2011.

Lisiecki, L. E. and Lisiecki, P. A.: Application of dynamic programming to the correlation of paleoclimate records, Paleoceanography, 17, 1–1—1–12, doi:10.1029/2001PA000733, 2002.

Malaize, B., Bender, M., Luz, B., Sucher, C., Grootes, P., and EJ, S.: Chronology of the Taylor Dome ice core based on the del 18-O of O2 in trapped air, EOS Transactions, 75, 226, 1994.

Marcott, S. A., Bauska, T. K., Buizert, C., Steig, E. J., Rosen, J. L., Cuffey, K. M., Fudge, T. J., Severinghaus, J. P., Ahn, J., Kalk, M. L., McConnell, J. R., Sowers,

T., Taylor, K. C., White, J. W. C., and Brook, E. J.: Centennial-scale changes in the global carbon cycle during the last deglaciation, Nature, 514, 616–619, doi:10.1038/nature13799, 2014.

Mitchell, L. E., Brook, E. J., Sowers, T., McConnell, J. R., and Taylor, K.: Multidecadal variability of atmospheric methane, 1000-1800 C.E., Journal of Geophysical Research: Biogeosciences, 116, G02 007, doi:10.1029/2010JG001441, 2011.

Moore, J. C., Nishio, F., Fujita, S., Narita, H., Pasteur, E., Grinsted, A., Sinisalo, A., and Maeno, N.: Interpreting ancient ice in a shallow ice core from the South Yamato (Antarctica) blue ice area using flow modeling and compositional matching to deep ice cores, Journal of Geophysical Research: Atmospheres, 111, D16 302, doi:10.1029/2005JD006343, 2006.

Morse, D. L., Waddington, E. D., and Steig, E. J.: Ice age storm trajectories inferred from radar stratigraphy at Taylor Dome, Antarctica, Geophysical Research Letters, 25, 3383–3386, doi:10.1029/98GL52486, 1998.

Morse, D. L., Waddington, E. D., and Rasmussen, L. A.: Ice deformation in the vicinity of the ice-core site at Taylor Dome, Antarctica, and a derived accumulation rate history, Journal of Glaciology, 53, 449–460, doi:10.3189/002214307783258530, 2007.

Petrenko, V.: Encyclopedia of Quaternary Science, 2nd ed., chap. Ice Core Records: Ice Margin Sites, pp. 416–430, Elsevier, 2013.

Petrenko, V., Severinghaus, J., Brook, E., Reeh, N., and Schaefer, H.: Gas records from the West Greenland ice margin covering the Last Glacial Termination: a horizontal ice core, Quaternary Science Reviews, 25, 865–875, doi:10.1016/j.quascirev.2005.09.005, 2006.

Popp, T. J.: The Speed and Timing of Climate Change: Detailed Ice Core Stable Isotope Records from NorthGRIP, Greenland and Mt. Moulton, West Antarctica, Ph.D. thesis, University of Colorado at Boulder, URL http://books.google.com/books?id=adEwXeIwUNwC, 2008.

Reeh, N., Oerter, H., Letréguilly, A., Miller, H., and Hubberten, H.-W.: A new, detailed ice-age oxygen-18 record from the ice-sheet margin in central West Greenland, Global and Planetary Change, 4, 373–383, doi:10.1016/0921-8181(91)90003-F, 1991.

Robinson, P.: Ice dynamics and thermal regime of Taylor Glacier, South Victoria Land, Antarctica, Journal of Glaciology, 30, 153–160, 1984.

Schaefer, H., Whiticar, M. J., Brook, E. J., Petrenko, V. V., Ferretti, D. F., and Severinghaus, J. P.: Ice Record of $\delta^{13}C$ for Atmospheric CH_4 Across

the Younger Dryas-Preboreal Transition, Science, 313, 1109–1112, doi:10.1126/science.1126562, 2006.

Schaefer, H., Petrenko, V., Brook, E., Severinghaus, J., Reeh, N., Melton, J., and Mitchell, L.: Ice stratigraphy at the Pakitsoq ice margin, West Greenland, derived from gas records, Journal of Glaciology, 55, 411–421, doi:10.3189/002214309788816704, 2009.

Schilt, A., Baumgartner, M., Schwander, J., Buiron, D., Capron, E., Chappellaz, J., Loulergue, L., Schüpbach, S., Spahni, R., Fischer, H., and Stocker, T. F.: Atmospheric nitrous oxide during the last 140,000 years, Earth and Planetary Science Letters, 300, 33–43, doi:10.1016/j.epsl.2010.09.027, 2010.

Severinghaus, J. P., Sowers, T., Brook, E. J., Alley, R. B., and Bender, M. L.: Timing of abrupt climate change at the end of the Younger Dryas interval from thermally fractionated gases in polar ice, Nature, 391, 141–146, doi:10.1038/34346, 1998.

Severinghaus, J. P., Beaudette, R., Headly, M. A., Taylor, K., and Brook, E. J.: Oxygen-18 of O_2 Records the Impact of Abrupt Climate Change on the Terrestrial Biosphere, Science, 324, 1431–1434, doi:10.1126/science.1169473, 2009.

Sinisalo, A. and Moore, J. C.: Antarctic blue ice areas - towards extracting palaeoclimate information, Antarctic Science, 22, 99–115, doi:10.1017/S0954102009990691, 2010.

Sinisalo, A., Grinsted, A., Moore, J. C., Meijer, H. A. J., Martma, T., and Van De Wal, R. S. W.: Inferences from stable water isotopes on the Holocene evolution of Scharffenbergbotnen blue-ice area, East Antarctica, Journal of Glaciology, 53, 427–434, doi:10.3189/002214307783258495, 2007.

Souney, J., Twickler, M., Hargreaves, G., Bencivengo, B., Kippenhan, M., Johnson, J., Cravens, E., Neff, P., Nunn, R., Orsi, A., Popp, T., Rhoades, J., Vaughn, B., Voigt, D., Wong, G., and Taylor, K.: Core handling and processing for the WAIS Divide ice-core project, Annals of Glaciology, 55, 15–26, doi:10.3189/2014AoG68A008, 2014.

Sowers, T. and Bender, M.: Climate Records Covering The Last Deglaciation, Science, 269, 210–214, doi:10.1126/science.269.5221.210, 1995.

Sowers, T., Bender, M., and Raynaud, D.: Elemental and isotopic composition of occluded O_2 and N_2 in polar ice, Journal of Geophysical Research: Atmospheres, 94, 5137–5150, doi:10.1029/JD094iD04p05137, 1989.

Spaulding, N. E., Higgins, J. A., Kurbatov, A. V., Bender, M. L., Arcone, S. A., Campbell, S., Dunbar, N. W., Chimiak, L. M., Introne, D. S., and Mayewski,

P. A.: Climate archives from 90 to 250 ka in horizontal and vertical ice cores from the Allan Hills Blue Ice Area, Antarctica, Quaternary Research, 80, 562–574, doi:10.1016/j.yqres.2013.07.004, 2013.

Steig, E. J., Brook, E. J., White, J. W. C., Sucher, C. M., Bender, M. L., Lehman, S. J., Morse, D. L., Waddington, E. D., and Clow, G. D.: Synchronous climate changes in Antarctica and the North Atlantic, Science, 282, 92–95, doi:10.1126/science.282.5386.92, 1998.

Steig, E. J., Morse, D. L., Waddington, E. D., Stuiver, M., Grootes, P. M., Mayewski, P. A., Twickler, M. S., and Whitlow, S. I.: Wisconsinan and Holocene climate history from an ice core at Taylor Dome, western Ross Embayment, Antarctica, Geografiska Annaler Series A-Physical Geography, 82A, 213–235, doi:10.1111/j.0435-3676.2000.00122.x, 2000.

Stibal, M., Sabacka, M., and Zarsky, J.: Biological processes on glacier and ice sheet surfaces, Nature Geoscience, 5, 771–774, doi:10.1038/ngeo1611, 2012.

Sucher, C. M.: Atmospheric gases in the Taylor Dome ice core: Implications for East Antarctic climate change, Master's thesis, University of Rhode Island, Narraganset, 1997.

WAIS Divide Project Members: Onset of deglacial warming in West Antarctica driven by local orbital forcing, Nature, 500, 440–444, doi:10.1038/nature12376, 2013.

Whillans, I. and Cassidy, W.: Catch a falling star: meteorites and old ice, Science, 222, 55–57, doi:10.1126/science.222.4619.55, 1983.

Chapter 3

A horizontal ice core from Taylor Glacier and its implications for the Taylor Dome climate history

Abstract

Ice core records from Antarctica show synchronous temperature variations during the deglacial transition, an indication that the climate of the entire continent reacted as one unit to the global changes. However, a record from the Taylor Dome ice core in the Ross Sea sector of East Antarctica has been suggested to show a rapid warming, similar in style and synchronous with the Oldest Dryas - Bølling warming in Greenland. Since publication of the Taylor Dome record, evidence has been mounting that this interpretation is flawed due to errors in the underlying time scale. Currently, the issues raised regarding the dating of Taylor Dome linger unresolved and the original time scale remains the de facto chronology. We present new water isotope and chemistry data from Taylor Glacier to resolve the confusion surrounding the Taylor Dome time scale. Taylor Glacier is located downstream and fed by ice deposited on Taylor Dome's northern flank, providing the opportunity to reproduce the disputed findings. We find that the Taylor Glacier record is incompatible with the original interpretation of the Taylor Dome record, showing

that the warming in the area was gradual and started at ∼18 ka BP (before 1950) just like in all other Antarctic ice cores. We create a consistent, up-to-date Taylor Dome chronology from 0 ka to 60 ka BP by combining new and old age markers based on synchronization to other ice core records. The most notable feature of the new TD2015 time scale is a gas age - ice age difference of up to 12,000 years during the Last Glacial Maximum, by far the largest ever observed. A modeling effort to gain insight into the very low accumulation rates necessary during this time interval is unable to reproduce the estimated firn column thickness.

3.1 Introduction

The transition from the last glacial period to the Holocene is of great interest because it is a time of large scale reorganization of the climate system. The global mean temperature increased by 3.5°C from 18 ka to 10 ka BP (Shakun et al. (2012)). In the polar regions, the temperature change was significantly larger because of polar amplification, roughly 12°C in Antarctica (WAIS Divide Project Members (2013)) and 15°C in Greenland (Cuffey and Clow (1997)). The spatial and temporal patterns of these large scale changes are important clues to understand their causes and mechanisms. The similarities and differences of the Greenland and Antarctic temperature records have been studied extensively (Blunier and Brook (2001), EPICA Community Members (2006)) but uncertainties of the relative timing of events still inhibit a more complete understanding of the interplay between the two hemispheres. The thermal bipolar seesaw model (Stocker and Johnsen (2003)) is able to explain most of the first order variability. It postulates that the state of the Atlantic Meridional Overturning Circulation (AMOC) determines the hemispheric temperature contrast in the North and the South through heat flux changes in the Atlantic and the Southern Ocean. The bipolar seesaw is manifested in an Antarctic warming trend while Greenland is cold, and an Antarctic cooling trend while Greenland is warm (EPICA Community Members (2006)). This pattern also seems to hold for the deglaciation: Antarctica starts warming from roughly 18 ka BP on, while Greenland is still in a cold state. At 14.7 ka BP the AMOC

switches on, leading to a net transport of heat to the northern hemisphere, which puts Greenland in a warm state while Antarctica is experiencing a cooling phase (termed the Antarctic Cold Reversal) because of the net energy loss. The meltwater from a rapidly thinning Laurentide ice sheet is then thought to have eventually shut off deep water formation and in turn the AMOC at 13 ka BP, which led to the Younger Dryas cold period in the North and a resumption of the warming in the South (McManus et al. (2004)). Finally, by 11.7 ka BP, the AMOC turns on again but now both hemispheres stay in a warm state, presumably because of strong greenhouse gas forcing (Menviel et al. (2011), Shakun et al. (2012)).

The response to large scale, abrupt changes in the climate system presents a challenge and a testing ground for global climate models. North Atlantic "hosing" experiments under glacial boundary conditions, where the AMOC is shut off by imposing large freshwater fluxes into the North Atlantic, have shown a range of changes in Antarctic climate as a result of the AMOC shutdown (Kageyama et al. (2013)). While most models indicate a continent-wide coherent warming, some models (e.g. Timmermann et al. (2010)) have produced changes of opposite signs in some coastal areas, implying that regional climate dynamics dominate the response. Buiron et al. (2012) also present a model that produces a dipole pattern (cooling in West Antarctica, warming in East Antarctica) in response to a forced AMOC shutdown under LGM conditions. The mechanism responsible for this behaviour appears to be atmospheric teleconnections originating from the tropics. However, in a synthesis of circum-Antarctic climate records from the last glacial period, Buiron et al. (2012) cannot find such a dipole signal. As a benchmark for global climate models but also for conceptual models it is crucial to know whether all of Antarctica went through the deglacial transition as a single unit. Furthermore, whether Antarctic climate responds to climate changes as a single unit could be important for predicting the spatial distribution of future mass loss.

Temperature proxy records from ice cores drilled throughout all of Antarctica mostly agree on a synchronous, spatially coherent deglacial warming signal (Pedro et al. (2011)). The prevalence of this pattern, along with Antarctica's isolation and the Southern Ocean's role as a buffer due to its large heat capacity,

has led to the belief that the continent reacted to the changes in the global climate system as a single unit. The only record that does not support this block behaviour is from the Taylor Dome ice core where a more Greenland-like warming has been reported (Steig et al. (1998)). This finding was subsequently challenged by Mulvaney et al. (2000) who questioned Steig et al.'s (1998) st9810 time scale because of poor agreement of the Taylor Dome decrease in calcium concentration during the deglaciation in comparison with other ice cores from East Antarctica. Dissolved calcium is a proxy for particulate dust (Ruth et al. (2008)), mostly of South American origin, the fine fraction of which is transported to Antarctica and deposited onto the ice sheet (Lunt and Valdes (2001)). Because the dust source is far removed from the deposition site, it is thought that changes in wind strength and precipitation in the source region as well as changing circulation patterns during the transport phase are the main factors influencing dust deposition in Antarctica (Fischer et al. (2007b), Lambert et al. (2008)). The result is that local deposition effects are second order at best and changes in the dust flux are expected to be qualitatively similar in all ice cores (Schüpbach et al. (2013)). In Grootes et al. (2001), the authors of the st9810 chronology acknowledge the error in the original time scale and tie the deep part of the record directly to Vostok δD variations. On this new time scale, the calcium record during the deglaciation is in good agreement with other ice cores, however, there are still major differences in the Last Glacial Maximum (LGM). Furthermore, the adjusted time scale is up to 7,000 years older than st9810, but the implications of this substantial modification are not discussed.

To understand how this came to be, it is instructive to take a step back and look at how st9810 was built. For every ice core, there are two separate time scales, one applying to the ice phase, and one to the gas phase, with the age difference of the two at a specific depth termed the gas age - ice age difference (Δage). This arises because air is able to mix relatively freely through the porous firn column and gets trapped in bubbles only at the bottom of the firn, where the ice is already hundreds to thousands of years old depending on site conditions (Schwander et al. (1988), Sowers et al. (1989)). Ice age time scales in high

accumulation sites are typically based on layer counting, but for most Antarctic ice cores (including Taylor Dome) this is not an option because the annual layers are too thin for accurate counting. The traditional workaround is to synchronize the gas time scale to a high accumulation rate core (commonly from Greenland) via globally well-mixed gases (Blunier et al. (2007)) and estimate Δage using firn densification models. Δage for Greenland ice cores is on the order hundreds of years and its uncertainty does not contribute much to the total uncertainty in this procedure. Because of smaller accumulation rates, Δage in Antarctic ice cores is generally larger, commonly a few thousands years, and less well known (Bender et al. (2006)). For Taylor Dome, Steig et al. (1998) used cosmogenic beryllium-10 concentrations (^{10}Be) as a proxy for accumulation rates under the assumption of constant flux of ^{10}Be from the atmosphere to the ice (Steig (1996)) and δD for temperature as inputs into the Herron-Langway densification model (Herron and Langway (1980)) to estimate Δage. The fact that they had to correct their initial time scale by 7,000 years means that ^{10}Be severely overestimated the actual accumulation rate during this time period. The explanation for this overestimation may be that their assumption of constant ^{10}Be flux to the ice was unwarranted. Snow deposited on Taylor Dome may have blown away, to be deposited elsewhere (probably in the Dry Valleys), carrying with it the highly particle-reactive ^{10}Be and dust particles. Finally, Morse et al. (2007) revisited this paradox by recreating the accumulation history necessary to produce the Grootes et al. (2001) time scale. They conclude that accumulation rate estimates from ^{10}Be and non-sea-salt sulfate overestimate the actual accumulation rate significantly during the LGM, possibly because of wind scour removing some of the initial snowfall. This somewhat confusing evolution of the Taylor Dome time scale has led many to believe that Taylor Dome is at best poorly dated (e.g. Jouzel et al. (2001), Morgan et al. (2002), Masson-Delmotte et al. (2011)), but it continues to be cited as an example of North-South synchronous climate change (e.g. Farmer et al. (2005), Davis et al. (2009), Timmermann et al. (2010), Buiron et al. (2011)). For lack of availability of an updated, consistent chronology, the st9810 time scale is still the de facto Taylor Dome time scale (Carlson and Clark (2012), Siddall et al. (2012), Schoen-

emann et al. (2014)). Recent results from another ice core drilled at nearby Talos Dome support the view that the Ross Sea sector of Antarctica did not exhibit a Greenland-like behavior (Stenni et al. (2011)).

The aim of this paper is to resolve the mystery of the Taylor Dome ice core and to present a new, up-to-date time scale. We use new data from the ablation zone of Taylor Glacier, a valley glacier formed by ice deposited on the northern slope of Taylor Dome (Figure 3.1), to confirm that the Taylor Dome deglacial temperature record is synchronous with the rest of Antarctica.

The concept of a horizontal ice core is based on the notion that ice buried in the accumulation zone surfaces again in the ablation zone (Reeh et al. (1991)). If a continuous record can be identified, this marginal ice may be a valuable source for easily accessible large volume samples for paleoclimate studies (Petrenko et al. (2009)). Ice from the northern flank of Taylor Dome descends eastward through the Transantarctic Mountains as Taylor Glacier and terminates in Taylor Valley (Kavanaugh et al. (2009)). We therefore hope to find essentially the same ice that is buried beneath Taylor Dome to be exposed at the surface on Taylor Glacier. Possible complications with this simplistic approach include deformation of the ice and finding very young/old ice if flow speeds are too fast/slow. An initial exploration of the Taylor Glacier ablation zone using stable water isotopes by Aciego et al. (2007) shows that vast quantities of glacial and deglacial transition ice are exposed over tens of kilometers. Subsequent work using atmospheric gases trapped in bubbles describes well-dated and continuous sections of ice covering the deglaciation and the LGM (cf. Chapter 2). Here, we present new water isotope and dust data from Taylor Glacier covering 49 ka to 16 ka BP. Section 2 describes the sampling and measurement setup in detail. The results are presented in Section 3, while Section 4 contains a discussion of the dating of Taylor Dome, its implications for continent-wide deglacial climate change, Δage and a δ^{15}N modeling exercise.

3.2 Sampling and analytical procedures

Our sampling approach is guided by the data presented in Chapter 2, that establishes transects and gas age models for Taylor Glacier. All samples used in this study are from a 120 m long section on the across flow transect that was dated to 47.7 ka to 14.6 ka BP using gases. The transect is oriented perpendicular to the flow direction which is the preferred sampling setup since layers of equal age (isochrons) lie parallel to the ice flow direction. The dip of the layers is approximately vertical based on gas measurements and visual evidence from a 1.5 m deep pit. We adopt the distance registration of the across flow transect (cf. Chapter 2), where our sampling section covers -90 m to -210 m. The main measurements are continuous flow analysis of non-sea-salt calcium (nssCa), δ^{18}O of ice, and insoluble particle mass of the full 120 m section. These data are supported by discrete measurements of insoluble dust mass and dust size distribution, as well as more continuous and discrete $\delta^{18}O_{ice}$ measurements performed in a different lab. Samples were collected in the 2010/11, 2011/12, and 2013/14 field seasons. The ice surface is sub-horizontal, with no crevasses but thermal contraction cracks are pervasive. Wind-blown dust gathers on surface irregularities and melts itself into the ice through radiative heating, forming cryoconite holes. The largest depth to which this surface contamination is observed is 40 cm. All our samples are from 70 cm to 100 cm depth to avoid surface contamination artifacts. Some thermal contraction cracks are filled with wind-blown snow, presumably during wintertime katabatic storms that blow fresh snow from the polar plateau into the valleys. These snow layers are up to 3 mm thick, and we estimate that they may contribute up to 1 percent of the total sample volume.

3.2.1 Continuous flow analysis

For the continuous samples, representing a true horizontal ice core, a trench of 50 cm depth was excavated, and an electric chainsaw was used to cut ice sticks with dimensions of 50 cm x 5 cm x 5 cm from the entire length of the trench (Figure 3.2a). The effective sampling depth for these samples was 70 cm to 80

cm. The ice sticks were later trimmed to 50 cm x 3.5 cm x 3.5 cm using a band saw in McMurdo. Major ion concentrations in the ice were measured at the Ultra Trace Chemistry Laboratory at the Desert Research Institute via continuous flow analysis. The ice stick samples were melted continuously on a melter head that divides the melt water into three parallel streams. Elemental measurements were made on melt water from the innermost part of the core with ultra-pure nitric acid added to the melt stream immediately after the melter head; potentially contaminated water from the outer part of the ice is discarded. Elemental analysis of the innermost melt water stream is performed in parallel on two inductively coupled plasma mass spectrometers (ICPMS), each measuring a different set of elements; some elements were analyzed on both. The dual ICPMS setup allows for measurement of a broad range of 30 elements and data quality control (McConnell et al. (2002), McConnell et al. (2007)). The continuous flow system also measures δ^{18}O of the melt water (Maselli et al. (2013)). The effective resolution of this sampling setup is approximately 1 cm.

3.2.2 Discrete samples for dust analysis

The same transect was discretely sampled with a PICO ice coring drill (3 inch diameter) for measurements of insoluble dust. For each sample, a 1 m deep core was drilled and a cylinder of 2 cm height was cut from the bottom of the core with a clean hand saw (Figure 3.2b). The sampling resolution is 30 cm from -90 m to -140 m, and 1 m from -140 m to -180 m. These samples were sent to the Laboratoire de Glaciologie et Géophysique de l'Environnement (LGGE) in Grenoble, France, for analysis of dust mass and dust size distribution. The ice samples were decontaminated by repeat washings in ultra-pure water. The measurements were performed using a Multisizer IIe(c) Coulter Counter set up in a class 100 clean room. Detailed decontamination and measurement procedures are described by Delmonte et al. (2002).

3.2.3 Additional measurements of $\delta^{18}O_{ice}$

We sub-sampled both the continuous ice sticks and the discrete cylindrical ice samples for stable water isotope analysis. 25 cm long slabs of 2 to 3 mm thickness were shaved off of one side of the continuous samples from -90 m to -170 m. The same procedure was applied to all discrete samples. These slabs of ice were later melted in ziploc bags and the meltwater was transferred into 30 ml wide mouth hdpe sampling bottles and sent to the Institute of Arctic and Alpine Research (INSTAAR) for analysis. Measurements were performed on a Micromass SIRA Series II Dual Inlet mass spectrometer using well established procedures. The stated 1-sigma precision of the $\delta^{18}O$ measurements is 0.036 ‰.

3.3 Results

3.3.1 Quality of the dust record

Patagonia has been identified as the major source of dust in Antarctic ice cores during the last glacial period (Grousset et al. (1992), Basile et al. (1997)) and changes in the dust flux are attributed to aridity and wind strength in the source region (Lunt and Valdes (2001)). The first order dust signal throughout Antarctica is quite uniform despite large differences in dust concentrations due to widely varying accumulation rates. For the Taylor Glacier dust record to be useful as a dating tool, we must show that (a) it has not been compromised by additional local dust sources either during deposition on the polar plateau or at our sampling site via cracks or cryoconites, and (b) that the dust signal is qualitatively similar to records from deep ice cores. Figure 3.3 shows the dust size distribution of 164 samples averaged in 20 bins. All parts of the record have a unimodal distribution with a maximum at 2 μm and virtually no particles larger than 5 μm. This size distribution is characteristic of long range dust transport and consistent with observations from e.g. EDC (Delmonte et al. (2004)), EDML (Wegner (2008)), or Talos Dome (Albani et al. (2012)), all of which show the same mode at 2 μm. The fact that there are no particles larger than 5 μm in the Taylor Glacier record

strongly suggests that there are no local dust sources contributing to the total measured dust load.

The raw dust and nssCa records are shown in Figure 3.4. Insoluble dust mass measured with different techniques on discrete ice samples and continuous ice samples agree well with each other on the main features, but a more detailed comparison is hampered by high levels of noise. The data from the discrete samples are consistently higher by approximately 0.1 ppb than the data from the continuous flow analysis. The discrepancy could be explained by differences in the measurement techniques, e.g. in the continuous flow analysis system the melt water stream is forced through a 10 μm filter which may also capture a non-negligible fraction of particles smaller than 10 μm. Nonetheless, the excellent agreement of insoluble dust mass and nssCa concentrations gives us confidence to use nssCa as a proxy for long range dust loading. From here on, we will use only nssCa as a dust proxy to compare with other ice cores because very few ice cores have published high resolution insoluble dust records whereas nssCa records are usually available.

The elevated values for nssCa concentration from -110 m to -150 m in the transect are indicative of the LGM. The shape of the dust record compares favourably with Antarctic deep ice cores, all of which have three distinctive maxima in dust concentration during the LGM, separated by Antarctic Isotope Maximum (AIM) 2 and AIM 4. Assuming no hiatuses in the record, the sections with very low dust loading from -170 m to -180 m and -195 m to -205 m should then correspond to AIM 8 and AIM 12, respectively.

3.3.2 $\delta^{18}\mathbf{O}_{ice}$

Stable oxygen isotopes of H_2O in the ice are commonly used to infer past surface temperatures at the ice core deposition site (Jouzel et al. (1997)). Figure 3.4 shows $\delta^{18}O_{ice}$ measured on discrete and continuous samples from the Taylor Glacier transect. The three records agree very well with each other. The absolute values at certain obvious features are identical to the $\delta^{18}O_{ice}$ values measured in the Taylor Dome ice core (Figure 3.5, Steig et al. (1998)): -39 ‰ during AIM 12, -40.5 ‰ during AIM 8, and -44 ‰ during the LGM. This close correspondance in

the absolute values is a strong indication that the deposition site for Taylor Glacier is at approximately the same elevation as the Taylor Dome ice core. It also means that small amounts of snow blown into winter time cracks and observed in our samples do not significantly alter the large scale nature of our record. However, the Taylor Glacier $\delta^{18}O_{ice}$ record is considerably more noisy then $\delta^{18}O_{ice}$ records from other ice cores, even when 25 cm averages are considered. One reason for this could be the small amounts of modern snow in our samples, however, modern snow is presumably less depleted in the heavy isotopologue and we would expect only outliers to the positive side, which is not what we are observing. Another possibility is that the Taylor Glacier deposition site experiences more decadal variability than other ice cores precisely because the accumulation rate is very low. In such an arid regime, single snowfall events contribute a larger fraction of the total snow accumulation, which could explain the increased variability. A third factor to consider is that post-depositional processes can modify $\delta^{18}O$ values by several ‰ in low accumulation settings, as shown with modern measurements for a site at Taylor Mouth by Neumann et al. (2005) and at Dome Fuji (Hoshina et al. (2014)). Ventilation can redistribute and remove vapor in the firn, which causes modification of isotope ratios through sublimation and condensation (Waddington et al. (2002)). The lower the accumulation rate, the longer the firn remains near the surface, where it can be modified by ventilation. On the other hand, even if diffusion causes a significant change in the $\delta^{18}O$ values, one would expect that such a re-distribution through vapor would smooth out the differences in $\delta^{18}O$ between different layers of ice.

3.4 Discussion

3.4.1 Dating Taylor Glacier

We take advantage of the fact that dust transport into Antarctica is the main factor in determining local dust deposition, and therefore reconstructed dust records from different locations all look very similar. This allows us to date our transect by synchronizing changes in nssCa concentration to equivalent changes in

the WAIS Divide ice core (Table 3.1, Figure 3.5). We chose the WAIS Divide ice core as our reference record because of its excellent dating and its high resolution nssCa data (WAIS Divide Project Members (2013), Buizert et al. (2015)). In between the tie points we apply a linear interpolation. Fudge et al. (2014) show that more complex interpolation schemes taking into account annual layer thicknesses or accumulation rates produce more accurate age models, but since we don't have good constraints on either annual layer thickness or accumulation rate we are forced to use the traditional method. The difference between the interpolation schemes should be small to negligible if a large number of tie points can be identified. In addition to the tie points from the nssCa synchronization, we were able to identify a number of volcanic events that are found in both cores based on sulphur and cadmium anomalies. This volcanic synchronization confirms and strengthens our time scale further. The resulting distance age relationship is close to linear from 49 ka to 17 ka BP with a hint of a steepening and higher accumulation rates from 17 ka to 16 ka BP. The inferred average annual layer thickness, calculated as horizontal distance divided by time without correcting for thinning, is 0.35 cm/yr.

3.4.2 Asynchronous climate changes at Taylor Dome and in the North Atlantic

At Taylor Glacier, $\delta^{18}O_{ice}$ starts to increase at approximately 18 ka BP (Figure 3.3). The timing of the increase is very well constrained via the 17.8 k volcanic event that is found in the WAIS Divide ice core and the Taylor Glacier horizontal ice core and can be unambiguously matched because of its unique chemical fingerprint (McConnell et al. (2015)). $\delta^{18}O$ of ice is typically interpreted as a proxy for the local condensation temperature, but changes in the atmospheric circulation and accumulation rate can also impact $\delta^{18}O_{ice}$ without affecting the local temperature. Naturally, changes in temperature, atmospheric circulation and accumulation rate are often convoluted, complicating the interpretation of a $\delta^{18}O_{ice}$ record. For our purposes, it is sufficient to recognize that either one of these factors, and probably all of them, are changing starting at 18 ka BP, and that this change has to affect the Taylor Dome deposition site as well because of its close proxim-

ity. This observation is directly contradicting the st9810 time scale that showed no change in $\delta^{18}O_{ice}$ until 15 ka BP. Furthermore, as pointed out by Mulvaney et al. (2000), the calcium records are also incompatible (Figure 3.5). Although it seems far fetched, one could have argued that Taylor Dome was indeed affected by different air masses and maybe should not have the same dust history as Dome C, especially if there was some sort of direct North-South Atlantic connection that determined climate in the western Ross Sea sector. But the new Taylor Glacier nssCa record is indisputably inconsistent with the st9810 chronology and proves that the dust flux history in the Taylor Dome area was not significantly different from the rest of Antarctica. Our new findings confirm that the isotope warming at the start of the deglaciation in the Taylor Dome area begins at approximately 18 ka BP, just like in other Antarctic ice cores.

3.4.3 TD2015 - a new time scale for Taylor Dome

Although the validity of the Taylor Dome ice time scale has been questioned previously, nobody has gone ahead and created an updated time scale for the deglaciation and the LGM. The additional evidence from Taylor Glacier provides motivation to revisit this issue and produce a new Taylor Dome time scale based on all available information. We start with the ice age time scale: Following the approach outlined by Mulvaney et al. (2000), we synchronize the Taylor Dome calcium record to our Taylor Glacier nssCa record from 16 ka to 49 ka BP (Appendix B, Figure 3.10). From 49 ka to 60 ka BP we apply the same procedure with WAIS Divide as the reference record. For the Holocene (0 ka to 11 ka BP) we use the ice age time scale of Monnin et al. (2004). Between 11 ka and 16 ka BP, there are no features in the calcium record that could inform the dating. We add two tie points at the beginning and the end of the Antarctic Cold Reversal (ACR) identified in the $\delta^{18}O_{ice}$ record, assuming that these large scale isotope changes are synchronous in all Antarctic ice cores (Pedro et al. (2011), Stenni et al. (2011)).

Unlike for the ice age time scale, a number of different gas age time scales have been published, most of them only valid for a certain part of the core (Figure 3.6): The Holocene (Indermuhle et al. (1999)) and deglaciation (Smith et al.

(1999)) CO_2 isotope papers both use the st9810 gas time scale which is based on CH_4 and $\delta^{18}O_{atm}$ synchronization to the Greenland Ice Sheet Project 2 (GISP2) ice core. Brook et al. (2000) also use methane and $\delta^{18}O_{atm}$ measured in Taylor Dome to synchronize to GISP2, but the resulting time scale is significantly different, especially during the Holocene. Indermuehle et al. (2000) present a CO_2 record from the last glacial period that is on a time scale built by matching CO_2 and CH_4 to the Vostok GT4 time scale. Monnin et al. (2004) matches the Holocene CO_2 record from Indermuhle et al. (1999) to the Dome C CO_2 record. Using new and existing CO_2 and CH_4 data from 65 ka to 35 ka BP, Ahn and Brook (2007) also produced a new chronology for Taylor Dome, synchronized to GISP2. Finally, Lourantou et al. (2010) synchronize the deglacial CO_2 record from Smith et al. (1999) to the GICC05 time scale (Blunier et al. (2007)). After careful deliberation we decided to use a combination of the Monnin et al. (2004) (during the Holocene), Brook et al. (2000) (during the deglaciation), and Ahn and Brook (2007) (during the last glacial period) time scales with two additional $\delta^{18}O_{atm}$ tie points during the LGM to build the TD2015 gas age time scale.

All used time scales were updated to the WD2014 standard as well as possible. For example, the Monnin et al. (2004) gas time scale that we use in the Holocene and is based on GICC05 is multiplied by 1.0063 as suggested by Buizert et al. (2015). For the Holocene ice age chronology the estimated Δage of Monnin et al. (2004) is then added to the gas age for each depth. The Ahn and Brook (2007) time scale that we adopt for our gas chronology from 65 ka to 35 ka BP originally uses tie points to line up Taylor Dome and GISP2. We re-map those tie points to the equivalent gas events in the WD2014 time scale.

The resulting depth-age curves for the gas and ice phase (Figure 3.7) are almost flat in the LGM because of the very low accumulation rate. A period of 8,000 years, from 24.5 ka to 16.5 ka BP, is compressed into 2.8 m depth. Our best estimate of the maximum Δage is $\sim$12,000 years (at 378.5 m depth), significantly larger than the next-largest value of 6,500 years that was estimated for the Vostok ice core in the LGM (Veres et al. (2013)). We believe our estimate is robust owing to good age constraints on both the gas and ice phase: At 378.5 m, CO_2 is already

220 ppm, methane is 450 ppb and rising, and $\delta^{18}O_{atm}$ is >1 ‰, which excludes any ages older than 15.5 ka BP. At the same depth, nssCa is 15 to 20 ppb, but elevated nssCa values between AIM 4 and AIM 2 preclude ages younger than 27 ka BP for the ice phase.

The Taylor Dome $\delta^{18}O_{ice}$ record, on the TD2015 time scale, looks qualitatively similar to isotope records from other Antarctic ice cores. AIM 2 features prominently during the LGM. Because of the spectacularly low accumulation rate the time resolution of the isotope record is reduced, making precise comparisons difficult. The following warming is gradual and starts at 18 ka BP. As already discussed by Steig et al. (2000), Taylor Dome is unusual in that almost all of the isotope warming is accomplished by 14.7 ka BP, during the first half of the deglaciation. On this particular point we see no evidence for problems with the original interpretation.

3.4.4 δ^{15}N modeling

There are no modern or past analogues for a firn column that takes 12,000 years for fresh snowfall to turn into ice, as required by our results. The relevant physics may be significantly different from the physics implicit in firn densification models, which are built and calibrated for present day conditions. For example, physical processes such as vapor transport may dominate over mechanical deformation as densification mechanisms under low driving stress on these long timescales. However, as an exercise to illuminate the possible model limitations, we model Δage using an empirical steady state firn densification model (Herron and Langway (1980)) together with δ^{15}N measurements (cf. Chapter 2) to gain insight into the firn column during that unusual time. We chose the Herron-Langway model instead of other, more recent modeling approaches (e.g. Goujon et al. (2003)) because it seems to have a more realistic sensitivity to accumulation variability (Buizert et al. (2015)) and because of its simplicity. A situation with 12 ka Δage and <.1 cm/yr water equivalent accumulation is well outside of the calibration range of any firn densification model (Landais et al. (2006)), so the results should be taken with a healthy dose of scepticism. The Herron-Langway model uses in-

puts of firn temperature and accumulation rate to predict density-depth profiles and thus indirectly firn thickness. Δage is approximated as the age of the ice at bubble close-off depth (parameterized as ice density $\rho = 0.8\ g/cm^3$), and the age of the gas at this depth is assumed negligible (on the order of a few decades). Firn thickness and accumulation rate then directly determine Δage. We run the Herron-Langway model in reverse, trying to find the accumulation rate that produces our observed Δage given a prescribed temperature. The temperature input is averaged over the measured Δage, representing an average temperature during the densification process. We convert the Taylor Dome isotope record into local temperature using $\alpha = 0.5\,‰\,(°C)^{-1}$ as in Steig et al. (2000). We use the same approach to model Δage for Taylor Glacier. However, we use the Taylor Dome temperature instead of the Taylor Glacier temperature because of gaps in the Taylor Glacier record and unresolved doubts about whether the Taylor Glacier isotope record is a good proxy for local temperature (see Section 3.3.2 for details).

The firn thickness can then be used to predict δ^{15}N assuming that gravitational settling is the only process affecting δ^{15}N in the firn (Sowers et al. (1989), Craig et al. (1988)). The predicted δ^{15}N is directly comparable to measured δ^{15}N in trapped air bubbles. In reality, a number of factors influence δ^{15}N in addition to gravitational enrichment, most notably thermal diffusion because of temperature gradients (Severinghaus et al. (1998)) and a convective zone at the top of the firn column because of strong surface winds and high porosity (Kawamura et al. (2006)). These other factors are not generally known for past times. For these reasons the δ^{15}N calculated in this way should be viewed as a maximum estimate (at least for Antarctic sites, where thermal diffusion signals are small or negative).

As expected, the firn model is able to reproduce the observed Δages for Taylor Dome and Taylor Glacier with arbitrary accumulation rates (Figure 3.8). The necessary accumulation rates for Taylor Dome are extremely low during the LGM and of similar magnitude as in Morse et al. (2007). A different approach, using the glaciological thinning function to un-thin our new TD2015 age model, yields comparable results. The fact that modeled accumulation rate is lowest at 30 ka BP and not later is merely reflective of the fact that we use a steady state

model that does not integrate accumulation over time, such that variations that are smaller than Δage should not be interpreted. The model does a good job of estimating δ^{15}N before and after the LGM, but it is unable to reproduce the measured δ^{15}N signal during the time of extremely low accumulation for Taylor Dome and also to a slightly lesser degree Taylor Glacier. The discrepancy could be explained by a substantial convective zone at the top of the firn column (as seen in one modern location with very low accumulation rates, Severinghaus et al. (2010), Kawamura et al. (2013)) or it may be indicative of the fact that the model is ill-suited for such extreme conditions.

3.5 Conclusions

We present new dust and temperature proxy records from a horizontal ice core on Taylor Glacier that are incompatible with synchronous North-South climate change in the Taylor Dome region and the North Atlantic as suggested by Steig et al. (1998). Following Mulvaney et al. (2000), we construct a new ice age time scale for Taylor Dome by synchronizing it with our well-dated Taylor Glacier record using the dust signal, and the argument that the close proximity of the Taylor Glacier and Taylor Dome deposition sites prohibits large differences in the dust records. For consistency, we also update the Taylor Dome gas time scale. The new TD2015 time scale covers 0 ka to 60 ka BP, and although it still suffers from poor resolution during the LGM, and less than optimal data quality in some parts, it is a clear improvement on previous dating efforts. During the LGM, Taylor Dome experienced a period of extremely low accumulation, along with a Δage of 12,000 years, the underestimation of which led to the initial erroneous interpretation of a direct North-South coupling. The Taylor Dome isotope record on the TD2015 chronology shows a similar deglacial transition as the rest of Antarctica. The warming starts around 18 ka BP and is gradual.

The good quality of the dust data indicates that Taylor Glacier is usable as a source of large volume samples for measurements of micro-particles and their isotopes in high temporal resolution for the section presented (49 ka to 16 ka BP)

and most likely also for other time intervals. More work is needed to establish precise ice age chronologies for e.g. the full deglaciation, or the penultimate interglacial, both of which have been identified and can be accessed at the glacier surface (cf. Chapter 2).

The extremely low accumulation rate during the LGM has implications for our understanding of the hydrology and atmospheric circulation at that time. It is well known that accumulation can vary significantly on small spatial scales, e.g. Morse et al. (1999) show a large gradient in accumulation across Taylor Dome at present. There is evidence that during the LGM this gradient was reversed, with moisture bearing storms arriving mainly from the north, whereas today they reach Taylor Dome from the south (Morse et al. (1998)). This finding is strengthened by the higher reconstructed LGM accumulation rates for Taylor Glacier ice, which was deposited to the north of Taylor Dome. Whether this low accumulation anomaly was due to local topographical effects only or if it is part of a larger regional accumulation anomaly is still unclear. In this context, it should be noted that snow deposited on Taylor Dome during the LGM could have been blown away, carrying with it trace constituents such as ^{10}Be and dust. For this reason, a constant-flux assumption for these species (or equivalently, a spatially-invariant flux to the ice) may be unwarranted.

3.5.1 Acknowledgements

The US Antarctic Program provided outstanding logistical support. IDDO (Ice Drilling Design and Operations) provided the drilling systems. The Polar Geospatial Center (PGC) provided satellite imagery. We thank Paul Rose for being a whiz and keeping the chain saws running. Thomas Bauska, Christo Buizert, Michael Dyonisius, Xavier Fain, Benjamin Hmiel, Robb Kulin, James Lee, Chandra Llewellyn, Logan Mitchell, Avery Palardy, Hinrich Schaefer, and Adrian Schilt and all helped with sampling in the field. This work is supported through NSF Grants #0839031 and #1246148.

This chapter, in part, is currently being prepared for submission of the material. Baggenstos, D., J.P. Severinghaus, J.R. McConnell, M. Sigl, O. Maselli,

J.-R. Petit, and B. Grente. The dissertation author was the primary investigator and author of this material.

3.A Small scale variability in chemistry from continuous samples

The sampling for the horizontal ice core for continuous flow analysis was performed in two separate seasons (2011 and 2013), with a 1 m long overlap between the two sampling lines to help combine the two parts into one record (Figure 3.9). By far the best match is found for $\delta^{18}O_{ice}$. The water isotopes are highly smoothed by diffusion in the firn and ice which removes a lot of the small scale variability present in the initial snow accumulation. The short lived and inert aerosols, however, do not experience any smoothing and it is therefore not surprising that individual nssCa peaks on the order of 5 ppb are not reproducible by replication. It is thus recommended to apply a smoothing filter to the raw dust proxy data for interpretation or comparison to other records.

3.B Synchronizing Taylor Glacier and Taylor Dome using nssCa concentrations

To facilitate the synchronization, we convert Taylor Dome calcium and sodium concentrations to nssCa as described in Bigler et al. (2006). Using continuous flow high resolution measurements from Dome C, they also determined the sodium/calcium ratios in sea salt and in crustal derived aerosols, which are necessary for the calculation of nssCa. We adopt their estimates assuming that the crustal and sea salt sources are similar for aerosols deposited at Dome C and Taylor Dome. The correction to Ca is small, less than 2 ppb excluding the LGM, and less than 5 ppb during the most dusty intervals. The nssCa concentration at Taylor Glacier and Taylor Dome are very similar, with slightly higher values for Taylor Glacier. This is somewhat surprising since in continental Antarctica dust

deposition is thought to occur mainly through dry deposition (Mahowald et al. (1999)). Taylor Glacier has higher accumulation rates during the LGM which should dilute the atmospheric dust flux more than at Taylor Dome, leading to lower nssCa concentrations at Taylor Glacier. Since we are observing the opposite, we must conclude that dry deposition is not the main deposition mechanism.

A precise synchronization is complicated by two factors: The time resolution of the Taylor Dome chemistry record is only approximately one measurement every few hundred years in this period, because of the very low accumulation rate during the LGM and a sample spacing of 0.2 m. In addition, there are no data available from a crucial part of the record, from 382.48 m to 383.5 m depth and from 383.7 m to 384.5 m depth. Taking this into account, there are two viable ways to synchronize the two records (Figure 3.10): Option (a) requires the accumulation rate to gradually decrease heading into the LGM, reaching a minimum at 25 ka to 20 ka BP, and then increase substantially into the early Holocene. For option (b) to work, accumulation has to fall sharply to extremely low levels at 32 ka BP, probably with significant hiatuses on the order of a few thousand years, before increasing gradually starting at 25 ka BP. This option has the advantage that the highest value measured in Taylor Dome matches the highest peak in Taylor Glacier, which is not the case for option (a). We reject option (b) for the following reasons: Independent estimates using ^{10}Be (Steig et al. (2000)) and SO_4 (Morse et al. (2007)) agree that the lowest accumulation rate was reached around 20 ka BP, with higher values around 30 ka BP. Furthermore, there are no signs of an accumulation rate hiatus in the stable water isotope record or any of the gas records.

Table 3.1: Fixed tie points used in the Taylor Glacier - WAIS Divide ice age synchronization. Tie points were selected manually based on nssCa. WAIS Divide is on the WD2014 age scale (Buizert et al. (2015)).

Ice age [yrs BP]	WAIS Divide depth [m]	TG across flow distance [m]	Type of tie point
15,225	2,293	-90.03	start pt guess (gas age+500)
16,380	2,368	-100.36	peak
17,660	2,423	-108.20	fast transition
21,180	2,535	-117.30	transition midpoint
22,560	2,575	-120.60	transition midpoint
24,900	2,646	-127.30	transition midpoint
26,820	2,709	-133.00	transition midpoint
28,600	2,772	-138.70	peak
30,020	2,817	-146.80	transition midpoint
31,820	2,861	-152.80	transition midpoint
33,280	2,890	-156.90	peak
35,080	2,932	-162.90	transition midpoint
36,500	2,971	-168.93	peak
37,480	2,993	-171.20	transition midpoint
39,700	3,046	-181.50	transition midpoint
42,400	3,102	-191.20	peak
43,740	3,128	-194.10	transition midpoint
48,380	3,216	-208.00	transition fast
49,000	3,226	-210.53	end pt guess

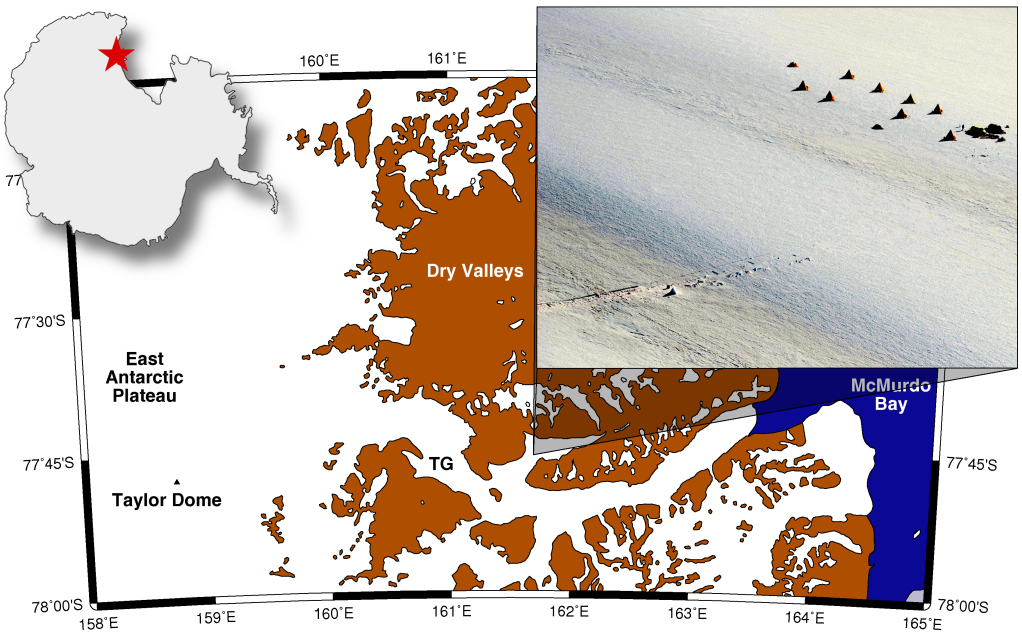

Figure 3.1: Map showing the location of the Taylor Glacier horizontal ice core in the southern McMurdo Dry Valleys, and Taylor Dome on the polar plateau. The McMurdo Dry Valleys are a series of snow-free valleys within Victoria Land. The region is one of the world's most extreme deserts. Ice flowing into Taylor Valley originates on the northern flank of Taylor Dome, on the polar plateau. The aerial photo shows a close up of the study site. In the lower left, the trench excavated for the horizontal ice core is visible. The trench cuts across a band of darker, slightly brown ice, representing the LGM and its high dust content. Photo by J. Schwander.

Figure 3.2: Impressions from sampling the horizontal ice core. (left) A. Palardy cutting a wedge of ice from the bottom of the trench for continuous analysis. (right) Sampling setup for discrete samples from 1 m depth. Some drilling holes are slightly offset to avoid cryoconite holes that could damage the cutters.

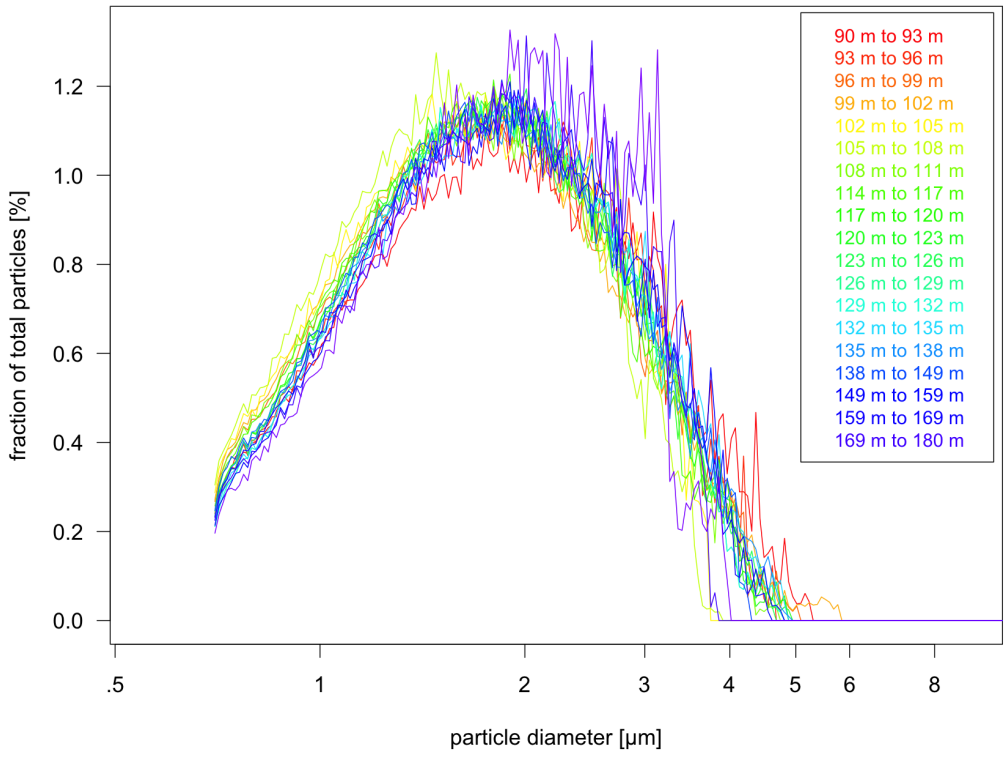

Figure 3.3: Average dust size distributions from different sections of the transect. Colors denote sections of increasing age, from youngest (red) to oldest (purple). There is no indication of any local dust sources. Measurements made by Benjamin Grente and Jean-Robert Petit at LGGE, Grenoble via Coulter counter.

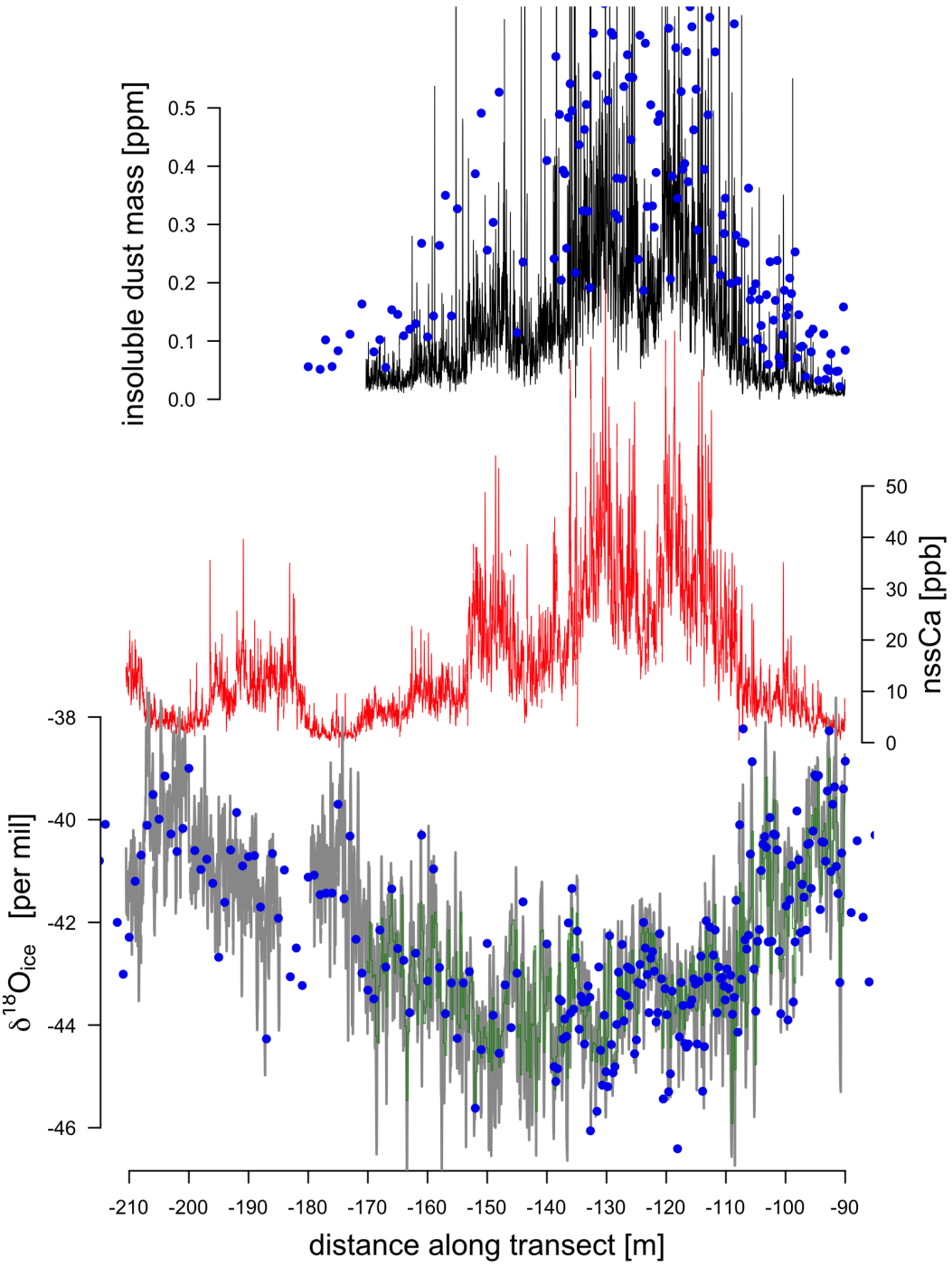

Figure 3.4: Raw data for insoluble dust mass (top), nssCa (center), and $\delta^{18}O_{ice}$ (bottom) from the Taylor Glacier horizontal ice core. Data from high resolution continuous flow analysis is shown in black (top), red (center), and gray (bottom). Discrete samples for insoluble dust and $\delta^{18}O_{ice}$ are shown as blue circles. $\delta^{18}O_{ice}$ 25 cm averages measured at INSTAAR are in excellent agreement with the continuous flow data (green line).

Figure 3.5: Antarctic ice phase records on a common timescale. From top to bottom: Taylor Glacier distance-age curve (orange) synchronized to the WD2014 time scale using nssCa tie points (orange) and volcanic events (black); Taylor Dome depth-age curve for the new TD2015 time scale (blue, solid) and Steig et al. (1998)'s st9810 time scale (blue, dotted); EPICA Dome C nssCa (black, Wolff et al. (2006), Fischer et al. (2007a)), WAIS Divide nssCa (black, Buizert et al. (2015)), Taylor Glacier nssCa (orange), Taylor Dome nssCa on TD2015 time scale (blue, solid), and st9810 (blue, dotted); Stable water isotopes for EPICA Dronning Maud Land (black, EPICA Community Members (2006)), Taylor Glacier (orange), and Taylor Dome (blue). All nssCa and water isotope records were binned into 100 year averages (except for Taylor Dome during the LGM where the sampling resolution is less than 100 years).

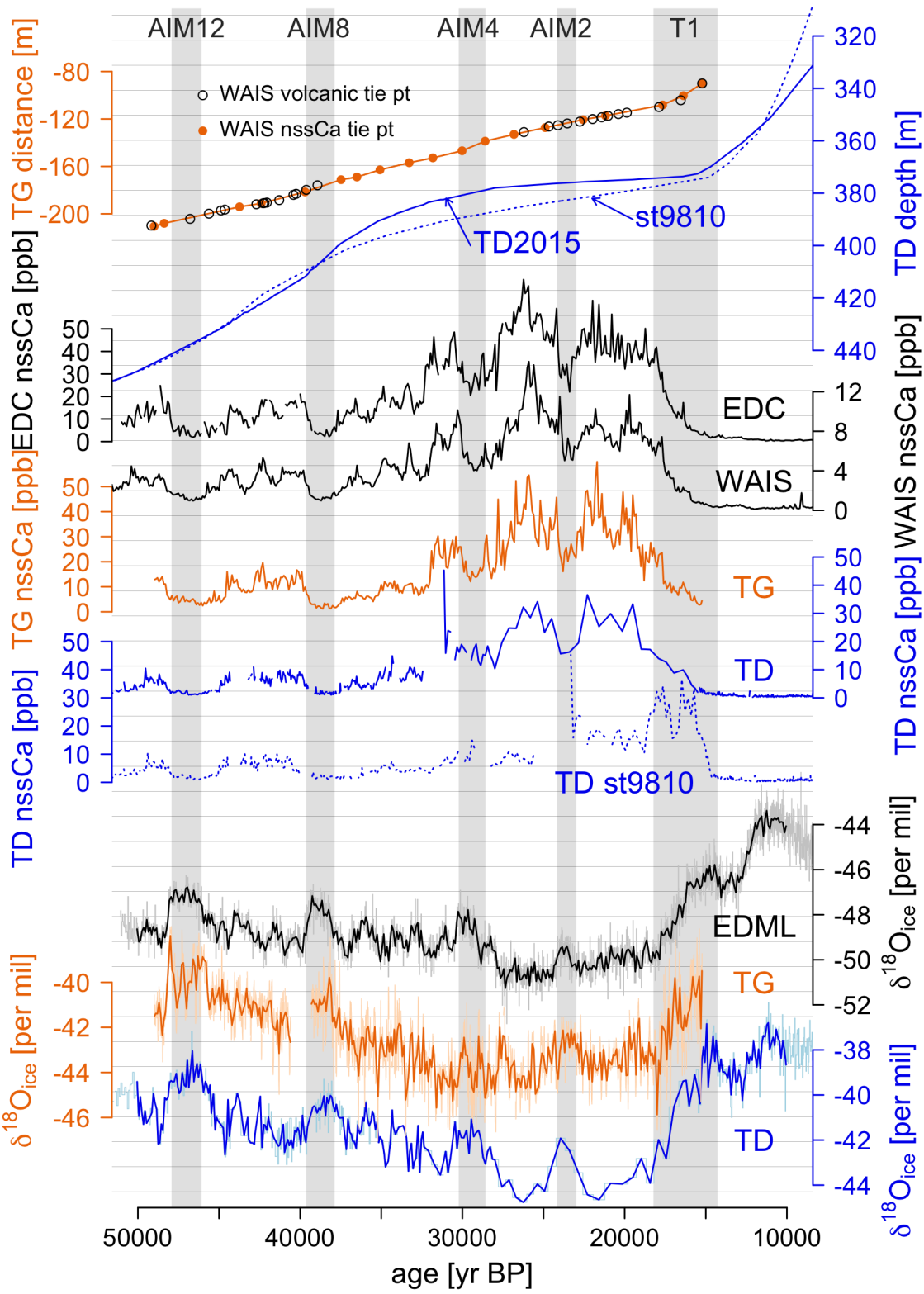
AIM12
AIM8
AIM4
AIM2
T1
WAIS volcanic tie pt
WAIS nssCa tie pt
TG distance [m]
TD depth [m]
TD2015
st9810
EDC nssCa [ppb]
WAIS nssCa [ppb]
EDC
WAIS
TG nssCa [ppb]
TG
TD nssCa [ppb]
TD
TD st9810
δ18Oice [per mil]
EDML
TG
TD
age [yr BP]

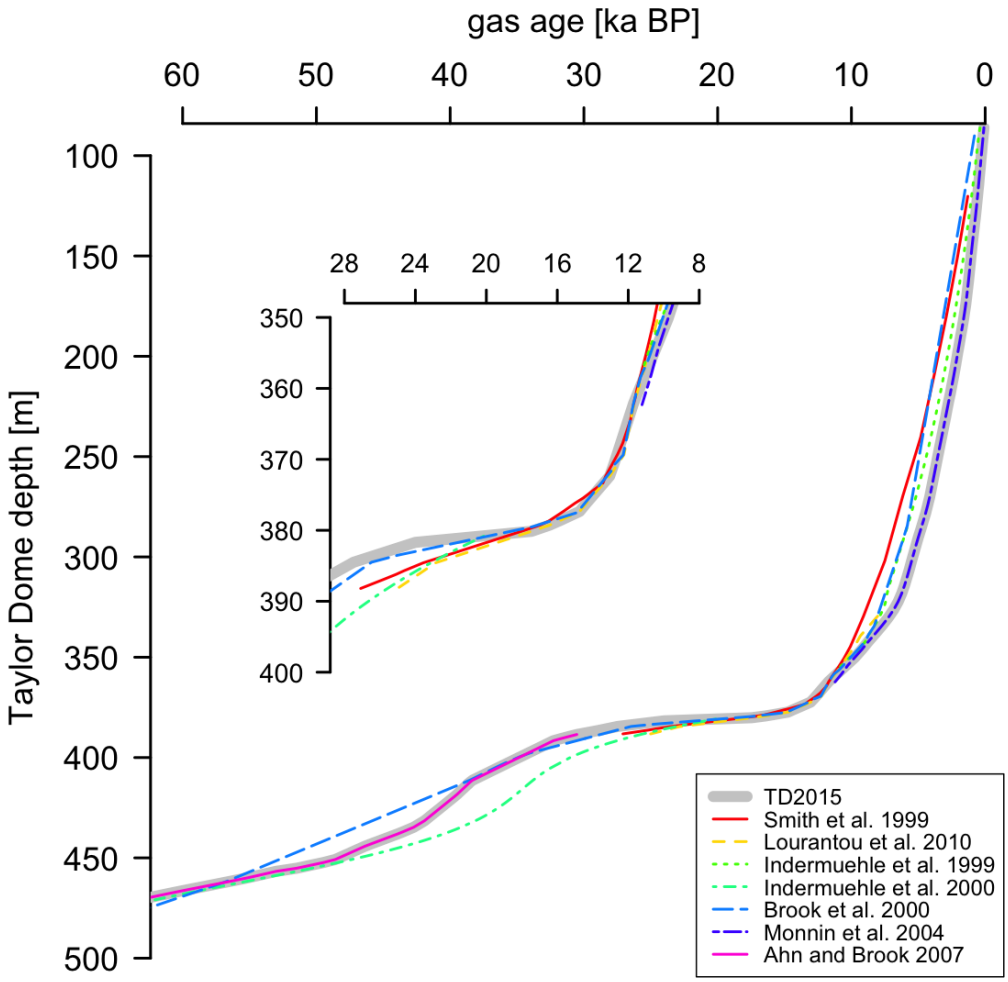

Figure 3.6: Existing Taylor Dome gas time scales and TD2015 from 0 ka to 60 ka BP. Insert shows close-up of the late LGM and the deglacial transition. There are large differences between individual time scales, especially from 35 ka to 55 ka BP, but also during the Holocene. During the deglacial transition the agreement between time scales is good, thanks to large and sometimes abrupt changes in all gases.

Figure 3.7: Δage, gas and ice phase records for Taylor Glacier and Taylor Dome. From top to bottom: CO_2 concentration from the Taylor Dome (blue, Smith et al. (1999), Ahn and Brook (2007)) and WAIS Divide (black, Marcott et al. (2014)) ice cores; CH_4 concentration from Taylor Dome (blue, Brook et al. (2000)), Taylor Glacier (orange), and WAIS Divide (black, Buizert et al. (2015), WAIS Divide Project Members (2013)); $\delta^{18}O_{atm}$ from Taylor Dome (blue, Sucher (1997)), Taylor Glacier (orange), and WAIS Divide (black); Taylor Dome ice age (blue solid) and gas age (blue dotted) curves; Taylor Glacier ice age (orange solid) and gas age (orange dotted) curves; Δage for Taylor Dome (blue) and Taylor Glacier (orange) including an estimate of the uncertainty; nssCa from Taylor Dome (blue) and Taylor Glacier (orange). Taylor Dome records are on the TD2015 time scale. Δage is plotted on the ice age time scale. Black arrows point to 378.5 m depth for the gas and ice age. At 378.5 m the Δage is approximately 12,000 years. Major Antarctic Isotope Maximum (AIM) events and the beginning of the deglacial transition are highlighted in gray bars.

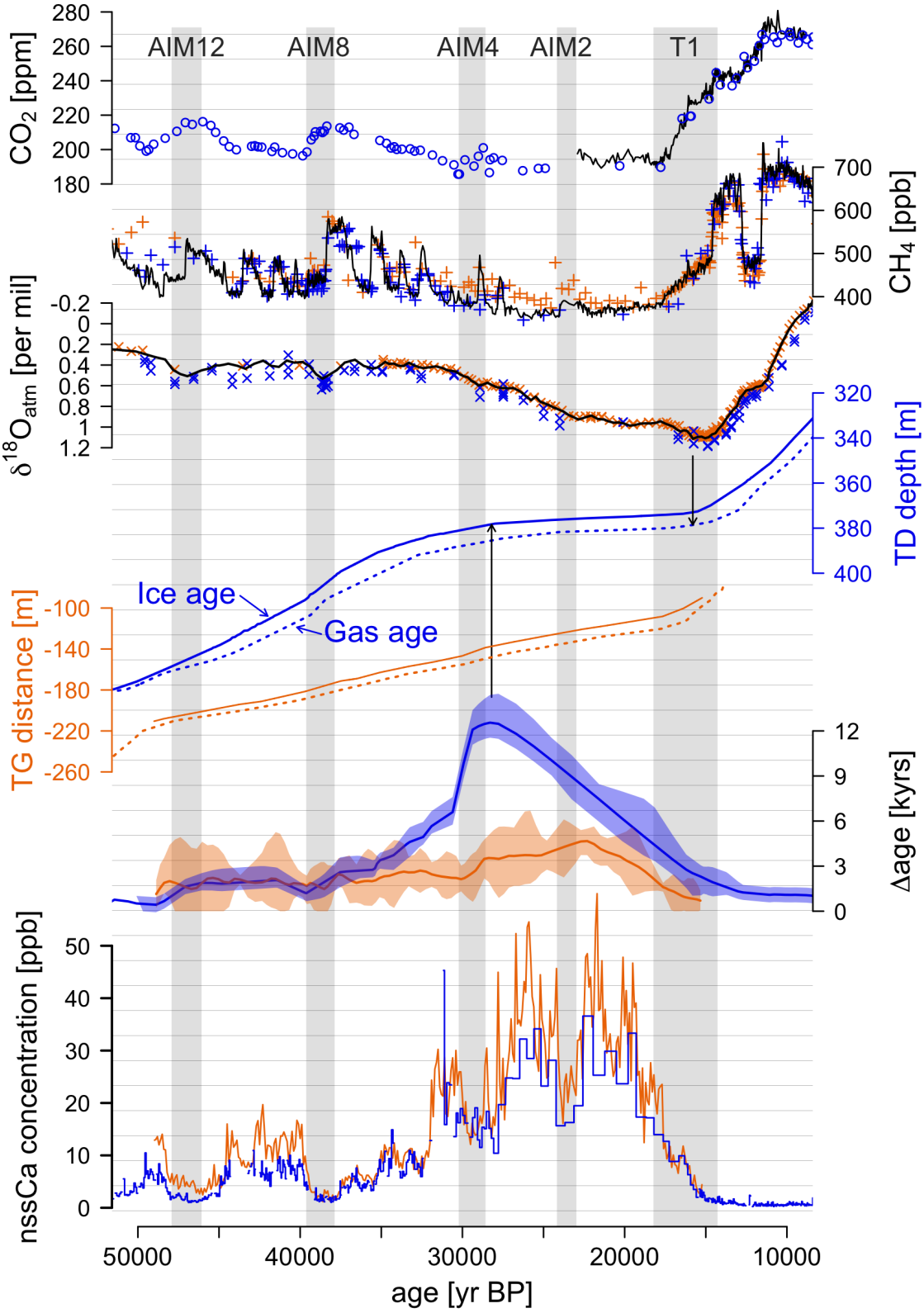
AIM12
AIM8
AIM4
AIM2
T1
CO2 [ppm]
CH4 [ppb]
δ18Oatm [per mil]
TD depth [m]
Ice age
Gas age
TG distance [m]
Δage [kyrs]
nssCa concentration [ppb]
age [yr BP]

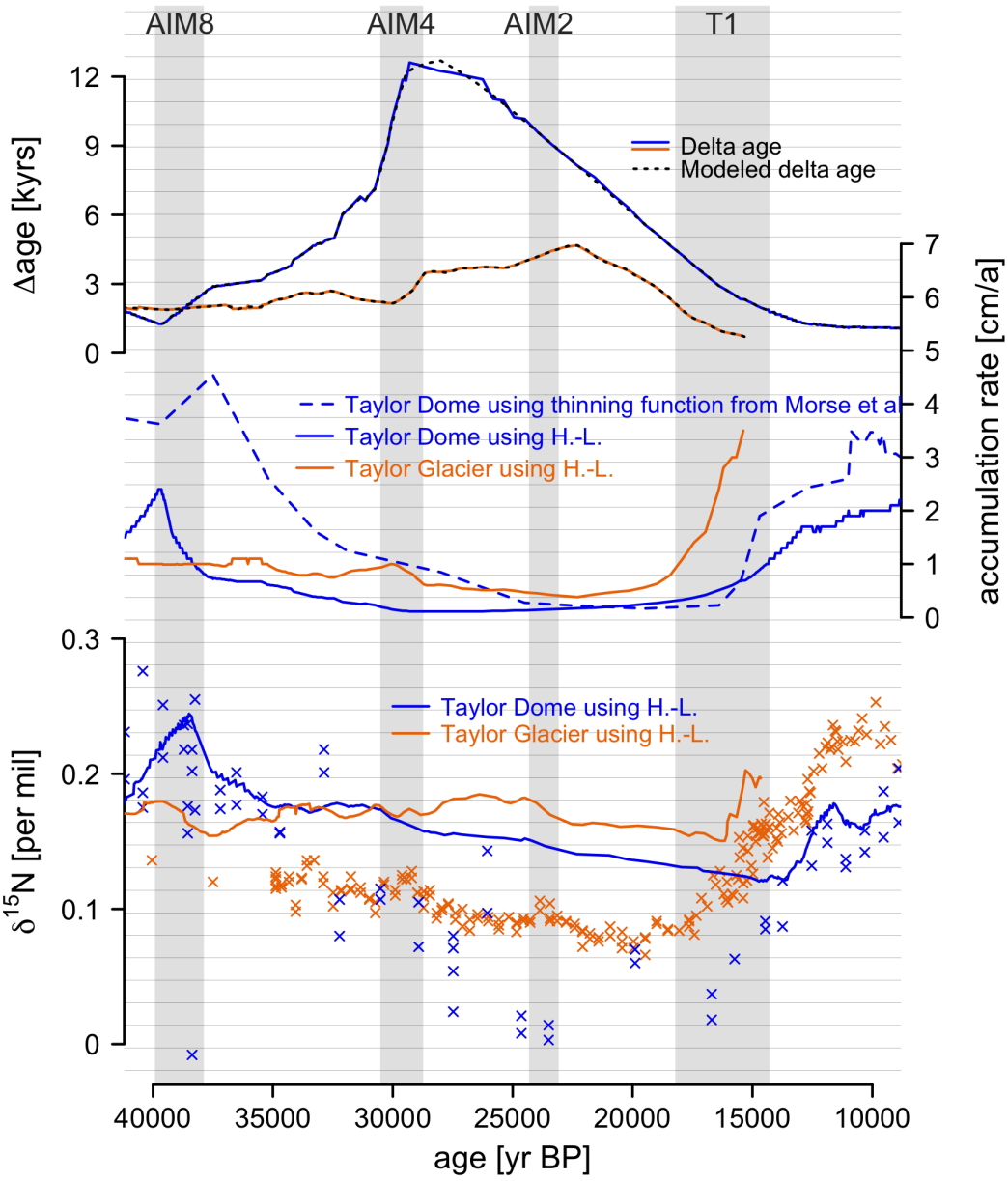

Figure 3.8: Δage modeling for Taylor Glacier and Taylor Dome and a comparison with δ^{15}N. For both Taylor Glacier and Taylor Dome, shown are modeled Δage (top), accumulation rate (center), and δ^{15}N (bottom), along with measurements of δ^{15}N (Sucher (1997)). For Taylor Dome, a second accumulation rate history (dashed) was reconstructed by un-thinning the TD2015 time scale using the thinning function from Morse et al. (2007). Major Antarctic Isotope Maximum (AIM) events and the beginning of the deglacial transition are shown in gray bars.

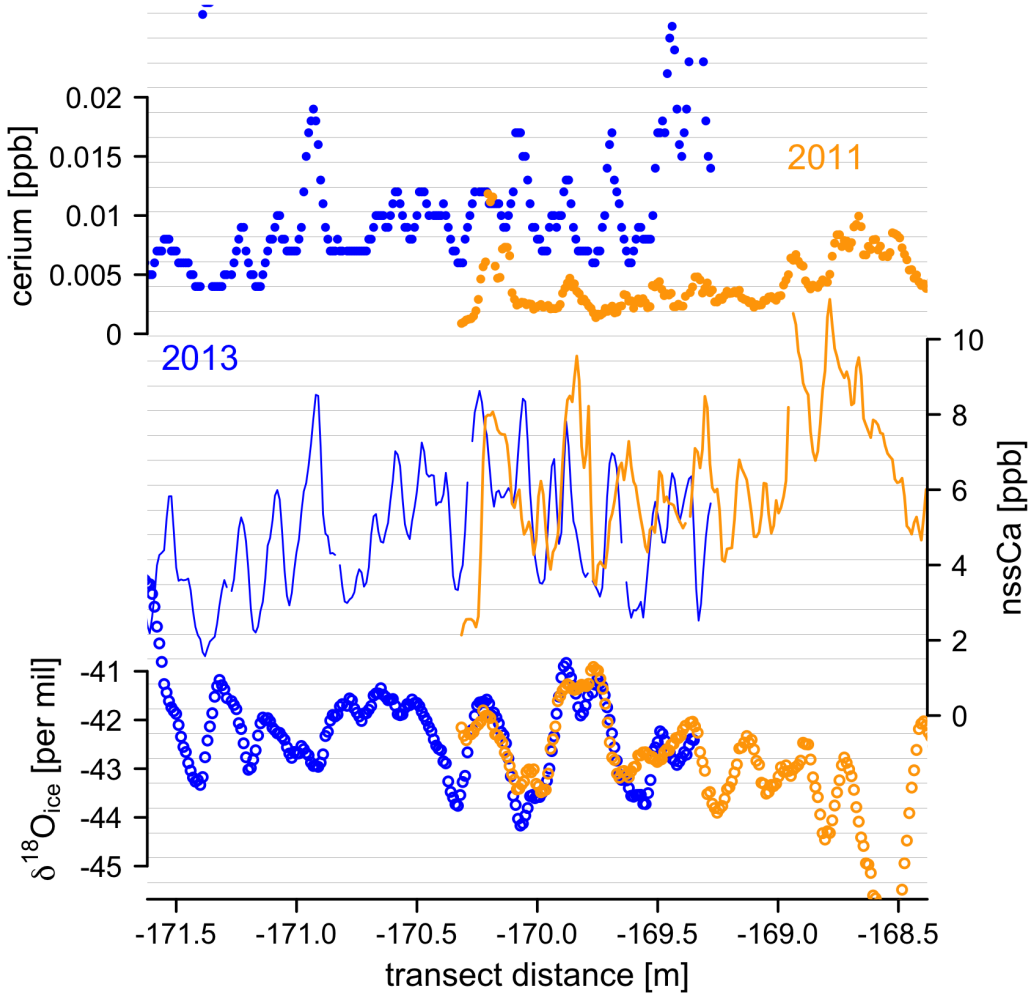

Figure 3.9: Ice phase chemistry measurements for overlap in the horizontal ice core. Cerium, nssCa and $\delta^{18}O_{ice}$ data are shown for a 3 m long section of the horizontal ice core, 1 m of which was replicated to facilitate the merging of the two records. The sampling lines were offset by 40 cm in the along flow direction. For cerium, not only is the noise uncorrelated as for nssCa, but there is a large difference in magnitude between the 2011 and 2013 data. We can only explain this discrepancy with the fact that we used a 10 μm filter on the extraction line in 2011 but not in 2013.

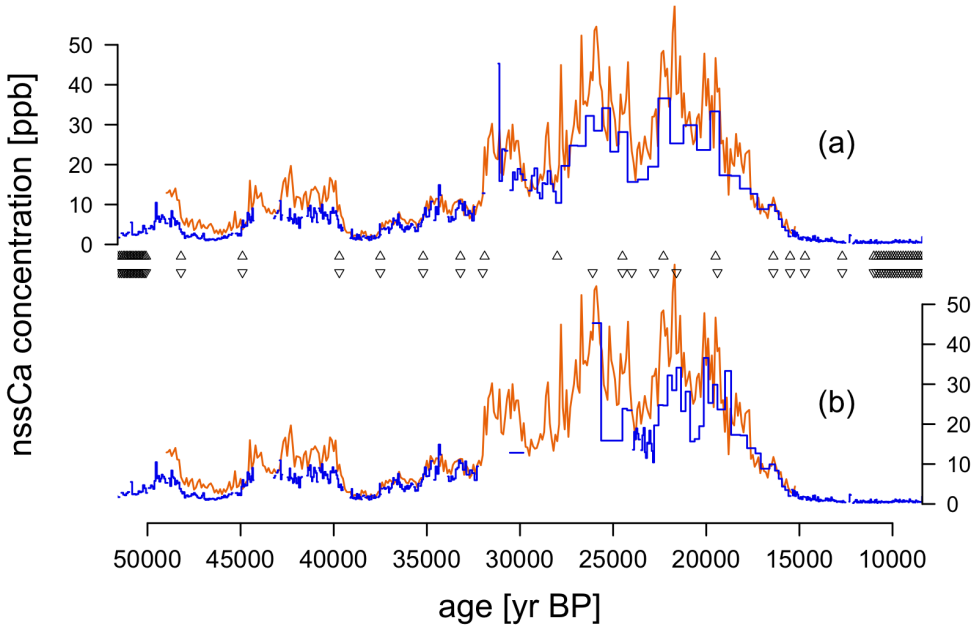

Figure 3.10: Synchronization of Taylor Glacier (orange) and Taylor Dome (blue, Steig et al. (2000)) nssCa records. Low sampling resolution and missing data complicate the synchronization. Shown are two options (a) and (b) along with the tie points used for both scenarios.

References

Aciego, S. M., Cuffey, K. M., Kavanaugh, J. L., Morse, D. L., and Severinghaus, J. P.: Pleistocene ice and paleo-strain rates at Taylor Glacier, Antarctica, Quaternary Research, 68, 303–313, doi:10.1016/j.yqres.2007.07.013, 2007.

Ahn, J. and Brook, E. J.: Atmospheric CO_2 and climate from 65 to 30 ka B.P., Geophysical Research Letters, 34, L10 703, doi:10.1029/2007GL029551, 2007.

Albani, S., Delmonte, B., Maggi, V., Baroni, C., Petit, J.-R., Stenni, B., Mazzola, C., and Frezzotti, M.: Interpreting last glacial to Holocene dust changes at Talos Dome (East Antarctica): Implications for atmospheric variations from regional to hemispheric scales, Climate of the Past, 8, 741–750, doi:10.5194/cp-8-741-2012, 2012.

Basile, I., Grousset, F. E., Revel, M., Petit, J. R., Biscaye, P. E., and Barkov, N. I.: Patagonian origin of glacial dust deposited in East Antarctica (Vostok and Dome C) during glacial stages 2, 4 and 6, Earth and Planetary Science Letters, 146, 573–589, doi:10.1016/S0012-821X(96)00255-5, 1997.

Bender, M. L., Floch, G., Chappellaz, J., Suwa, M., Barnola, J.-M., Blunier, T., Dreyfus, G., Jouzel, J., and Parrenin, F.: Gas age-ice age differences and the chronology of the Vostok ice core, 0-100 ka, Journal of Geophysical Research: Atmospheres, 111, D21 115, doi:10.1029/2005JD006488, 2006.

Bigler, M., Röthlisberger, R., Lambert, F., Stocker, T. F., and Wagenbach, D.: Aerosol deposited in East Antarctica over the last glacial cycle: Detailed apportionment of continental and sea-salt contributions, Journal of Geophysical Research: Atmospheres, 111, D08 205, doi:10.1029/2005JD006469, 2006.

Blunier, T. and Brook, E. J.: Timing of millennial-scale climate change in Antarctica and Greenland during the last glacial period, Science, 291, 109–112, doi:10.1126/science.291.5501.109, 2001.

Blunier, T., Spahni, R., Barnola, J.-M., Chappellaz, J., Loulergue, L., and Schwander, J.: Synchronization of ice core records via atmospheric gases, Climate of the Past, 3, 325–330, doi:10.5194/cp-3-325-2007, 2007.

Brook, E. J., Harder, S., Severinghaus, J., Steig, E. J., and Sucher, C. M.: On the origin and timing of rapid changes in atmospheric methane during the last glacial period, Global Biogeochemical Cycles, 14, 559–572, doi:10.1029/1999GB001182, 2000.

Buiron, D., Chappellaz, J., Stenni, B., Frezzotti, M., Baumgartner, M., Capron, E., Landais, A., Lemieux-Dudon, B., Masson-Delmotte, V., Montagnat, M., Parrenin, F., and Schilt, A.: TALDICE-1 age scale of the Talos Dome deep ice

core, East Antarctica, Climate of the Past, 7, 1–16, doi:10.5194/cp-7-1-2011, 2011.

Buiron, D., Stenni, B., Chappellaz, J., Landais, A., Baumgartner, M., Bonazza, M., Capron, E., Frezzotti, M., Kageyama, M., Lemieux-Dudon, B., Masson-Delmotte, V., Parrenin, F., Schilt, A., Selmo, E., Severi, M., Swingedouw, D., and Udisti, R.: Regional imprints of millennial variability during the MIS 3 period around Antarctica, Quaternary Science Reviews, 48, 99–112, doi:10.1016/j.quascirev.2012.05.023, 2012.

Buizert, C., Cuffey, K. M., Severinghaus, J. P., Baggenstos, D., Fudge, T. J., Steig, E. J., Markle, B. R., Winstrup, M., Rhodes, R. H., Brook, E. J., Sowers, T. A., Clow, G. D., Cheng, H., Edwards, R. L., Sigl, M., McConnell, J. R., and Taylor, K. C.: The WAIS Divide deep ice core WD2014 chronology - Part 1: Methane synchronization (68-31 ka BP) and the gas age-ice age difference, Climate of the Past, 11, 153–173, doi:10.5194/cp-11-153-2015, 2015.

Carlson, A. E. and Clark, P. U.: Ice sheet sources of sea level rise and freshwater discharge during the last deglaciation, Reviews of Geophysics, 50, RG4007, doi:10.1029/2011RG000371, 2012.

Craig, H., Horibe, Y., and Sowers, T.: Gravitational Separation Of Gases And Isotopes In Polar Ice Caps, Science, 242, 1675–1678, doi:10.1126/science.242.4886.1675, 1988.

Cuffey, K. M. and Clow, G. D.: Temperature, accumulation, and ice sheet elevation in central Greenland through the last deglacial transition, Journal of Geophysical Research: Oceans, 102, 26 383–26 396, doi:10.1029/96JC03981, 1997.

Davis, P. T., Menounos, B., and Osborn, G.: Holocene and latest Pleistocene alpine glacier fluctuations: a global perspective, Quaternary Science Reviews, 28, 2021–2033, doi:10.1016/j.quascirev.2009.05.020, 2009.

Delmonte, B., Petit, J., and Maggi, V.: Glacial to Holocene implications of the new 27000-year dust record from the EPICA Dome C (East Antarctica) ice core, Climate Dynamics, 18, 647–660, doi:10.1007/s00382-001-0193-9, 2002.

Delmonte, B., Petit, J. R., Andersen, K. K., Basile-Doelseh, I., Maggi, V., and Lipenkov, V. Y.: Dust size evidence for opposite regional atmospheric circulation changes over east Antarctica during the last climatic transition, Climate Dynamics, 23, 427–438, doi:10.1007/s00382-004-0450-9, 2004.

EPICA Community Members: One-to-one coupling of glacial climate variability in Greenland and Antarctica, Nature, 444, 195–198, doi:10.1038/nature05301, 2006.

Farmer, E. C., deMenocal, P. B., and Marchitto, T. M.: Holocene and deglacial ocean temperature variability in the Benguela upwelling region: Implications for low-latitude atmospheric circulation, Paleoceanography, 20, PA2018, doi: 10.1029/2004PA001049, 2005.

Fischer, H., Fundel, F., Ruth, U., Twarloh, B., Wegner, A., Udisti, R., Becagli, S., Castellano, E., Morganti, A., Severi, M., Wolff, E., Littot, G., Röthlisberger, R., Mulvaney, R., Hutterli, M. A., Kaufmann, P., Federer, U., Lambert, F., Bigler, M., Hansson, M., Jonsell, U., de Angelis, M., Boutron, C., Siggaard-Andersen, M.-L., Steffensen, J. P., Barbante, C., Gaspari, V., Gabrielli, P., and Wagenbach, D.: Reconstruction of millennial changes in dust emission, transport and regional sea ice coverage using the deep EPICA ice cores from the Atlantic and Indian Ocean sector of Antarctica, Earth and Planetary Science Letters, 260, 340–354, doi:10.1016/j.epsl.2007.06.014, 2007a.

Fischer, H., Siggaard-Andersen, M. L., Ruth, U., Rothlisberger, R., and Wolff, E.: Glacial/interglacial changes in mineral dust and sea-salt records in polar ice cores: Sources, transport, and deposition, Reviews of Geophysics, 45, RG1002, doi:10.1029/2005RG000192, 2007b.

Fudge, T. J., Waddington, E. D., Conway, H., Lundin, J. M. D., and Taylor, K.: Interpolation methods for Antarctic ice-core timescales: application to Byrd, Siple Dome and Law Dome ice cores, Climate of the Past, 10, 1195–1209, doi: 10.5194/cp-10-1195-2014, 2014.

Goujon, C., Barnola, J.-M., and Ritz, C.: Modeling the densification of polar firn including heat diffusion: Application to close-off characteristics and gas isotopic fractionation for Antarctica and Greenland sites, Journal of Geophysical Research: Atmospheres, 108, 4792, doi:10.1029/2002JD003319, 2003.

Grootes, P. M., Steig, E. J., Stuiver, M., Waddington, E. D., and Morse, D. L.: The Taylor Dome Antarctic O-18 record and globally synchronous changes in climate, Quaternary Research, 56, 289–298, doi:10.1006/qres.2001.2276, 2001.

Grousset, F. E., Biscaye, P. E., Revel, M., Petit, J.-R., Pye, K., Joussaume, S., and Jouzel, J.: Antarctic (Dome C) ice-core dust at 18 k.y. B.P.: Isotopic constraints on origins, Earth and Planetary Science Letters, 111, 175–182, doi:10.1016/ 0012-821X(92)90177-W, 1992.

Herron, M. and Langway, C. C.: Firn densification - an empirical-model, Journal of Glaciology, 25, 373–385, URL http://www.igsoc.org/journal/25/#part93, 1980.

Hoshina, Y., Fujita, K., Nakazawa, F., Iizuka, Y., Miyake, T., Hirabayashi, M., Kuramoto, T., Fujita, S., and Motoyama, H.: Effect of accumulation rate on water stable isotopes of near-surface snow in inland Antarctica, Journal of Geophysical

Research: Atmospheres, 119, 274–283, doi:10.1002/2013JD020771, 2014.

Indermuehle, A., Monnin, E., Stauffer, B., Stocker, T. F., and Wahlen, M.: Atmospheric CO_2 concentration from 60 to 20 kyr BP from the Taylor Dome Ice Core, Antarctica, Geophysical Research Letters, 27, 735–738, doi:10.1029/1999GL010960, 2000.

Indermuhle, A., Stocker, T. F., Joos, F., Fischer, H., Smith, H. J., Wahlen, M., Deck, B., Mastroianni, D., Tschumi, J., Blunier, T., Meyer, R., and Stauffer, B.: Holocene carbon-cycle dynamics based on CO_2 trapped in ice at Taylor Dome, Antarctica, Nature, 398, 121–126, doi:10.1038/18158, 1999.

Jouzel, J., Alley, R., Cuffey, K., Dansgaard, W., Grootes, P., Hoffmann, G., Johnsen, S., Koster, R., Peel, D., Shuman, C., Stievenard, M., Stuiver, M., and White, J.: Validity of the temperature reconstruction from water isotopes in ice cores, Journal of Geophysical Research: Oceans, 102, 26 471–26 487, doi:10.1029/97JC01283, 1997.

Jouzel, J., Masson, V., Cattani, O., Falourd, S., Stievenard, M., Stenni, B., Longinelli, A., Johnsen, S. J., Steffenssen, J. P., Petit, J. R., Schwander, J., Souchez, R., and Barkov, N. I.: A new 27 ky high resolution East Antarctic climate record, Geophysical Research Letters, 28, 3199–3202, doi:10.1029/2000GL012243, 2001.

Kageyama, M., Merkel, U., Otto-Bliesner, B., Prange, M., Abe-Ouchi, A., Lohmann, G., Ohgaito, R., Roche, D. M., Singarayer, J., Swingedouw, D., and Zhang, X.: Climatic impacts of fresh water hosing under Last Glacial Maximum conditions: a multi-model study, Climate of the Past, 9, 935–953, doi:10.5194/cp-9-935-2013, 2013.

Kavanaugh, J. L., Cuffey, K. M., Morse, D. L., Conway, H., and Rignot, E.: Dynamics and mass balance of Taylor Glacier, Antarctica: 1. Geometry and surface velocities, Journal Of Geophysical Research: Earth Surface, 114, F04 010, doi:10.1029/2009JF001309, 2009.

Kawamura, K., Severinghaus, J. P., Ishidoya, S., Sugawara, S., Hashida, G., Motoyama, H., Fujii, Y., Aoki, S., and Nakazawa, T.: Convective mixing of air in firn at four polar sites, Earth and Planetary Science Letters, 244, 672–682, doi:10.1016/j.epsl.2006.02.017, 2006.

Kawamura, K., Severinghaus, J. P., Albert, M. R., Courville, Z. R., Fahnestock, M. A., Scambos, T., Shields, E., and Shuman, C. A.: Kinetic fractionation of gases by deep air convection in polar firn, Atmospheric Chemistry and Physics, 13, 11 141–11 155, doi:10.5194/acp-13-11141-2013, 2013.

Lambert, F., Delmonte, B., Petit, J. R., Bigler, M., Kaufmann, P. R., Hutterli,

M. A., Stocker, T. F., Ruth, U., Steffensen, J. P., and Maggi, V.: Dust-climate couplings over the past 800,000 years from the EPICA Dome C ice core, Nature, 452, 616–619, doi:10.1038/nature06763, 2008.

Landais, A., Barnola, J., Kawamura, K., Caillon, N., Delmotte, M., Ommen, T. V., Dreyfus, G., Jouzel, J., Masson-Delmotte, V., Minster, B., Freitag, J., Leuenberger, M., Schwander, J., Huber, C., Etheridge, D., and Morgan, V.: Firn-air δ^{15}N in modern polar sites and glacial-interglacial ice: a model-data mismatch during glacial periods in Antarctica?, Quaternary Science Reviews, 25, 49–62, doi:10.1016/j.quascirev.2005.06.007, 2006.

Lourantou, A., Lavric, J. V., Köhler, P., Barnola, J.-M., Paillard, D., Michel, E., Raynaud, D., and Chappellaz, J.: Constraint of the CO_2 rise by new atmospheric carbon isotopic measurements during the last deglaciation, Global Biogeochemical Cycles, 24, GB2015, doi:10.1029/2009GB003545, 2010.

Lunt, D. J. and Valdes, P. J.: Dust transport to Dome C, Antarctica, at the Last Glacial Maximum and present day, Geophysical Research Letters, 28, 295–298, doi:10.1029/2000GL012170, 2001.

Mahowald, N., Kohfeld, K., Hansson, M., Balkanski, Y., Harrison, S. P., Prentice, I. C., Schulz, M., and Rodhe, H.: Dust sources and deposition during the last glacial maximum and current climate: A comparison of model results with paleodata from ice cores and marine sediments, Journal of Geophysical Research: Atmospheres, 104, 15 895–15 916, doi:10.1029/1999JD900084, 1999.

Marcott, S. A., Bauska, T. K., Buizert, C., Steig, E. J., Rosen, J. L., Cuffey, K. M., Fudge, T. J., Severinghaus, J. P., Ahn, J., Kalk, M. L., McConnell, J. R., Sowers, T., Taylor, K. C., White, J. W. C., and Brook, E. J.: Centennial-scale changes in the global carbon cycle during the last deglaciation, Nature, 514, 616–619, doi:10.1038/nature13799, 2014.

Maselli, O. J., Fritzsche, D., Layman, L., McConnell, J. R., and Meyer, H.: Comparison of water isotope-ratio determinations using two cavity ring-down instruments and classical mass spectrometry in continuous ice-core analysis, Isotopes in Environmental and Health Studies, 49, 387–398, doi:10.1080/10256016.2013.781598, pMID: 23713832, 2013.

Masson-Delmotte, V., Buiron, D., Ekaykin, A., Frezzotti, M., Gallée, H., Jouzel, J., Krinner, G., Landais, A., Motoyama, H., Oerter, H., Pol, K., Pollard, D., Ritz, C., Schlosser, E., Sime, L. C., Sodemann, H., Stenni, B., Uemura, R., and Vimeux, F.: A comparison of the present and last interglacial periods in six Antarctic ice cores, Climate of the Past, 7, 397–423, doi:10.5194/cp-7-397-2011, 2011.

McConnell, J., Dunbar, N., Köhler, P., Thomas, J., Adkins, J., Baggenstos, D., Brook, E., Buizert, C., Burke, A., Chellman, N., Cole-Dai, J.and Fleet, L., Fudge, T., Knorr, G., Grieman, M., Layman, L., Marcott, S., Maselli, O., McGwire, K., Mulvaney, R., Paris, G., Pasteris, D., Rhodes, R., Saltzman, E., Severinghaus, J., Sigl, M., Steffensen, J., Taylor, K., and Winckler, G.: Accelerated deglaciation linked to ozone depletion from volcanic eruptions 17.8k years ago, submitted to Science, 2015.

McConnell, J. R., Lamorey, G. W., Lambert, S. W., and Taylor, K. C.: Continuous Ice-Core Chemical Analyses Using Inductively Coupled Plasma Mass Spectrometry, Environmental Science & Technology, 36, 7–11, doi:10.1021/es011088z, pMID: 11811493, 2002.

McConnell, J. R., Aristarain, A. J., Banta, J. R., Edwards, P. R., and Simões, J. C.: 20th-Century doubling in dust archived in an Antarctic Peninsula ice core parallels climate change and desertification in South America, Proceedings of the National Academy of Sciences, 104, 5743–5748, doi:10.1073/pnas.0607657104, 2007.

McManus, J. F., Francois, R., Gherardi, J. M., Keigwin, L. D., and Brown-Leger, S.: Collapse and rapid resumption of Atlantic meridional circulation linked to deglacial climate changes, Nature, 428, 834–837, doi:10.1038/nature02494, 2004.

Menviel, L., Timmermann, A., Timm, O. E., and Mouchet, A.: Deconstructing the Last Glacial termination: the role of millennial and orbital-scale forcings, Quaternary Science Reviews, 30, 1155–1172, doi:10.1016/j.quascirev.2011.02.005, 2011.

Monnin, E., Steig, E. J., Siegenthaler, U., Kawamura, K., Schwander, J., Stauffer, B., Stocker, T. F., Morse, D. L., Barnola, J.-M., Bellier, B., Raynaud, D., and Fischer, H.: Evidence for substantial accumulation rate variability in Antarctica during the Holocene, through synchronization of CO_2 in the Taylor Dome, Dome C and DML ice cores, Earth and Planetary Science Letters, 224, 45–54, doi:10.1016/j.epsl.2004.05.007, 2004.

Morgan, V., Delmotte, M., van Ommen, T., Jouzel, J., Chappellaz, J., Woon, S., Masson-Delmotte, V., and Raynaud, D.: Relative timing of deglacial climate events in Antarctica and Greenland, Science, 297, 1862–1864, doi:10.1126/science.1074257, 2002.

Morse, D. L., Waddington, E. D., and Steig, E. J.: Ice age storm trajectories inferred from radar stratigraphy at Taylor Dome, Antarctica, Geophysical Research Letters, 25, 3383–3386, doi:10.1029/98GL52486, 1998.

Morse, D. L., Waddington, E. D., Marshall, H.-P., Neumann, T. A., Steig, E. J.,

Dibb, J. E., Winebrenner, D. P., and Arthern, R. J.: Accumulation Rate Measurements at Taylor Dome, East Antarctica: Techniques and Strategies for Mass Balance Measurements in Polar Environments, Geografiska Annaler: Series A, Physical Geography, 81, 683–694, doi:10.1111/1468-0459.00106, 1999.

Morse, D. L., Waddington, E. D., and Rasmussen, L. A.: Ice deformation in the vicinity of the ice-core site at Taylor Dome, Antarctica, and a derived accumulation rate history, Journal of Glaciology, 53, 449–460, doi:10.3189/002214307783258530, 2007.

Mulvaney, R., Röthlisberger, R., Wolff, E. W., Sommer, S., Schwander, J., Hutteli, M. A., and Jouzel, J.: The transition from the last glacial period in inland and near-coastal Antarctica, Geophysical Research Letters, 27, 2673–2676, doi:10.1029/1999GL011254, 2000.

Neumann, T., Waddington, E., Steig, E., and Grootes, P.: Non-climate influences on stable isotopes at Taylor Mouth, Antarctica, Journal of Glaciology, 51, 248–258, doi:10.3189/172756505781829331, 2005.

Pedro, J. B., van Ommen, T. D., Rasmussen, S. O., Morgan, V. I., Chappellaz, J., Moy, A. D., Masson-Delmotte, V., and Delmotte, M.: The last deglaciation: timing the bipolar seesaw, Climate of the Past, 7, 671–683, doi:10.5194/cp-7-671-2011, 2011.

Petrenko, V. V., Smith, A. M., Brook, E. J., Lowe, D., Riedel, K., Brailsford, G., Hua, Q., Schaefer, H., Reeh, N., Weiss, R. F., Etheridge, D., and Severinghaus, J. P.: $^{14}CH_4$ Measurements in Greenland Ice: Investigating Last Glacial Termination CH_4 Sources, Science, 324, 506–508, doi:10.1126/science.1168909, 2009.

Reeh, N., Oerter, H., Letréguilly, A., Miller, H., and Hubberten, H.-W.: A new, detailed ice-age oxygen-18 record from the ice-sheet margin in central West Greenland, Global and Planetary Change, 4, 373–383, doi:10.1016/0921-8181(91)90003-F, 1991.

Ruth, U., Barbante, C., Bigler, M., Delmonte, B., Fischer, H., Gabrielli, P., Gaspari, V., Kaufmann, P., Lambert, F., Maggi, V., Marino, F., Petit, J.-R., Udisti, R., Wagenbach, D., Wegner, A., and Wolff, E. W.: Proxies and Measurement Techniques for Mineral Dust in Antarctic Ice Cores, Environmental Science & Technology, 42, 5675–5681, doi:10.1021/es703078z, pMID: 18754492, 2008.

Schoenemann, S. W., Steig, E. J., Ding, Q., Markle, B. R., and Schauer, A. J.: Triple water-isotopologue record from WAIS Divide, Antarctica: Controls on glacial-interglacial changes in $^{17}O_{excess}$ of precipitation, Journal of Geophysical Research: Atmospheres, 119, 8741–8763, doi:10.1002/2014JD021770, 2014.

Schüpbach, S., Federer, U., Kaufmann, P. R., Albani, S., Barbante, C., Stocker, T. F., and Fischer, H.: High-resolution mineral dust and sea ice proxy records from the Talos Dome ice core, Climate of the Past, 9, 2789–2807, doi:10.5194/cp-9-2789-2013, 2013.

Schwander, J., Stauffer, B., and Sigg, A.: Air mixing in firn and the age of the air at pore close-off, Annals of Glaciology, 10, 141–145, 1988.

Severinghaus, J. P., Sowers, T., Brook, E. J., Alley, R. B., and Bender, M. L.: Timing of abrupt climate change at the end of the Younger Dryas interval from thermally fractionated gases in polar ice, Nature, 391, 141–146, doi:10.1038/34346, 1998.

Severinghaus, J. P., Albert, M. R., Courville, Z. R., Fahnestock, M. A., Kawamura, K., Montzka, S. A., Mühle, J., Scambos, T. A., Shields, E., Shuman, C. A., Suwa, M., Tans, P., and Weiss, R. F.: Deep air convection in the firn at a zero-accumulation site, central Antarctica, Earth and Planetary Science Letters, 293, 359–367, doi:10.1016/j.epsl.2010.03.003, 2010.

Shakun, J. D., Clark, P. U., He, F., Marcott, S. A., Mix, A. C., Liu, Z., Otto-Bliesner, B., Schmittner, A., and Bard, E.: Global warming preceded by increasing carbon dioxide concentrations during the last deglaciation, Nature, 484, 49–54, doi:10.1038/nature10915, 2012.

Siddall, M., Milne, G. A., and Masson-Delmotte, V.: Uncertainties in elevation changes and their impact on Antarctic temperature records since the end of the last glacial period, Earth and Planetary Science Letters, 315-316, 12–23, doi:10.1016/j.epsl.2011.04.032, sea Level and Ice Sheet Evolution: A PALSEA Special Edition, 2012.

Smith, H. J., Fischer, H., Wahlen, M., Mastroianni, D., and Deck, B.: Dual modes of the carbon cycle since the Last Glacial Maximum, Nature, 400, 248–250, doi:10.1038/22291, 1999.

Sowers, T., Bender, M., and Raynaud, D.: Elemental and isotopic composition of occluded O_2 and N_2 in polar ice, Journal of Geophysical Research: Atmospheres, 94, 5137–5150, doi:10.1029/JD094iD04p05137, 1989.

Steig, E.: Beryllium-10 in the Taylor Dome Ice Core: Applications to Antarctic Glaciology and Paleoclimatology, Ph.D. thesis, University of Washington, 1996.

Steig, E. J., Brook, E. J., White, J. W. C., Sucher, C. M., Bender, M. L., Lehman, S. J., Morse, D. L., Waddington, E. D., and Clow, G. D.: Synchronous climate changes in Antarctica and the North Atlantic, Science, 282, 92–95, doi:10.1126/science.282.5386.92, 1998.

Steig, E. J., Morse, D. L., Waddington, E. D., Stuiver, M., Grootes, P. M., Mayewski, P. A., Twickler, M. S., and Whitlow, S. I.: Wisconsinan and Holocene climate history from an ice core at Taylor Dome, western Ross Embayment, Antarctica, Geografiska Annaler Series A-Physical Geography, 82A, 213–235, doi:10.1111/j.0435-3676.2000.00122.x, 2000.

Stenni, B., Buiron, D., Frezzotti, M., Albani, S., Barbante, C., Bard, E., Barnola, J. M., Baroni, M., Baumgartner, M., Bonazza, M., Capron, E., Castellano, E., Chappellaz, J., Delmonte, B., Falourd, S., Genoni, L., Iacumin, P., Jouzel, J., Kipfstuhl, S., Landais, A., Lemieux-Dudon, B., Maggi, V., Masson-Delmotte, V., Mazzola, C., Minster, B., Montagnat, M., Mulvaney, R., Narcisi, B., Oerter, H., Parrenin, F., Petit, J. R., Ritz, C., Scarchilli, C., Schilt, A., Schuepbach, S., Schwander, J., Selmo, E., Severi, M., Stocker, T. F., and Udisti, R.: Expression of the bipolar see-saw in Antarctic climate records during the last deglaciation, Nature Geoscience, 4, 46–49, doi:10.1038/ngeo1026, 2011.

Stocker, T. F. and Johnsen, S. J.: A minimum thermodynamic model for the bipolar seesaw, Paleoceanography, 18, 1087, doi:10.1029/2003PA000920, 2003.

Sucher, C. M.: Atmospheric gases in the Taylor Dome ice core: Implications for East Antarctic climate change, Master's thesis, University of Rhode Island, Narraganset, 1997.

Timmermann, A., Menviel, L., Okumura, Y., Schilla, A., Merkel, U., Timm, O., Hu, A., Otto-Bliesner, B., and Schulz, M.: Towards a quantitative understanding of millennial-scale Antarctic warming events, Quaternary Science Reviews, 29, 74–85, doi:10.1016/j.quascirev.2009.06.021, climate of the Last Million Years: New Insights from EPICA and Other Records, 2010.

Veres, D., Bazin, L., Landais, A., Toyé Mahamadou Kele, H., Lemieux-Dudon, B., Parrenin, F., Martinerie, P., Blayo, E., Blunier, T., Capron, E., Chappellaz, J., Rasmussen, S. O., Severi, M., Svensson, A., Vinther, B., and Wolff, E. W.: The Antarctic ice core chronology (AICC2012): an optimized multi-parameter and multi-site dating approach for the last 120 thousand years, Climate of the Past, 9, 1733–1748, doi:10.5194/cp-9-1733-2013, 2013.

Waddington, E., Steig, E., and Neumann, T.: Using characteristic times to assess whether stable isotopes in polar snow can be reversibly deposited, Annals of Glaciology, 35, 118–124, doi:10.3189/172756402781817004, International Symposium on Ice Cores and Climate, Kangerlussuaq, Greenland, Aug 19-23, 2001, 2002.

WAIS Divide Project Members: Onset of deglacial warming in West Antarctica driven by local orbital forcing, Nature, 500, 440–444, doi:10.1038/nature12376, 2013.

Wegner, A.: Sources and Transport Characteristics of Mineral Dust in Dronning Maud Land, Antarctica, Ph.D. thesis, Universität Bremen, 2008.

Wolff, E. W., Fischer, H., Fundel, F., Ruth, U., Twarloh, B., Littot, G. C., Mulvaney, R., Röthlisberger, R., de Angelis, M., Boutron, C. F., Hansson, M., Jonsell, U., Hutterli, M. A., Lambert, F., Kaufmann, P., Stauffer, B., Stocker, T. F., Steffensen, J. P., Bigler, M., Siggaard-Andersen, M. L., Udisti, R., Becagli, S., Castellano, E., Severi, M., Wagenbach, D., Barbante, C., Gabrielli, P., and Gaspari, V.: Southern Ocean sea-ice extent, productivity and iron flux over the past eight glacial cycles, Nature, 440, 491–496, doi:10.1038/nature04614, 2006.

Chapter 4

A second look at the Taylor Glacier ice stratigraphy using gas records

Abstract

Ice sheet margin sites, where ancient ice is exposed at the glacier surface, offer unique opportunities for paleo-studies of trace components requiring large sample volumes. Following previous work on Taylor Glacier, Antarctica, we use a combination of geochemical parameters measured in air occlusions (δ^{18}O of atmospheric oxygen, methane and carbon dioxide concentration) to date ice layers from specific climate intervals. We present results from six sampling lines and two deep cores. The data expand our understanding of the stratigraphy and three-dimensional structure of ice layers outcropping at Taylor Glacier. Sections containing ice from every distinct climatic interval of the last glacial cycle, including the Holocene, deglacial transition, Last Glacial Maximum, Marine Isotope Stage 3, 4, and 5, are identified. The age of the ice generally increases with distance along the flow axis, but at any point on the glacier the across flow age gradient is much larger.

4.1 Introduction

Paleoclimate reconstructions of the past 800,000 years have relied heavily on ice cores drilled deep into the polar ice sheets, both in Greenland and Antarctica (Andersen et al. (2004), Augustin et al. (2004)). One limitation of traditional deep ice core drilling is the very finite amount of core retrieved, setting restrictions on what kind of measurements can be performed. One remedy for this problem is replicate coring (Shturmakov et al. (2014)), which allows us to re-drill certain sections of the ice core that are of particular interest. Another solution is to turn to the margin of the great ice sheets, where ancient ice is found in large quantities (Reeh et al. (1991)). As snow continues to fall on top of an ice sheet, individual layers of ice get buried deeper and become thinner with time as a consequence of the overburden pressure. The thinning leads to ice flow towards the ice margin, where the ice will eventually melt or sublimate. It is to be expected that ice layers will acquire a deformation history through shearing and folding on their path through the ice sheet. The main challenge at ice margin sites is then to map the stratigraphy, identify the deformation patterns, and establish a chronology.

In Chapter 2 we presented data from two sampling lines, one parallel and one perpendicular to the glacier flow (called the along flow profile respectively the across flow transect). Here we introduce six more sampling lines as well as two deep cores to further our understanding of the surface age distribution and the associated deformation pattern. The methodology to date individual sections of ice is the same as in Chapter 2; we use a combination of globally well-mixed gases (methane and molecular oxygen) for gas synchronization (Petrenko et al. (2006), Schaefer et al. (2009)). Both methane concentration and molecular oxygen isotopic composition ($\delta^{18}O_{atm}$) have varied in the past in response to changes in their sources and sinks (Bender et al. (1994b); Loulergue et al. (2008)). They both changed in broadly similar ways, but the timing of these changes is different, with $\delta^{18}O_{atm}$ lagging behind methane by several thousand years. Therefore the relationship of $\delta^{18}O_{atm}$ and methane is not linear and varies with time. This time dependency allows us to date ice of unknown age by matching it to well-dated gas records from deep ice cores (Figure 2.4 and 2.7). Another way to visualize

the evolution of methane concentrations and $\delta^{18}O_{atm}$ through time is via a phase diagram (Figure 4.1). Interglacials (Holocene, MIS 5e) are characterized by high methane and low $\delta^{18}O_{atm}$. In contrast, the Last Glacial Maximum (LGM) is distinguished by very low methane and high $\delta^{18}O_{atm}$. MIS 3 has $\delta^{18}O_{atm}$ of 0.2 ‰ to 0.5 ‰ but widely varying methane values. MIS 4 also is marked by a narrow band of $\delta^{18}O_{atm}$ (0.6 ‰ to 0.75 ‰) and large variations in methane. Finally, MIS 5a to 5d covers a large area in the phase plot with no distinctive value for either $\delta^{18}O_{atm}$ or methane, which makes this time interval generally difficult to date.

4.2 Sampling procedures and transects

All sampling locations are shown in Figure 4.2. We collected samples covering most of the ablation zone of Taylor Glacier, from 1120 m elevation above sea level (ASL) on the upstream end, to 160 m ASL near the terminus, over a distance of approximately 40 km (with an average topographical slope of 1.4°). The sampling was confined to a relatively narrow band in the center of the glacier, because we expect this part to be less deformed than anything closer to the lateral margins, and therefore more useful and easier to interpret. Thermal contraction cracks, found everywhere on the glacier, were avoided to the extent possible. All locations were GPS registered with a hand-held unit. Samples from transects A, B, C, and F were collected in 2009/2010, E in 2010/2011, and D in 2013/2014. The exact sampling procedure was different for every profile/transect, so we describe each separately in the following paragraphs.

Along-flow profile A is an extension of the original along-flow profile from Chapter 2 and reaches almost to the equilibrium line of Taylor Glacier. Samples were collected from the near-surface ice with a gas powered chainsaw by cutting an upside-down pyramid into the surface which was then extracted from the glacier using an ice screw (Figure 4.3). A small sample of 50 to 100 grams was cut off the tip of the pyramid for analysis. Because of the shallow sampling depth (20 cm to 30 cm) most samples include cracks. A total of 37 samples were collected with 500 m spacing. 10 of these samples are overlapping the original along flow profile

to check if the shallow sampling depth has a significant effect on the data.

Across-flow transect B lies perpendicular to the along flow profile at 18.7 km distance from the terminus. Samples were collected from 2 m depth with a PICO shallow coring drill assisted with a Sidewinder electric power head after clearing the top 2 m with a Jiffy® ice auger. A total of 50 samples were collected spanning 490 meters with a constant spacing of 10 m.

Across-flow transect C is just downstream and parallel to the main across flow transect. Samples were again collected from the near-surface with a chainsaw as described for along-flow profile A. A total of 288 samples were collected over 615 m in mostly 2 m resolution. This transect crosses the Taylor-Ferrar suture and a small number of samples were collected on Ferrar ice.

Across flow transect D is located 4 km downstream of transect C. Samples were collected from 4.5 m to 5 m depth using the PICO/Sidewinder/Jiffy shallow coring technique. The length of the transect is 200 m, with 100 m to either side of the along flow profile. The sampling resolution varies from 10 m at the edges to 2 m in the center for a total of 43 samples.

Across flow transect E crosses the along flow profile at 4.5 km from the terminus at a spot where the along flow data suggested the presence of Eemian (the last interglacial) ice. Again, samples were collected from 4.5 m to 5 m depth using the electric assisted shallow drill. Eighty-nine samples were collected over 200 m (-100 m to 100 m, with 0 m being the intersection with the along flow profile), with a section (72.0 m to 95.5 m) that was sampled in 0.5 m resolution, whereas the remaining samples had a 5 m spacing. The data from this transect is already published in Buizert et al. (2014), but their implications for the stratigraphy are not discussed, which will be done in the following.

Along flow profile F is an extension of the original along flow profile, continuing for another 2.9 km towards the terminus in 100 m resolution. Samples were collected from the near-surface ice using a hand drill (Figure 4.3). 40 samples were collected from ∼30 cm depth. Of the 40 samples, 10 were replicates of 5 m depth along flow profile samples.

In addition to the horizontal sampling lines, we will present data from two

depth profiles: One located at -380 m on the original across flow transect (hereafter called the -380 m core), and one from 87 m on transect E (hereafter 87 m core). Both were drilled from the surface to a depth of 15 m (-380 m core) resp. 9 m (87 m core). 26 samples were collected from the -380 m core; 8 for the 87 m core.

Samples from shallower than 4 m depth, i.e. all of profile A, transect B, transect C, and profile F, were only analyzed for $\delta^{18}O_{atm}$ because it is far less susceptible to contamination than methane or CO_2 (cf. Section 2.3.1). Profiles D and E, as well as the deep cores were analyzed for methane in addition to $\delta^{18}O_{atm}$. The procedures for laboratory measurements of $\delta^{18}O_{atm}$ and methane are outlined in Petrenko et al. (2006) and Mitchell et al. (2011). The corrections are identical to the ones applied in Chapter 2, and described in detail in the methods section there. A small number of samples were also analyzed for CO_2 concentration. The method for measuring CO_2 from air bubbles trapped in ice is presented in Marcott et al. (2014).

4.3 Results and discussion

4.3.1 Extension of the along flow profile

We added two profiles of near-surface sampling (A and F) to either end of the original along flow profile (Figure 4.4). On the upper glacier, the agreement with the 4 m depth data is generally good, but two samples are depleted in the heavy isotopologue by 0.15 ‰ (at 22.5 km and 23.5 km), probably because of modern air contamination. Another possibility is that there is a large age gradient between 4 m depth and the surface such that these samples are closer in age to the sample immediately upstream, with which they are in good agreement. The new data from 30 km to 40 km indicate Holocene ages for this ice, as expected since this part of the glacier is relatively close to the equilibrium line. The data are a little too noisy to be able to determine if the record follows the trend from the minimum at 6 ka BP to modern day values (0 ‰ by definition).

On the downstream end, close to the terminus, the data are less well behaved. There appear to be large age differences both between the surface and 4 m

depth as well as for adjacent samples, as evidenced in the large sample to sample variability. Ice that outcrops close to the terminus was buried deep in the ice sheet and compressed more strongly than ice from further upstream. It is also to be expected that a substantial amount of folding is present. It is therefore not surprising to see large variations in $\delta^{18}O_{atm}$ over short distances, and unfortunately it makes identifying individual climatic periods very difficult. The $\delta^{18}O_{atm}$ variability of -0.2 ‰ to 0.6 ‰ suggests that most of this ice could be 70 ka to 115 ka old (MIS 5a to 5d), but more high resolution sampling would be necessary to determine the exact age sequence.

4.3.2 Folding in transect B

In transect B we find three distinct maxima of $\delta^{18}O_{atm}$ at 1.1 ‰ (Figure 4.5). However, in the last 100,000 years there is only one point in time when $\delta^{18}O_{atm}$ was at 1.1 ‰, at 15 ka BP. This implies that all three maxima are in fact the same layer, and they are part of a syncline/anticline fold structure. This is confirmed by visual evidence in form of satellite imagery that also shows three distinct layers of similar color. $\delta^{18}O_{atm}$ decreases from 1.1 ‰ to 0.7 ‰ in all three instances, from the young side to the old side of the brown colored layer (i.e. from right to left in Figure 4.5 for the upright limbs, and left to right for the overturned limb). To determine the structure of the fold (whether it's an anticline/syncline pair or the opposite), one can follow the outcropping layers upstream or downstream until the fold axis becomes apparent (not shown). Our best guess estimate of the 2-D fold geometry is incorporated into Figure 4.5.

After accounting for the fold, the record is straightforward to interpret: At 0 m, $\delta^{18}O_{atm}$ is 0.8 ‰. It then increases to 1.1 ‰ over a short distance, before decreasing to 0.4 ‰ at 380 m. This $\delta^{18}O_{atm}$ sequence can be uniquely classified as 12 ka to ∼40 ka BP. It encompasses (from southeast to northwest) parts of MIS 3, the Last Glacial Maximum, and the beginning of the deglaciation.

4.3.3 Across flow transect C

Figure 4.6 shows $\delta^{18}O_{atm}$ measured on 288 near-surface samples in high spatial resolution. The data quality is clearly affected by the sampling depth. Modern air contamination adds noise of up to 0.2 ‰ to the record. It is still possible to deduce the large scale features of the stratigraphy with these data, but precise dating and identification of small amplitude features are not achievable.

Ice on the northwestern side, from -200 m to -100 m, is of LGM age with a distinct $\delta^{18}O_{atm}$ value of 1.0 ‰. $\delta^{18}O_{atm}$ then decreases to ∼0.4 ‰, which marks the beginning of MIS 3, at -50 m. The step in $\delta^{18}O_{atm}$ at 20 m indicates Antarctic Isotope Maximum (AIM) 12, or ∼46 ka BP (cf. Figure 2.4). Continuing along the transect, one would expect a sharp increase of $\delta^{18}O_{atm}$ into AIM 4. But the data show only a marginal increase to 0.4 ‰, which signifies an age reversal, and a return to late MIS 3 ice ages by 200 m transect distance. $\delta^{18}O_{atm}$ is then flat until the suture to the Ferrar ice is crossed (at 360 m). The satellite imagery also contains hints of an age reversal and the subsequent flattening of the stratigraphy as sharp, linear features on the northwest side get replaced with broad, sweeping structures associated with stratigraphical layers that outcrop at a very shallow angle.

4.3.4 Deep core -380 m finds MIS 4 at depth

In the -380 m core (Figure 4.7), $\delta^{18}O_{atm}$ ranges from 0.6 ‰ to 0.75 ‰, a spectrum of values indicative of MIS 4 (in principle it could also be of LGM or deglaciation age, but we can exclude those possibilities with CO_2 and methane). The agreement with $\delta^{18}O_{atm}$ and methane records from Siple Dome is striking, confirming our age assessment (Figure 4.7). There is a strong age gradient, 5,000 years in 10 m depth. This is consistent with the observation from the previous section that the stratigraphy in this area is relatively flat, and thus behaves more like a traditional ice core, with age increasing with depth.

4.3.5 Transect D captures MIS 5/4 transition

The interval from 100 m to 20 m in across-flow transect D is MIS 3 in age based on $\delta^{18}O_{atm}$ (Figure 4.8). Large variations in methane during this time are consistent with this age estimate, but methane as an age marker is non-unique and thus of reduced usefulness because numerous Dansgaard-Oeschger events (Dansgaard et al. (1993)) with associated changes in methane concentration are observed in the glacial period. Two $\delta^{18}O_{atm}$ data points around 0.6 ‰ at 10 m and 5 m give a hint of MIS 4 ice. From 0 m to -25 m $\delta^{18}O_{atm}$ decreases gradually to -0.1 ‰, marking the transition from MIS 4 to MIS 5a. Continuing in the transect, the most logical progression is MIS 5b from -40 m to -70 m and MIS 5c from -75 m to -100 m, although a fold and a repeat of MIS 5a cannot be excluded based on the data. Both MIS 4 and MIS 5a are quite compressed in this section, spanning roughly 10 m each. The data quality appears to be slightly worse than at other locations. This could be an artifact of a highly compressed section of ice sampled in too low resolution, or there could be small scale deformation in the form of folding that affects our record.

4.3.6 Penultimate deglaciation in ice near the terminus

The most outstanding feature in the gas records from transect E is the maximum of $\delta^{18}O_{atm}$ enrichment at 80 m. $\delta^{18}O_{atm}$ values of 1.1 ‰ are only found at deglacial transitions in the known record from the past 800,000 years (Landais et al. (2010)). In our case, only the last deglaciation (Termination I) and the penultimate deglaciation (Termination II) are viable candidates because the deepest part of the Taylor Dome ice core has been dated to ∼150 ka BP (Steig et al. (2000)), which makes it unlikely that there would be even older ice in Taylor Glacier. Buizert et al. (2014) dated a core from this location using Kr-81 to 120 ±20 ka BP, firmly establishing the age of this ice as Termination II.

From 80 m to 90 m $\delta^{18}O_{atm}$ decreases to -0.4 ‰, a typical value for the Eemian interglacial (MIS 5e). Continuing in this direction, the ice appears to get younger with a full sequence of MIS 5d, 5c, 5b, and 5a, although a number of more complex scenarios are also possible and cannot be rejected based on the

data. Towards the south side of 80 m, we observe an even more abrupt transition to interglacial $\delta^{18}O_{atm}$ values followed by a section of flat $\delta^{18}O_{atm}$ values from 45 m to 0 m. We have not been able to interpret this sequence in a useful fashion.

Finally, Figure 4.10 shows a depth core drilled at 87 m in transect E. $\delta^{18}O_{atm}$ and methane compare favourably to gas records from the EDML deep ice core. Here again, the fact that a high time resolution record can be obtained by drilling down into the ice surface suggests that the stratigraphy dips at a shallow angle at this location. However, unlike at the -380 m deep core site, the ice appears to get older with depth, implying that the stratigraphy here is upside down. The most plausible explanation is that the core drilled was located in the overturned part of a recumbent fold, a feature we have not observed anywhere else on the glacier.

4.3.7 Coherent deformation

The most obvious signs of deformation in the Taylor Glacier ice are the z-folds, best seen in the trace of the outcropping 'dusty band', and described in Chapter 2 and Section 4.3.2. The dusty band can be followed between the two z-folds in a straight line, suggesting only simple folding with relatively undisturbed stratigraphy. The elevation difference between transect B and transect C or the original across flow transect is approximately 150 m. This allows us a glimpse into the 3-D structure of the folding as evidenced by the 'dusty band' (Figure 4.11). The two syncline/anticline pairs appear to be minor folds in a limb of a larger underlying structure.

4.3.8 Age map

After identifying individual climate periods in transects and profiles at different locations on Taylor Glacier, we try to synthesize the established ages on a map (Figure 4.12). Tens of kilometers of Pleistocene ice are exposed at the surface, including ice from every climate period in the last 125,000 years. The stratigraphy becomes increasingly compressed with decreasing distance to the terminus. In all across glacier transects, age increases from northwest to southeast, perpendicular

to the flow direction (except in the overturned limbs of the folds). At the same time, there is also an age gradient in the along flow direction, from young ice near the equilibrium line, to old ice near the terminus, as one would expect. As already discussed in Chapter 2, we can offer no testable hypotheses to explain this age distribution.

In general, the stratigraphy is quite well behaved. Even though large scale folds have been identified, they do not complicate the stratigraphy inordinately, and do not in any way diminish the usefulness of Taylor Glacier as an archive of ancient ice. Only at the Eemian transect, close to the terminus, did we encounter a record that was not interpretable with our gas dating method. Therefore, it is possible to interpolate with confidence between ice of identical age in adjacent transects to create a surface age map (Figure 4.12). Still, there are large areas of Taylor Glacier that we have not tried to date.

4.4 Conclusions

Following earlier work on the Taylor Glacier ablation zone, we use the same combination of gas tracers to confirm the initial stratigraphic interpretation and expand our dating approach to other areas of the glacier. We show that the Taylor Glacier ancient air archive contains ice from all climatic periods of the last glacial cycle. This work lays the foundation for further studies focusing on distinct climate intervals. A number of potential targets for future studies on paleo-atmospheric trace gases have been identified. A continuous sequence of the penultimate deglaciation and the MIS 5/4 transition are of particular interest because large quantities of ice from these periods are not available from deep ice cores.

Much remains to be understood about the processes that produce the folding and the stratigraphic pattern in general at Taylor Glacier. However, we have shown that the deformation is not prohibitively complicated and that our gas dating tools are well-suited to assess the completeness of the chrono-stratigraphic record. Volcanic ash layers, visible as sharp but continuous features in satellite

imagery, are a resource that has not yet been tapped into. If it is possible to identify a known eruption by chemical fingerprinting, a lot could be learned both about the glacier's deformation history but also about the volcanic eruption itself, thanks to large ice volumes available at Taylor Glacier.

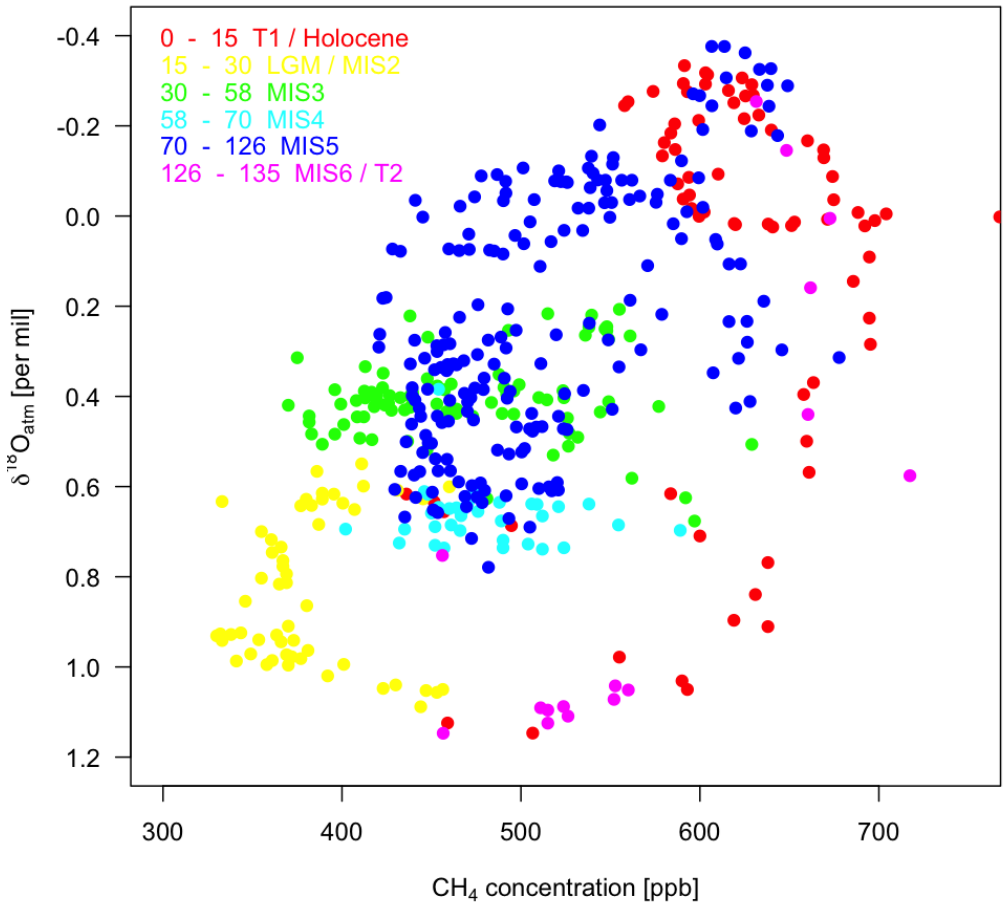

Figure 4.1: Phase diagram of methane and $\delta^{18}O_{atm}$ for the last 135,000 years. Points are colored according to age intervals. Data used for this plot are from the Siple Dome (0 ka to 50 ka, Brook et al. (2005), Severinghaus et al. (2009)), Greenland Ice Sheet Project 2 (50 ka to 70 ka, Bender et al. (1994a), Brook et al. (2000)), and EPICA Dronning Maud Land (70 ka to 125 ka, Capron et al. (2010)) ice cores. In order to keep the time resolution constant, all records were averaged into 200 year bins, which are shown as individual points in the plot.

Figure 4.2: Overview of the Taylor Glacier ablation zone with sampling locations. The along flow profile and across flow transect from Chapter 2 are shown in gray (cf. Figure 2.2). All across flow transects are registered with distance increasing to the northwest, with a (usually) arbitrary zero point. Landsat imagery courtesy of NASA Goddard Space Flight Center and US Geological Survey.

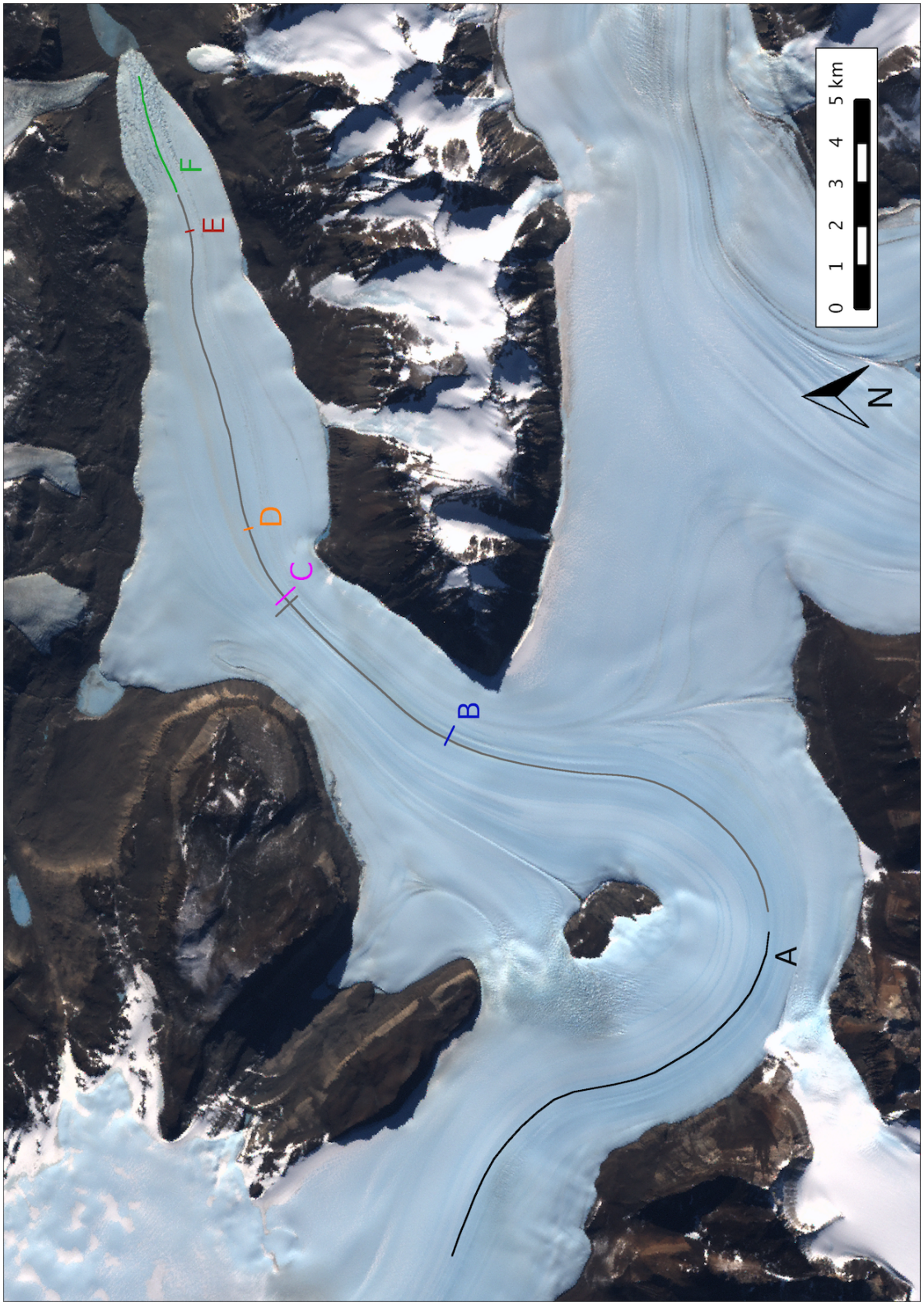
A
B
C
D
E
F
N
0 1 2 3 4 5 km

Figure 4.3: Impressions from sample collection. (top) Transect C after sampling, showing the inverted pyramids that were extracted for each sample. (center) Paul Rose using an electric chain saw to cut the aforementioned ice pyramids. (bottom) Hand-drilling a sample for profile F in between melt channels.

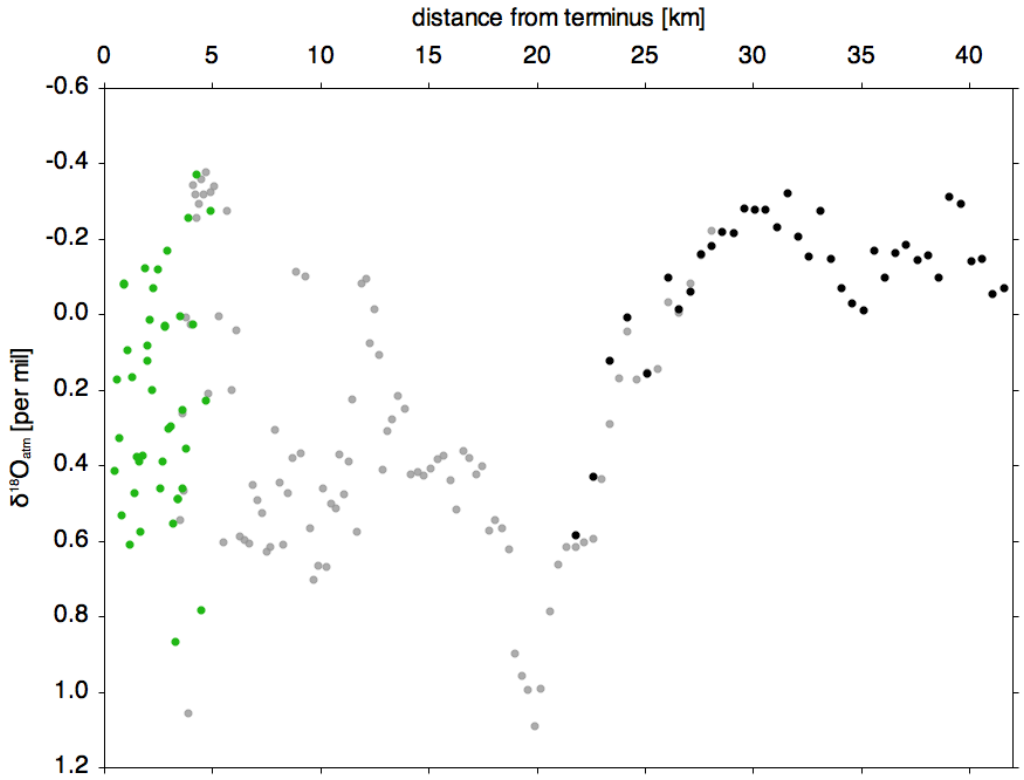

Figure 4.4: Extension of the along flow profile. Data from Chapter 2 are shown in gray. Shallow sampling profile A (black) and F (green) continue on both ends of the original profile. The agreement between near-surface samples and 4 m depth samples is good.

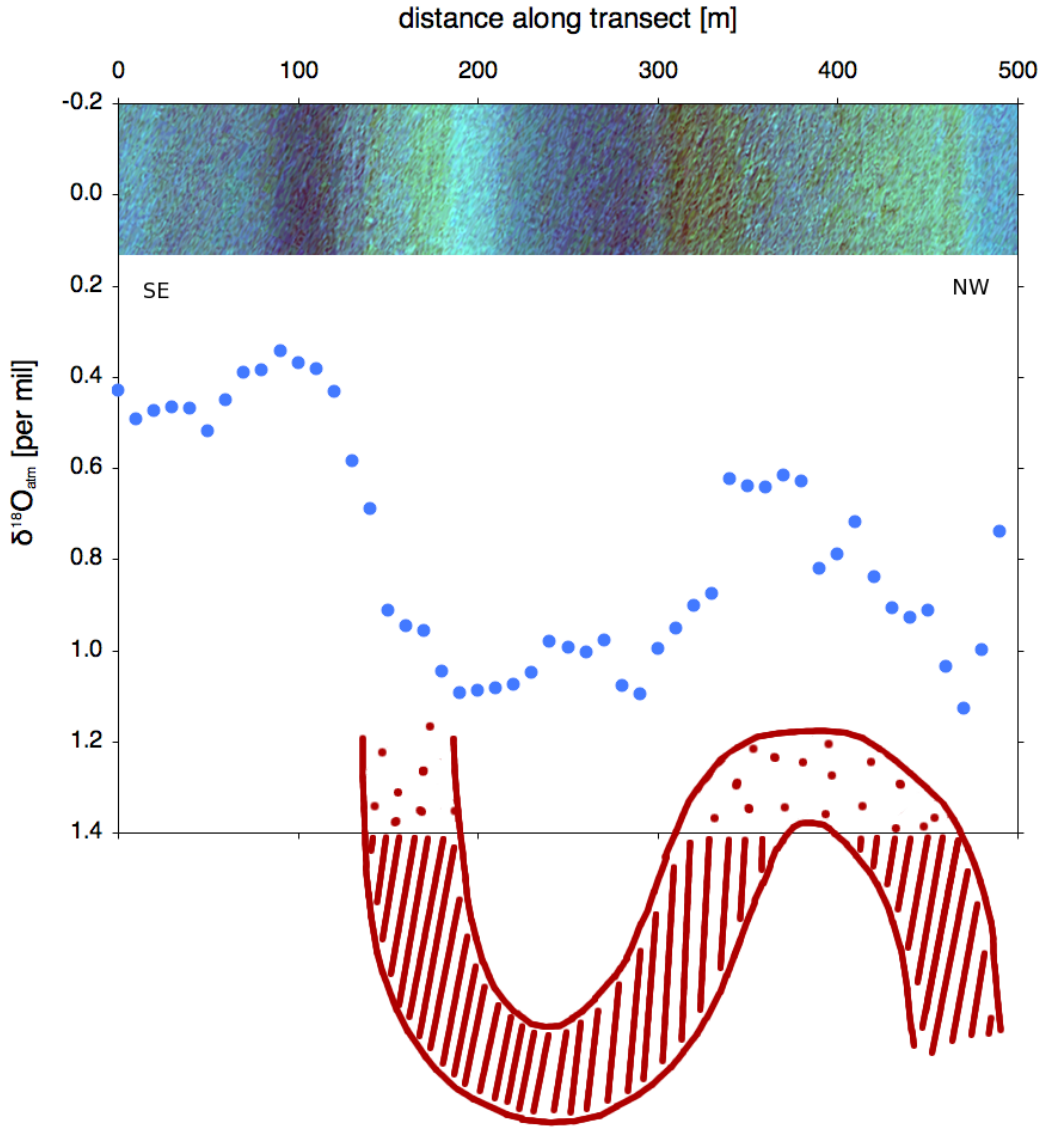

Figure 4.5: Transect B data, satellite imagery, and interpretation. Top shows a color enhanced satellite image of the transect B location, on the same distance registration as the gas data. Bottom shows our interpretation of the stratigraphy in the form of a cross-section through the glacier at the transect sampling line. The plot margin is used as the glacier surface. The along flow profile crosses this transect at 340 m and is dated at approximately 28 ka at the intersection of the two sampling lines. Satellite image courtesy of Google Earth (Google Earth (2015)).

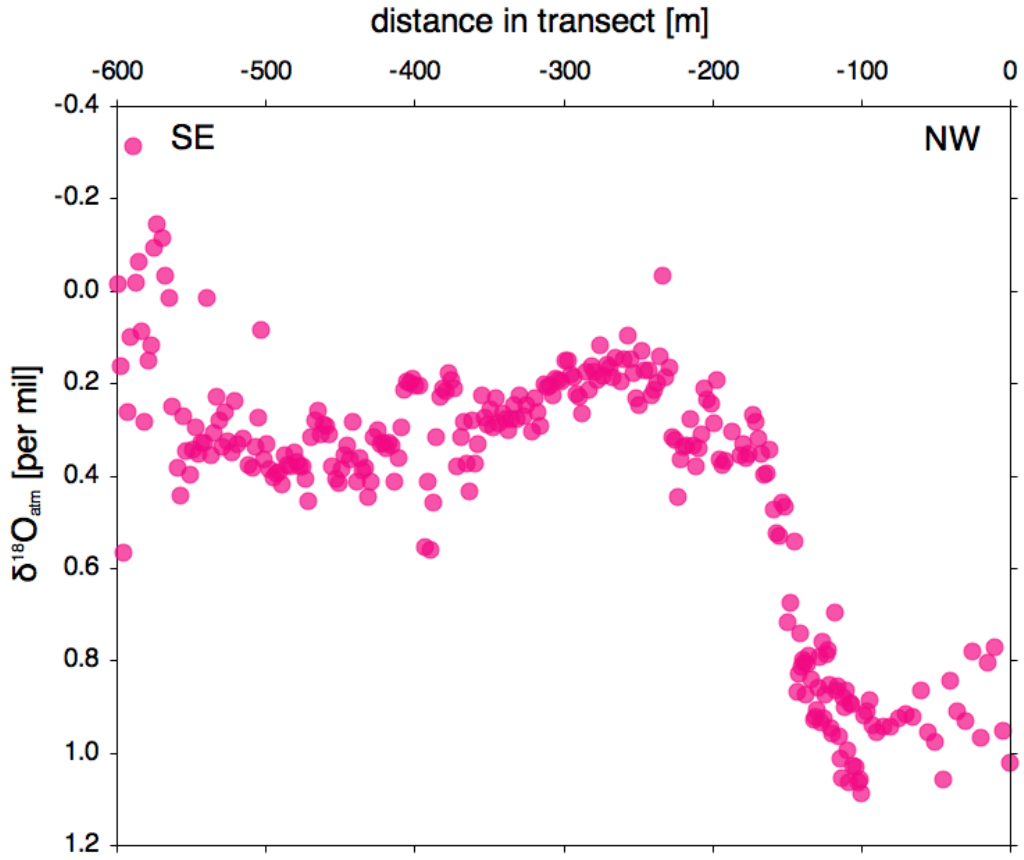

Figure 4.6: Across flow transect C data showing the deglacial transition. Data quality is clearly affected by proximity to surface of samples. The along flow profile crosses this transect at -260 m, and is dated to approximately 50 ka at the intersection. Measurements from -560 m to -600 m are from Ferrar ice.

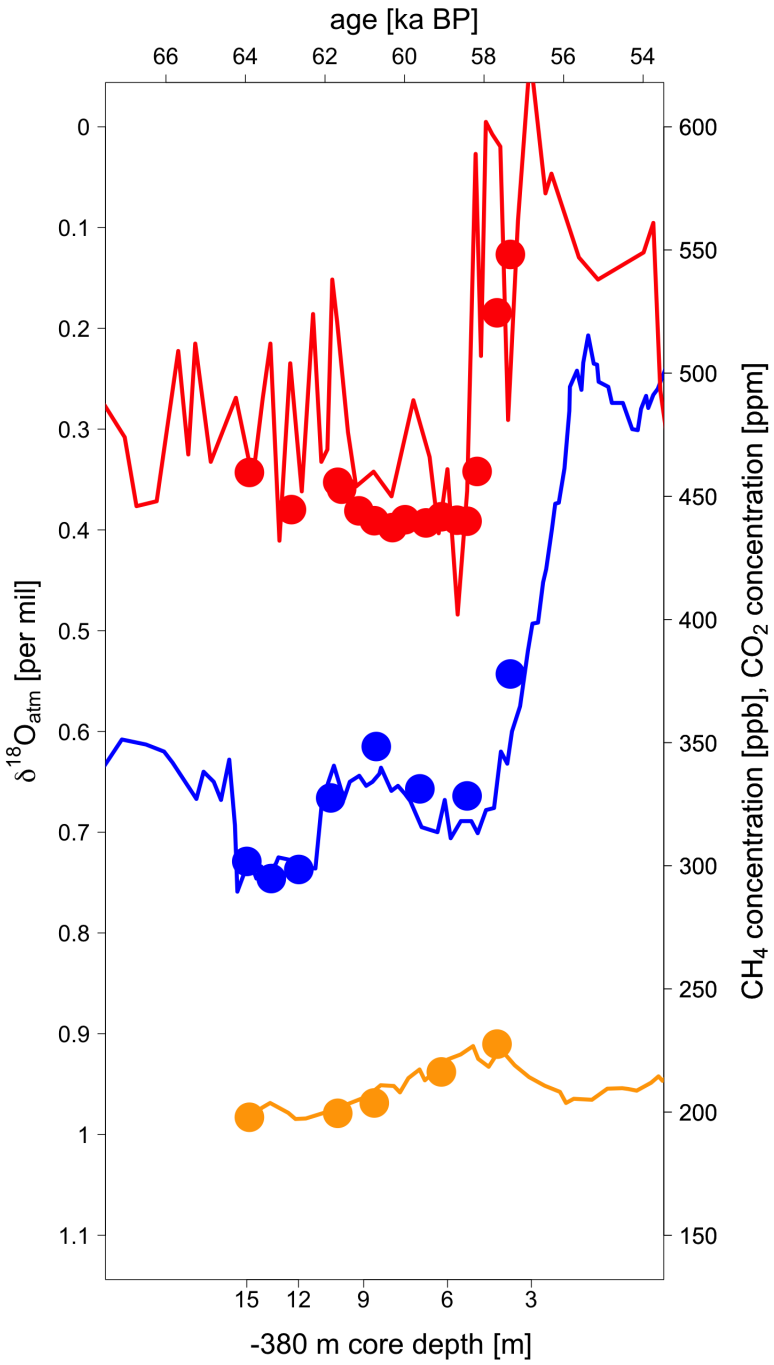

Figure 4.7: Gas data for the -380 m deep core. Methane (red), $\delta^{18}O_{atm}$ (blue), and CO_2 (orange) data are shown on the depth scale (solid dots). Deep ice core records of methane (red, Brook et al. (2000)), $\delta^{18}O_{atm}$ (blue, Severinghaus et al. (2009)), and CO_2 (orange, Lüthi et al. (2010)) are shown on an age scale for reference. The data are consistent with an age of 63 ka BP to 58 ka BP, which is the second half of MIS 4. Note that the -380 m core depth scale is compressed for depths deeper than 10 m.

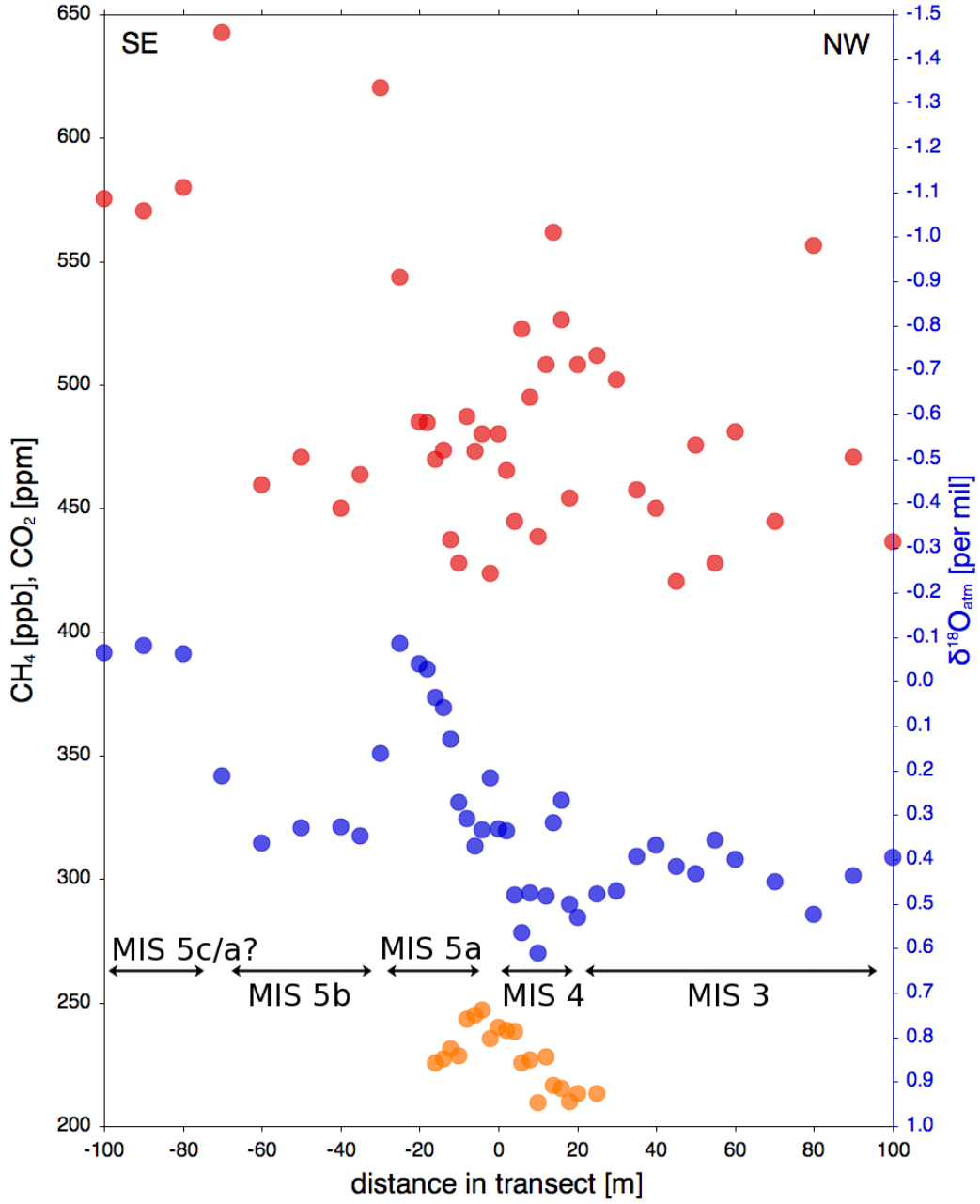

Figure 4.8: Gas data for across flow transect D. Methane (red), $\delta^{18}O_{atm}$ (blue) and CO_2 (orange) show a highly compressed sequence of MIS 3, 4, and 5. The along flow profile crosses this transect at 0 m.

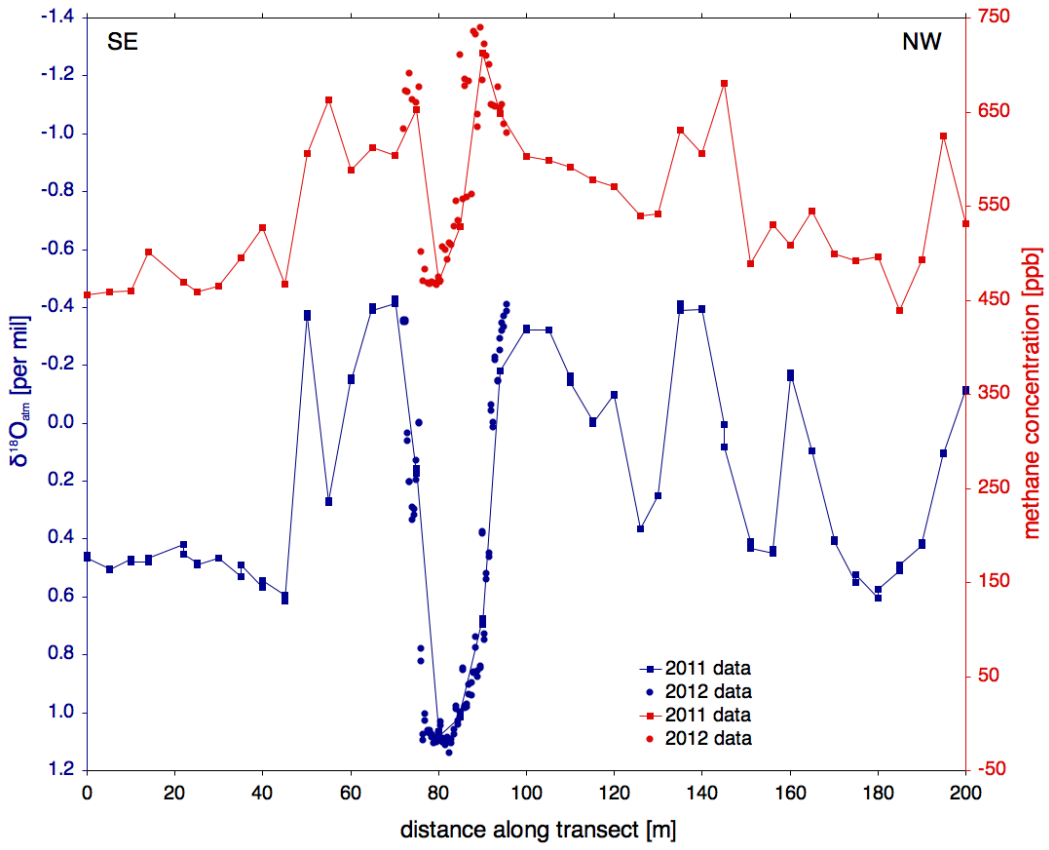

Figure 4.9: Gas data for the Eemian transect (transect E). Methane (red) and $\delta^{18}O_{atm}$ (blue) data are shown. The reproducibility of the low resolution (2011) and the high resolution (2012) data in the overlapping region is excellent. The along flow profile crosses this transect at 100 m. These data are already published in Buizert et al. (2014).

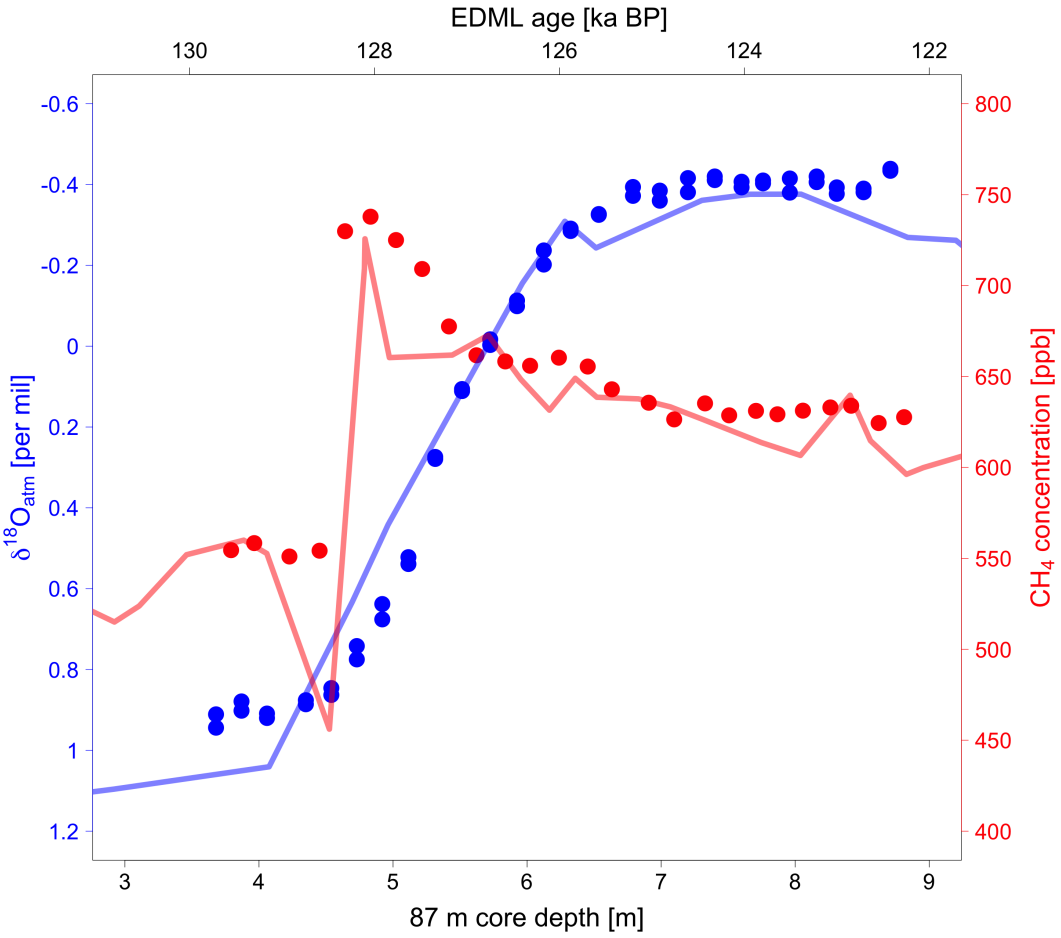

Figure 4.10: Deep core gas data from 87 m on the Eemian transect. Methane (red dots) and $\delta^{18}O_{atm}$ (blue dots) outline the penultimate deglaciation nicely with depth. The agreement with EDML gas records (Capron et al. (2010), Schilt et al. (2010)) is excellent. This core was drilled by our collaborator Hinrich Schaefer in the 2012/2013 season.

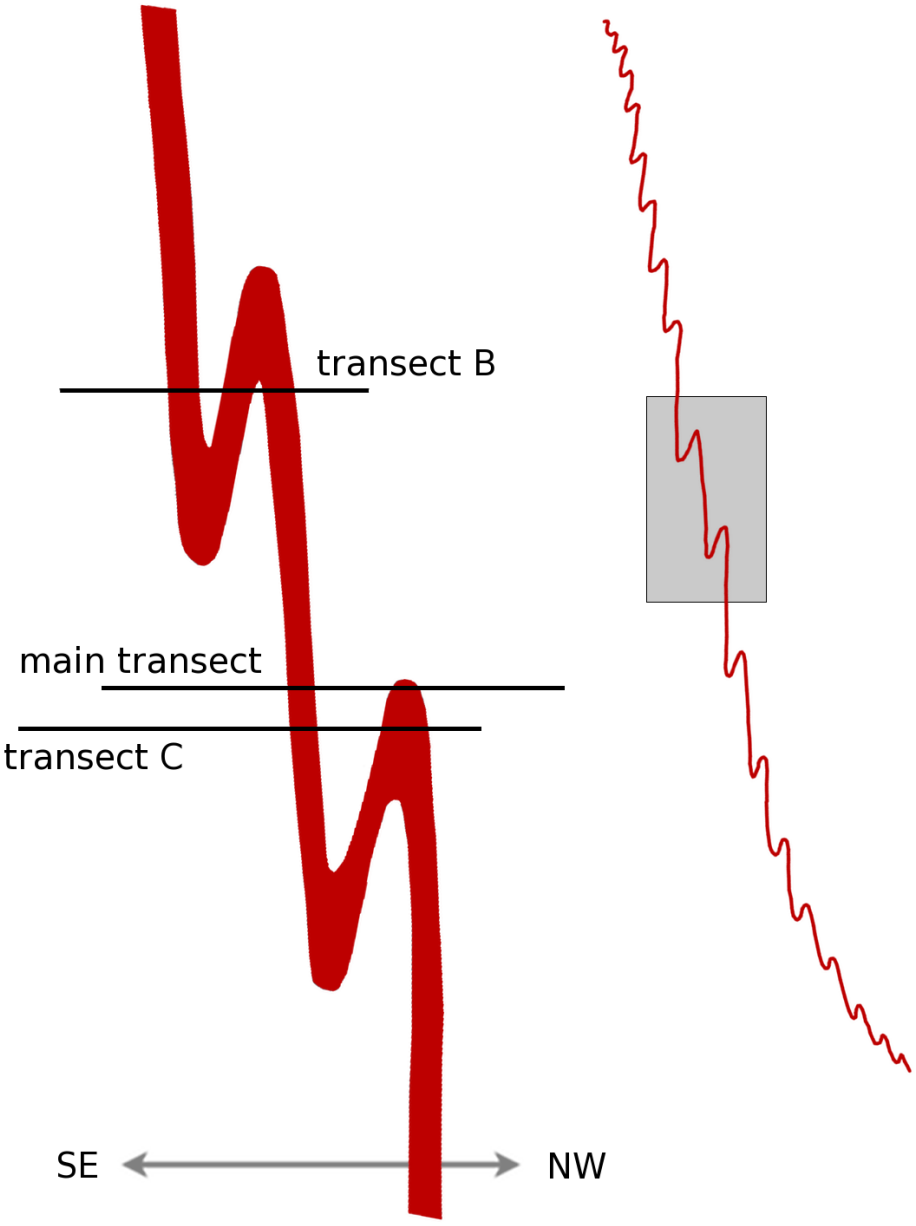

Figure 4.11: Sketch of a hypothetical cross-section through Taylor Glacier perpendicular to the flow direction highlighting the deformation in the dusty band. Across flow transects are indicated as black lines. (right) Interpretation of the two observed z-folds as minor folds in a larger deformation structure (Bell (1981), Hudleston and Treagus (2010)).

Figure 4.12: Age map of the outcropping ice on the Taylor Glacier surface. Established ages along sampling lines (solid lines) and a manual 'best guess' interpolation (semi-transparent colored area) are shown. Ice to the southeast of the black boundary is from Ferrar Glacier, and probably of Holocene age. Landsat imagery courtesy of NASA Goddard Space Flight Center and US Geological Survey.

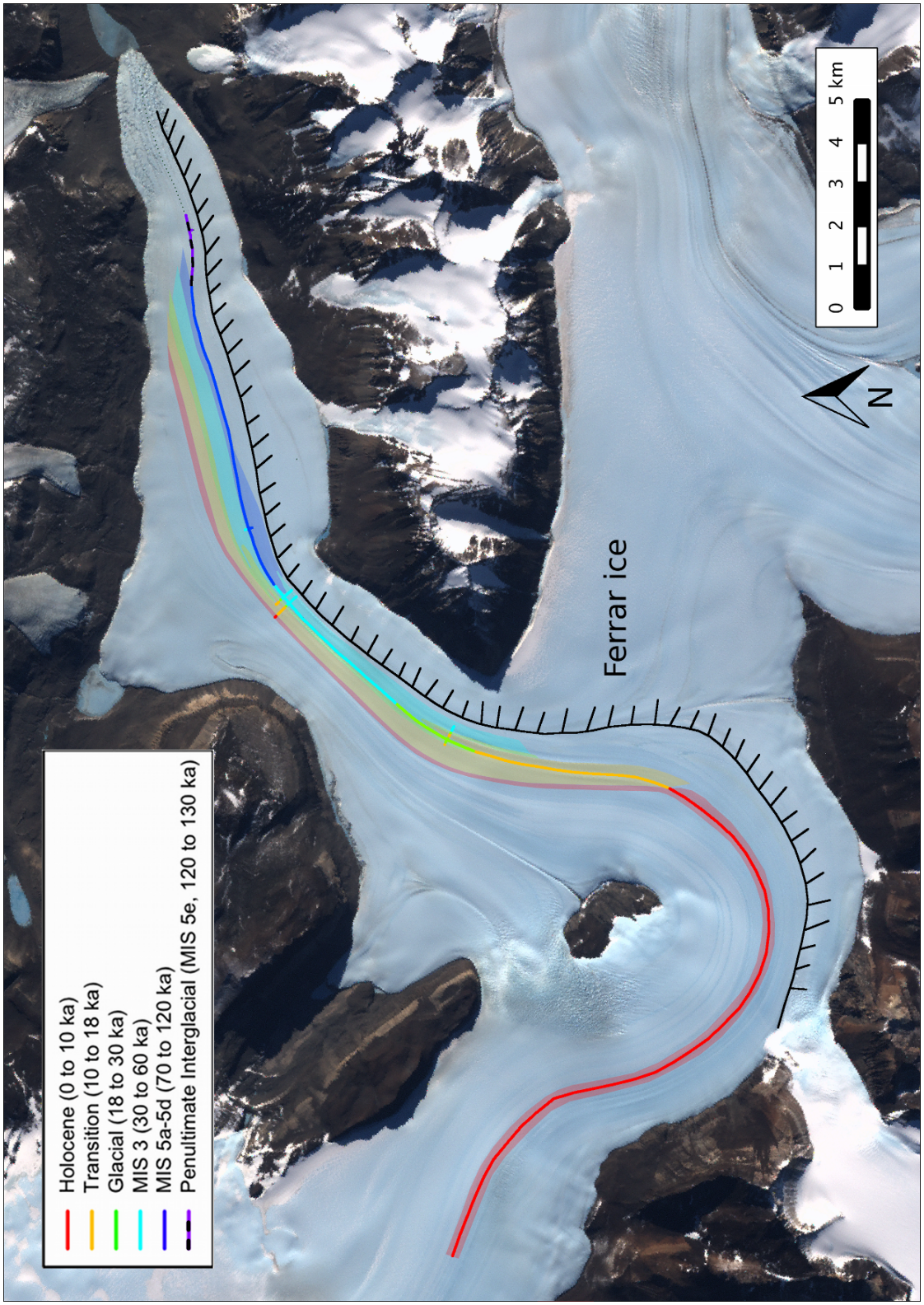
Holocene (0 to 10 ka)
Transition (10 to 18 ka)
Glacial (18 to 30 ka)
MIS 3 (30 to 60 ka)
MIS 5a-5d (70 to 120 ka)
Penultimate Interglacial (MIS 5e, 120 to 130 ka)
Ferrar ice
0 1 2 3 4 5 km
N

References

Andersen, K., Azuma, N., Barnola, J., Bigler, M., Biscaye, P., Caillon, N., Chappellaz, J., Clausen, H., DahlJensen, D., Fischer, H., Fluckiger, J., Fritzsche, D., Fujii, Y., Goto-Azuma, K., Gronvold, K., Gundestrup, N., Hansson, M., Huber, C., Hvidberg, C., Johnsen, S., Jonsell, U., Jouzel, J., Kipfstuhl, S., Landais, A., Leuenberger, M., Lorrain, R., Masson-Delmotte, V., Miller, H., Motoyama, H., Narita, H., Popp, T., Rasmussen, S., Raynaud, D., Röthlisberger, R., Ruth, U., Samyn, D., Schwander, J., Shoji, H., Siggard-Andersen, M., Steffensen, J., Stocker, T., Sveinbjornsdottir, A., Svensson, A., Takata, M., Tison, J., Thorsteinsson, T., Watanabe, O., Wilhelms, F., White, J., and Project, N. G. I. C.: High-resolution record of Northern Hemisphere climate extending into the last interglacial period, Nature, 431, 147–151, doi:10.1038/nature02805, 2004.

Augustin, L., Barbante, C., Barnes, P., Barnola, J., Bigler, M., Castellano, E., Cattani, O., Chappellaz, J., DahlJensen, D., Delmonte, B., Dreyfus, G., Durand, G., Falourd, S., Fischer, H., Flückiger, J., Hansson, M., Huybrechts, P., Jugie, R., Johnsen, S., Jouzel, J., Kaufmann, P., Kipfstuhl, J., Lambert, F., Lipenkov, V., Littot, G., Longinelli, A., Lorrain, R., Maggi, V., Masson-Delmotte, V., Miller, H., Mulvaney, R., Oerlemans, J., Oerter, H., Orombelli, G., Parrenin, F., Peel, D., Petit, J., Raynaud, D., Ritz, C., Ruth, U., Schwander, J., Siegenthaler, U., Souchez, R., Stauffer, B., Steffensen, J., Stenni, B., Stocker, T., Tabacco, I., Udisti, R., van de Wal, R., van den Broeke, M., Weiss, J., Wilhelms, F., Winther, J., Wolff, E., Zucchelli, M., and Members, E. C.: Eight glacial cycles from an Antarctic ice core, Nature, 429, 623–628, doi:10.1038/nature02599, 2004.

Bell, A.: Vergence: an evaluation, Journal of Structural Geology, 3, 197–202, doi:10.1016/0191-8141(81)90015-8, 1981.

Bender, M., Sowers, T., Dickson, M. L., Orchardo, J., Grootes, P., Mayewski, P. A., and Meese, D. A.: Climate Correlations Between Greenland And Antarctica During The Past 100,000 Years, Nature, 372, 663–666, doi:10.1038/372663a0, 1994a.

Bender, M., Sowers, T., and Labeyrie, L.: The Dole Effect And Its Variations During The Last 130,000 Years As Measured In The Vostok Ice Core, Global Biogeochemical Cycles, 8, 363–376, doi:10.1029/94GB00724, 1994b.

Brook, E. J., Harder, S., Severinghaus, J., Steig, E. J., and Sucher, C. M.: On the origin and timing of rapid changes in atmospheric methane during the last glacial period, Global Biogeochemical Cycles, 14, 559–572, doi:10.1029/1999GB001182, 2000.

Brook, E. J., White, J. W. C., Schilla, A. S. M., Bender, M. L., Barnett, B., Severinghaus, J. P., Taylor, K. C., Alley, R. B., and Steig, E. J.: Tim-

ing of millennial-scale climate change at Siple Dome, West Antarctica, during the last glacial period, Quaternary Science Reviews, 24, 1333–1343, doi: 10.1016/j.quascirev.2005.02.002, 2005.

Buizert, C., Baggenstos, D., Jiang, W., Purtschert, R., Petrenko, V. V., Lu, Z.-T., Müller, P., Kuhl, T., Lee, J., Severinghaus, J. P., and Brook, E. J.: Radiometric ^{81}Kr dating identifies 120,000-year-old ice at Taylor Glacier, Antarctica, Proceedings of the National Academy of Sciences, 111, 6876–6881, doi: 10.1073/pnas.1320329111, 2014.

Capron, E., Landais, A., Lemieux-Dudon, B., Schilt, A., Masson-Delmotte, V., Buiron, D., Chappellaz, J., Dahl-Jensen, D., Johnsen, S., Leuenberger, M., Loulergue, L., and Oerter, H.: Synchronising EDML and NorthGRIP ice cores using δ^{18}O of atmospheric oxygen ($\delta^{18}O_{atm}$) and CH_4 measurements over MIS5 (80–123 kyr), Quaternary Science Reviews, 29, 222–234, doi:10.1016/j.quascirev.2009.07.014, climate of the Last Million Years: New Insights from EPICA and Other Records, 2010.

Dansgaard, W., Johnsen, S. J., Clausen, H. B., Dahl-Jensen, D., Gundestrup, N. S., Hammer, C. U., Hvidberg, C. S., Steffensen, J. P., Sveinbjornsdottir, A. E., Jouzel, J., and Bond, G.: Evidence for general instability of past climate from a 250-kyr ice-core record, Nature, 364, 218–220, doi:10.1038/364218a0, 1993.

Google Earth: v7.1.2.2041. 11/14/2009. Taylor Glacier, Antarctica. -77.795°S, 161.590°E. DigitalGlobe 2015., http://www.earth.google.com, 2015.

Hudleston, P. J. and Treagus, S. H.: Information from folds: a review, Journal of Structural Geology, 32, 2042–2071, doi:10.1016/j.jsg.2010.08.011, Structural Diagenesis, 2010.

Landais, A., Dreyfus, G., Capron, E., Masson-Delmotte, V., Sanchez-Goñi, M., Desprat, S., Hoffmann, G., Jouzel, J., Leuenberger, M., and Johnsenca, S.: What drives the millennial and orbital variations of $\delta^{18}O_{atm}$?, Quaternary Science Reviews, 29, 235–246, doi:10.1016/j.quascirev.2009.07.005, climate of the Last Million Years: New Insights from EPICA and Other Records, 2010.

Loulergue, L., Schilt, A., Spahni, R., Masson-Delmotte, V., Blunier, T., Lemieux, B., Barnola, J.-M., Raynaud, D., Stocker, T. F., and Chappellaz, J.: Orbital and millennial-scale features of atmospheric CH_4 over the past 800,000 years, Nature, 453, 383–386, doi:10.1038/nature06950, 2008.

Lüthi, D., Bereiter, B., Stauffer, B., Winkler, R., Schwander, J., Kindler, P., Leuenberger, M., Kipfstuhl, S., Capron, E., Landais, A., Fischer, H., and Stocker, T. F.: CO_2 and O_2/N_2 variations in and just below the bubble–clathrate trans-

formation zone of Antarctic ice cores, Earth and Planetary Science Letters, 297, 226–233, doi:10.1016/j.epsl.2010.06.023, 2010.

Marcott, S. A., Bauska, T. K., Buizert, C., Steig, E. J., Rosen, J. L., Cuffey, K. M., Fudge, T. J., Severinghaus, J. P., Ahn, J., Kalk, M. L., McConnell, J. R., Sowers, T., Taylor, K. C., White, J. W. C., and Brook, E. J.: Centennial-scale changes in the global carbon cycle during the last deglaciation, Nature, 514, 616–619, doi:10.1038/nature13799, 2014.

Mitchell, L. E., Brook, E. J., Sowers, T., McConnell, J. R., and Taylor, K.: Multidecadal variability of atmospheric methane, 1000-1800 C.E., Journal of Geophysical Research: Biogeosciences, 116, G02 007, doi:10.1029/2010JG001441, 2011.

Petrenko, V., Severinghaus, J., Brook, E., Reeh, N., and Schaefer, H.: Gas records from the West Greenland ice margin covering the Last Glacial Termination: a horizontal ice core, Quaternary Science Reviews, 25, 865–875, doi:10.1016/j.quascirev.2005.09.005, 2006.

Reeh, N., Oerter, H., Letréguilly, A., Miller, H., and Hubberten, H.-W.: A new, detailed ice-age oxygen-18 record from the ice-sheet margin in central West Greenland, Global and Planetary Change, 4, 373–383, doi:10.1016/0921-8181(91)90003-F, 1991.

Schaefer, H., Petrenko, V., Brook, E., Severinghaus, J., Reeh, N., Melton, J., and Mitchell, L.: Ice stratigraphy at the Pakitsoq ice margin, West Greenland, derived from gas records, Journal of Glaciology, 55, 411–421, doi:10.3189/002214309788816704, 2009.

Schilt, A., Baumgartner, M., Schwander, J., Buiron, D., Capron, E., Chappellaz, J., Loulergue, L., Schüpbach, S., Spahni, R., Fischer, H., and Stocker, T. F.: Atmospheric nitrous oxide during the last 140,000 years, Earth and Planetary Science Letters, 300, 33–43, doi:10.1016/j.epsl.2010.09.027, 2010.

Severinghaus, J. P., Beaudette, R., Headly, M. A., Taylor, K., and Brook, E. J.: Oxygen-18 of O_2 Records the Impact of Abrupt Climate Change on the Terrestrial Biosphere, Science, 324, 1431–1434, doi:10.1126/science.1169473, 2009.

Shturmakov, A. J., Lebar, D. A., and Bentley, C. R.: DISC drill and replicate coring system: a new era in deep ice drilling engineering, Annals Of Glaciology, 55, 189–198, doi:10.3189/2014AoG68A017, 2014.

Steig, E. J., Morse, D. L., Waddington, E. D., Stuiver, M., Grootes, P. M., Mayewski, P. A., Twickler, M. S., and Whitlow, S. I.: Wisconsinan and Holocene climate history from an ice core at Taylor Dome, western Ross Embayment, Antarctica, Geografiska Annaler Series A-Physical Geography, 82A, 213–235, doi:10.1111/j.0435-3676.2000.00122.x, 2000.

Chapter 5

Measurements of inert gas isotopes for estimation of possible convective zone

5.1 Introduction

A long standing problem in ice core science concerns the mismatch between modeled $^{29}N_2/^{28}N_2$ (called $\delta^{15}N$) and measured $\delta^{15}N$ for East Antarctic ice cores during the last glacial period (Landais et al. (2006)). The discrepancy casts a shadow of doubt over many studies looking at the timing of greenhouse gas changes and related climate change based on data from Antarctic ice cores. Firn densification models (e.g. Herron and Langway (1980), Goujon et al. (2003)) use inputs of temperature and accumulation rate to estimate the thickness of the firn column. The firn column also provides a domain in which diffusion is the dominant form of gas movement, allowing atmospheric gases to un-mix in a diffusive equilibrium between the base of the firn and the overlying atmosphere (Schwander et al. (1988), Sowers et al. (1989)). The main force driving this fractionation is gravity. This process is manifested in an enrichment of heavy isotopes at the base of the firn, where gases are trapped in bubbles and the fractionation signal is thus preserved in the ice. The enrichment in the heavy isotopologue of nitrogen, $\delta^{15}N$,

is commonly used as a proxy for firn thickness, since the amount of enrichment is nearly linearly related to the height of the firn column (Sowers et al. (1992), Rasmussen et al. (2013), Buizert et al. (2015)).

δ^{15}N has been measured extensively in the air trapped in ice cores from Greenland (e.g. Schwander et al. (1997), Severinghaus and Brook (1999)) and Antarctica (e.g. Caillon et al. (2003), Capron et al. (2013)). Firn densification models have been able to reproduce the measured δ^{15}N for ice cores in Greenland and coastal Antarctica using reconstructed temperature and accumulation histories (Landais et al. (2006)). However, for ice cores from East Antarctica (such as Vostok, Dome F, or Dome C), such a data-model agreement during the last glacial period has been elusive. Two solutions for this discrepancy have been proposed, one concerning the densification physics, and one the validity of δ^{15}N as a direct proxy for firn thickness in low accumulation periods. The former is based on the observation that the correlation between calcium concentration and firn density increases with depth in modern firn profiles, implying that impurities may have a significant impact on the densification process (Hörhold et al. (2012)). The last glacial period was substantially dustier than today, possibly enhancing densification, which may explain why firn models were not able to produce a firn that was consistent with independent constraints on firn thickness. Freitag et al. (2013) implemented the impurity effect into a model with good results, however, Capron et al. (2013) could not find any evidence that impurity content and δ^{15}N discrepancy were correlated in several East Antarctic ice cores. Still, other studies have confirmed that densification models overestimate Δage for low accumulation sites (Loulergue et al. (2007)).

The second possible explanation for the δ^{15}N model-data mismatch is that δ^{15}N underestimates the actual firn thickness because of a substantial convective zone at the top of the firn column (Kawamura et al. (2006), Severinghaus et al. (2010)). Deep convection, enabled by large ice grains or even cracks typically formed by intense metamorphosis at low accumulation sites, prevents isotopic fractionation by turbulent mixing. Because the last glacial period in East Antarctica was characterized by very low accumulation, it is conceivable that large convective

zones masked the true thickness of the firn layer. To test this theory, Kawamura et al. (2013) developed a new proxy indicator of past convection in firn. Using isotopes of xenon, krypton, argon, and nitrogen, they show that convective mixing leads to a kinetic fractionation signal that should be measurable in ice core samples.

In Chapter 2 we identified a period of extremely low accumulation and anomalously low δ^{15}N in the Taylor Dome ice core, which is also observed (albeit to a slightly lesser degree) in the Taylor Glacier ice, providing an ideal test for the method proposed by Kawamura et al. (2013). In this chapter, we present new measurements of the isotopes of all major noble gases and nitrogen, including the first ever measurements of xenon isotopes of occluded gas in ice, to examine if a signal of the kinetic fractionation effect can be detected.

5.1.1 Gas fractionation in the firn

Diffusive separation of the isotopes is possible in the stagnant layer of air in porous firn by the following processes: (1) Gravitational settling causes heavier isotopes to be enriched at the bottom of the firn, as predicted by the barometric equation for a pair of gases (Craig et al. (1988), Sowers et al. (1989)): $\delta = [e^{\Delta mgz_d/(RT)} - 1] \cdot 10^3‰ \cong \Delta mgz_d/(RT) \cdot 10^3‰$, where δ is the isotopic variation, Δm is the mass difference between the two isotopes, g is the gravitational acceleration, z_d is the depth of the diffusive column, R is the gas constant, and T is the temperature of the firn. Because gravitational fractionation at any point in time depends only on the mass difference, in principle a correction for any gas pair is straightforward if an ideal isotope pair affected only by gravitational settling can be found. In reality, there is no such ideal pair, however, often δ^{86}Kr is used because of its weak thermal diffusion sensitivity (Headly (2008)).

(2) Gases will also fractionate if there are temperature gradients present in the firn, with an enrichment of heavy isotopes in the colder regions (Grew and Ibbs (1952)). Because the thermal diffusion coefficients are different for each gas, a combination of gases (typically nitrogen and argon) can be used to deduce the temperature signal. This can be exploited at times of rapid climate change to

estimate the change in temperature as first shown by Severinghaus et al. (1998), and has been used extensively since (e.g. Caillon et al. (2001), Landais et al. (2004), Kobashi et al. (2007)). Thermal diffusion is described mathematically by $\delta = \Omega_{x-y}\Delta T$, where ΔT is the temperature difference between the top and bottom of the diffusive column and Ω_{x-y} is the thermal diffusion sensitivity, an empirical characteristic for gas pair x-y that can be determined precisely in the laboratory (Grachev and Severinghaus (2003a) for δ^{15}N, Grachev and Severinghaus (2003b) for δ^{40}Ar, Kawamura et al. (2013) for δ^{86}Kr and δ^{136}Xe).

(3) A substantial convective zone at the top of the firn column is another potential source of fractionation, in the form of a kinetic fractionation. Turbulent mixing continually disturbs the diffusive equilibrium set up by gravity and thermal gradients. The molecular diffusivity, a quantity specific to each pair of gases, governs how fast gases diffuse back to the equilibrium. In the presence of a convective zone, slowly diffusing gases will have less gravitational enrichment than fast diffusing gases at the bottom of the firn and in the ice core record (Kawamura and Severinghaus (2006)), because the diffusive column is slightly thinner for slowly diffusing gases. A detailed mathematical description of this effect is given by Kawamura et al. (2013), developed for a modern site with a ∼25 m thick convective zone. Because gas diffusivities depend on physical properties of the pore space in the firn, it is not clear to what degree the Kawamura et al. (2013) model is applicable to other sites. However, it does provide a framework to estimate the amount of depletion in slowly diffusing gases in an idealized case (Kawamura et al. (2013)'s equation 10 and 11). The resulting fractionation δ for a slowly diffusing gas with respect to δ^{15}N can be expressed as $\delta_{x-y}/\Delta m \cong g z_c \Gamma_{x-y}/(RT)$, where z_c is the minimum thickness of the convective zone and Γ_{x-y} is the convective fractionation sensitivity of gas pair x-y, defined as

$$\Gamma_{x-y} = \left(\frac{\Delta m_{x-29}}{1 + \frac{D_{15}}{D_{x-29}}} - \frac{\Delta m_{y-29}}{1 + \frac{D_{15}}{D_{y-29}}} \right) \frac{1}{\Delta M_{x-y}} - \frac{\Delta m_{29-28}}{2} \tag{5.1}$$

with Δm_{x-29} the difference in molecular mass between gas x and air, D_{15} the diffusivity of $^{29}N_2$ into air, and D_{x-29} the diffusivity of gas x into ^{29}air. The

primary assumption that we make to get this relatively simple form is that the Peclet number ($Pe = D_{eddy}/D_{mol}$) is constant with depth and equal to 1. In this case, the eddy diffusivity and the molecular diffusivity are the same at each depth which is the most effective way to fractionate gases of different molecular diffusivities. This approach will therefore yield a minimum convective thickness, because in reality Pe decreases with depth in the firn.

(4) At some high accumulation sites, another type of kinetic fractionation has been observed with rapid snow accumulation causing a slight disequilibrium similar to the one produced by a convective zone (Headly (2008)). Again, slowly diffusing gases will be less enriched compared to faster diffusing gases. Since the Taylor Dome area is not a high accumulation environment we will not consider this fractionation further.

Finally, gas loss, which occurs during coring, transport, and storage of an ice core (Bender et al. (1995), Ikeda-Fukazawa et al. (2005)), appears to be accompanied by isotopic fractionation of argon and oxygen isotopes, while not affecting larger molecules (Severinghaus et al. (2003), Kobashi et al. (2008)).

Any measurement of gas isotopic ratios in ice cores is affected by the previously described fractionations, and corrections need to be applied to reconstruct the actual atmospheric values. Since inert gas isotopic composition in the atmosphere is considered constant on 10^5 year timescales, we can invert the problem to study the fractionation taking place in the firn column. To separate the contributions from gravitational, thermal, and convective fractionation, at least three independent isotope pairs are needed. Here we use the isotopic ratios of δ^{15}N, δ^{86}Kr, δ^{136}Xe to do exactly that. If gas loss is minor, δ^{40}Ar can add a further constraint to the scheme.

5.2 Methods

In this section we describe the sample collection, the extraction of the noble gases from trapped air bubbles, and the analytical setup for measurements of noble gas elemental and isotopic ratios.

5.2.1 Sample collection

Eleven samples were collected on the main across flow transect described in Chapter 2, from -90 m to -130 m with varying spacing. Each sample was extracted with the Blue Ice Drill (BID, Kuhl et al. (2014)) from 7 m depth to avoid modern air contamination (Figure 5.1). The BID produces ice cores of 1 m length and 24 cm diameter, each weighing 35 kg to 40 kg. To facilitate handling and transport, the samples were trimmed to rectangular blocks with dimensions of 50 cm x 15 cm x 18 cm.

5.2.2 Noble gas extraction

The experimental protocol for the extraction of inert gases for measurements of δ^{15}N, δ^{40}Ar, $\delta^{86/82}$Kr, δKr/Ar, and δXe/Ar from ice cores samples is described by Headly (2008), and partly updated by Orsi (2013). In short, a 700-1000 g piece of ice is melted under vacuum. The released gases are transferred through a water trap at -100°C and frozen at 4 K into a 10 cc stainless steel tube (called a 'dip tube') for further processing. The dip tube is connected to a 180 cc volume. After evacuating the volume, the dip tube is opened and the entire assembly is left to equilibrate overnight in a water bath (for 12 h to 16 h) to eliminate temperature gradients. The following morning, the homogenized gas sample is separated into two parts by closing a valve. The smaller part, containing approximately 1/40 of the total sample volume, is transferred into another dip tube for analysis of nitrogen and oxygen isotopes as well as oxygen/nitrogen and argon/nitrogen elemental ratios. The remaining gas is also transferred into a dip tube, which is then connected to a getter oven, where all reactive gases are consumed by a zirconium/aluminium alloy at high temperature. The remaining noble gases are transferred into another dip tube, to be analyzed for noble gas isotopic and elemental ratios.

To measure xenon isotopes in addition to nitrogen, argon, and krypton isotopes, a larger amount of gas is needed. We apply the following modifications to the original procedure to quadruple the quantity of gas. A total of 4 kg ice is used in four separate extractions, each following the standard protocol. After the

gettering step, all four sub-samples are trapped in the same dip tube. The dip tube, containing the noble gas aliquots of four sub-samples, is left overnight for the gases to homogenize before being run on the mass spectrometer.

Xenon freeze test

In the first part of the extraction, the whole sample is transferred through a glass u-trap at -100°C to freeze out water vapor. The boiling point of pure xenon at standard pressure is -108°C. During the extraction, the pressure in the line is much lower than atmospheric pressure, which will decrease the boiling point if the freezing/melting process is governed by thermodynamics. However, the relevant mechanism for freezing xenon in a low pressure environment appears to be surface adsorption. It depends critically on the type of material used in the trap (glass or steel) but has the potential to capture xenon at higher temperatures than expected from pure thermodynamics (Lott (2001)). In practice, we have seen that the boiling point of noble gases at standard pressure is similar to the temperature at which they start adsorbing onto a surface. To verify that our water trap does not capture a significant amount of xenon, we ran 8 aliquots of the standard gas through the trap at different temperatures and then measured each aliquot against another standard gas (Figure 5.2). The results suggest that xenon does start to freeze on to the trap around -110°C, and that a trap at -100°C does not influence xenon isotopes, xenon mixing ratios, or other noble gases in a measurable way. Setting the trap to a certain homogeneous temperature is not straightforward. The fluid used to cool the trap is ethanol, to which liquid nitrogen is added until the desired temperature is reached. At temperatures colder than approximately -90°C the ethanol becomes very viscous, allowing for substantial temperature gradients within the trap. Still, a careful examination of the data does not show any signs of xenon being captured by the trap.

5.2.3 Mass spectrometry

The analysis of $\delta^{15}N$, $\delta^{18}O$, $\delta O_2/N_2$, and $\delta Ar/N_2$ on a Thermo Finnigan MAT DeltaV mass spectrometer is described by Petrenko et al. (2006), which we

adopt with minor modifications (e.g. 16 measurement blocks instread of 4). The noble gas isotopic and elemental ratios are measured on a Thermo Finnigan MAT 253 mass spectrometer using methods outlined by Orsi (2013) and Kawamura et al. (2013). Typical measurement parameters are shown in Table 5.1. Routine corrections for pressure imbalance and chemical slope are applied to the data. All measurements are standardized to air collected at the end of the Scripps pier (called La Jolla air).

The precision of repeat measurements of a argon/krypton/xenon standard gas mixture is shown in Table 5.1. The standard deviation for 9 samples of La Jolla air is 2 per meg for δ^{15}N, 123 per meg for δAr/N_2, 13 per meg for δ^{40}Ar, 8 per meg for $\delta^{86/82}$Kr, 25 per meg for $\delta^{136/129}$Xe, 151 per meg for δKr/Ar, and 246 per meg for δXe/Ar. La Jolla air samples include the processing and gas handling steps except for the actual melt-extraction. Since we don't have replicates of ice samples, it is difficult to estimate the true reproducibility of the data. The best we can do is to take the standard deviation of measurements made on samples from a similar climate period. 6 of our samples are from the LGM, which is the closest to a stable climate period that is present in our record. The standard deviation for 5 of those 6 samples (1 is clearly different than the others for unknown reasons) is 2 per meg for δ^{15}N, 597 per meg for δAr/N_2, 4 per meg for δ^{40}Ar, 9 per meg for $\delta^{86/82}$Kr, 24 per meg for $\delta^{136/129}$Xe, 742 per meg for δKr/Ar, and 619 per meg for δXe/Ar. The precision of the elemental ratios is significantly worse for ice samples compared to La Jolla air replicates. This may be due to a size-dependent process of expulsion of gases during bubble close off, or selective gas loss of small atoms during transport and storage of the ice (Severinghaus and Battle (2006)). Both of these processes affect mainly argon, and have also been observed to affect argon isotopic ratios (Kobashi et al. (2008)). In our data it is not obvious if the argon isotopic composition has been altered because of gas loss. Because argon is compromised, it is beneficial to eliminate it by combining elemental ratios:

$$\delta x/^{28}N_2 = \left(\left\{ \frac{(\frac{\delta x/^{36}Ar}{1000} + 1)}{(\frac{\delta^{40}Ar/^{36}Ar}{1000} + 1)} (\frac{\delta^{40}Ar/^{28}N_2}{1000} + 1) \right\} - 1 \right) \cdot 1000 \qquad (5.2)$$

with x either ^{84}Kr or ^{132}Xe. The resulting precision for δKr/N$_2$ is 245 per meg, and 316 per meg for δXe/N$_2$, both significantly better than any elemental ratio involving argon.

5.3 Results and Discussion

The results are shown in Table 5.2 and in Figure 5.3. δ^{15}N data from the large 4 kg samples agree well with high resolution δ^{15}N data from small samples. The positive trend starting at ∼17 ka is due to a general thickening of the firn because of increasing accumulation rates during the deglaciation. The elemental ratios δKr/N$_2$ and δXe/N$_2$ are strongly depleted compared to δ^{15}N during the LGM. This depletion gradually disappears in the younger samples. The depletion can be explained by the temperature dependency of the solubility coefficients. Xenon is not only more soluble than nitrogen at a given temperature, its solubility also changes more strongly as the temperature changes. During the LGM, when the mean ocean temperature was significantly colder than today, more xenon was dissolved in the ocean with respect to nitrogen, leading to a depletion in atmospheric xenon mixing ratios (Craig and Wiens (1996)). This effect can be used to quantify the mean ocean temperature change (Headly and Severinghaus (2007); Ritz et al. (2011)) after careful corrections for the gravitational, thermal, and convective fractionations.

For all 11 samples there is a distinct order to the measured isotopic ratios. δ^{40}Ar is most enriched, followed by δ^{15}N, δ^{86}Kr, and finally δ^{136}Xe. Because all isotope results are scaled with their respective mass difference, the gravitational fractionation cannot explain this partitioning of the isotopes. A combination of thermal fractionation and convective fractionation (and possibly gas loss for δ^{40}Ar) must therefore be responsible for the observed results.

5.3.1 Estimation of the convective zone thickness

We use a linear least squares approach to estimate the contribution of each kind of fractionation. For each isotope pair, the measured value is the sum of all fractionations:

$$\delta^{15}N_{meas} = \delta^{15}N_{grav} + \delta^{15}N_{therm} \tag{5.3}$$

$$\delta^{40}Ar_{meas} = \delta^{40}Ar_{grav} + \delta^{40}Ar_{therm} + \delta^{40}Ar_{conv}\ [+\delta^{40}Ar_{gasloss}] \tag{5.4}$$

$$\delta^{86}Kr_{meas} = \delta^{86}Kr_{grav} + \delta^{86}Kr_{therm} + \delta^{86}Kr_{conv} \tag{5.5}$$

$$\delta^{136}Xe_{meas} = \delta^{136}Xe_{grav} + \delta^{136}Xe_{therm} + \delta^{136}Xe_{conv} \tag{5.6}$$

Note that Equation 5.3 does not contain a convective fractionation term because the convective fractionation effects of the noble gases are determined with respect to δ^{15}N. We can replace all the gravitational terms with $\Delta m_{x-y} g z_c/(RT)$, all thermal terms with $\Omega_{x-y}\Delta T$, and all convective terms with $g z_d \Gamma_{x-y}/(RT)$. We then divide both sides of Equations 5.3-5.6 with the respective mass difference for better comparison, and get

$$\delta^{15}N = g z_d/(RT) + \Delta T \Omega_{29-28} \tag{5.7}$$

$$\delta^{40}Ar/4 = g z_d/(RT) + \Delta T \Omega_{40-36}/4 + g z_c \Gamma_{40-36}/(RT)\ [+\delta^{40}Ar_{gasloss}/4] \tag{5.8}$$

$$\delta^{86}Kr/4 = g z_d/(RT) + \Delta T \Omega_{86-82}/4 + g z_c \Gamma_{86-82}/(RT) \tag{5.9}$$

$$\delta^{136}Xe/7 = g z_d/(RT) + \Delta T \Omega_{136-129}/7 + g z_c \Gamma_{136-129}/(RT) \tag{5.10}$$

which constitutes a system of four equations with four unknowns (z_d, ΔT, z_c, and $\delta^{40}Ar_{gasloss}$), or a 3x3 system if we disregard δ^{40}Ar. Note that the per mass unit scaling is already incorporated into Γ. The thermal diffusion sensitivities and the convective fractionation sensitivities for all gas pairs are shown in Table 5.3.

It would be possible to solve this set of equations for each sample separately, but we choose to average the 6 Last Glacial Maximum (LGM) samples to improve the signal to noise ratio. We focus on the LGM because it is the time period during which we most expect a large convective zone to form due to very low accumulation rates. The 4x4 system is redundant since adding one equation (δ^{40}Ar = ...) while

also adding an unconstrained unknown ($\delta^{40}Ar_{gasloss}$) will produce the same result for z_d, ΔT, and z_c as the 3x3 system. The results for the 3x3 system and a 4x3 system (including δ^{40}Ar but not the gas loss term) are shown in Table 5.4. The 4x3 system produces a convective zone thickness of 85 m, and a temperature gradient of 3.3°C over 23 m. Both values seem unrealistic, probably because neglecting the gas loss term for δ^{40}Ar is not a valid assumption.

The 3x3 system produces more realistic results, with a 51 m convective zone, a 19 m diffusive column, and a temperature difference of 1.6°C between the top and the bottom of the diffusive column. Because ΔT is negative, the bottom of the firn is warmer than the surface. To inform the evaluation of the temperature gradient it is instructive to consider a limiting case with zero accumulation. In such a situation, the temperature in the ice sheet would increase linearly with depth, while both the surface and the basal temperature are fixed. Assuming that the basal temperature is the same as today (-26°C, Clow and Waddington (1996); Grootes et al. (2001)), the surface temperature during the LGM was -50°C (as reconstructed by Steig et al. (2000)), and that the ice sheet elevation change was small (as suggested by Steig et al. (1998) but challenged by Siddall et al. (2012)), the maximum possible temperature difference in a 20 m diffusive column is 0.9°C. Accumulation would then disturb this equilibrium by advecting cold ice downwards, which would decrease the temperature gradient in the firn. Under these assumptions, a ΔT of 1.6°C must be deemed unrealistic.

Along with the temperature gradient, a 50 m convective zone is needed to explain our measured isotope data. The thickest modern day convective zone that we know about is ∼30 m, in a location of wandering snow dunes that cause an accumulation hiatus on the lee side of every dune that lasts for several hundred years (Severinghaus et al. (2010)). In this setting, snow at the surface has time to metamorphose, thereby increasing the average grain size but also creating larger pore spaces that allow for more efficient wind pumping, causing turbulent mixing to penetrate deeper into the firn. We have already shown in Chapter 3 that the accumulation rate in the Taylor Dome region was extremely small for many millennia, and it is conceivable that the deposition site for the Taylor Glacier ice

was similarly metamorphosed. Our model predicts a total firn thickness (convective zone + diffusive zone) of 70 m. In today's climate, firn thicknesses of the order of 70 m are typically found at high accumulation sites (Landais et al. (2006)).

The model presented requires an unrealistically large temperature gradient and a very thick convective zone to explain the measured data. The thermal diffusion sensitivity and the convective fractionation diffusivity of δ^{86}Kr and δ^{136}Xe are not very different, thus a very large convective zone is needed to explain the $\sim$6 per meg difference between these two isotope pairs. To compensate for the large convective zone, a large thermal gradient is needed. A better approach to estimate the convective thickness might be to impose a temperature gradient and solve only for the convective zone thickness. However, for reasonable values of the firn top to bottom temperature difference (0.5°C for a 20 m thick diffusive column), it is not possible to explain the measured isotope values by imposing an arbitrary convective zone.

There are many reasons to distrust this reconstruction of the convective zone thickness. The results, even though not totally implausible, are not very convincing, especially the large temperature gradient and the reconstructed total firn thickness. We have no way of evaluating the assumptions that went into Kawamura et al. (2013)'s equation 11 (especially the diffusivity profiles resp. the assumption that $Pe = 1$) and test their validity for our site. Our system of equations to separate the contributions from gravitational, thermal, and convective fractionation is not well suited to determine the convective zone thickness and the firn temperature difference. Furthermore, the fractionation effects manifested in the measured δ-values for the LGM seem to be present also in the samples of the deglaciation. In fact, one could argue that the isotopic separation is the same for all samples that we measured, even though the accumulation rate clearly increases from 17 ka onwards. Still, it is impossible to explain the measured δ-values without a substantial convective zone, especially the large difference between δ^{15}N and δ^{86}Kr/4.

5.4 Conclusions

We present the first ever measurements of xenon isotopes from occluded gas in ice samples, along with measurements of krypton isotopes, argon isotopes, and nitrogen isotopes. The combination of 4 isotope pairs is sufficient to partition the contribution of different types of fractionation happening in the firn. Our results point to a substantial convective zone, along with an inverted temperature gradient (colder at the surface than at the base of the firn). However, the absolute value of the reconstructed firn thickness and temperature gradients appears overestimated by our method.

Table 5.1: Typical mass spectrometry measurement parameters. The 1σ error is calculated as the standard deviation of measurements of repeated aliquots from a standard gas mixture. Note that $^{84}Kr/^{36}Ar$ and $^{132}Xe/^{36}Ar$ are measured by peak jumping.

Mass pair	Mass spectrometer	Sample size [mL_{STP} air]	Resistors [$10^9\Omega$]	Ion beam intensity [V]	Integration time [s]	Change-over cycles	1σ error [‰]	Δm [10^{-3} kg mol^{-1}]	1σ error/ Δm
$^{29}N_2/^{28}N_2$	Delta V	2	300/0.3	4.2	16	256	0.002	1	0.002
$^{40}Ar/^{28}N_2$	Delta V	2	100/0.3	4.2	16	256	0.016	12	0.001
$^{40}Ar/^{36}Ar$	MAT 253	350	0.3/100	9.0	16	64	0.007	4	0.002
$^{86}Kr/^{82}Kr$	MAT 253	350	1000/1000	1.5	26	250	0.010	4	0.003
$^{136}Xe/^{129}Xe$	MAT 253	350	1000/1000	0.85	26	250	0.021	7	0.003
$^{84}Kr/^{36}Ar$	MAT 253	350	1000/100	2.2/5.5	16/8	24	0.085	48	0.002
$^{132}Xe/^{36}Ar$	MAT 253	350	1000/100	0.2/5.5	16/8	24	0.152	96	0.002

Table 5.2: Isotopic and elemental ratios for the 11 measured samples. Taylor Glacier gas age scale is developed and described in Chapter 2.

distance in transect [m]	age [ka BP]	δ^{15}N [‰]	δ^{40}Ar [‰]	δ^{86}Kr [‰]	δ^{136}Xe [‰]	δAr/N_2 [‰]	δKr/Ar [‰]	δXe/Ar [‰]	δKr/N_2 [‰]	δXe/N_2 [‰]
-130	22.08	0.077	0.348	0.284	0.429	-4.997	8.394	9.417	3.006	4.023
-127	20.93	0.077	0.355	0.270	0.469	-6.004	9.837	10.937	3.418	4.511
-125	19.96	0.068	0.304	0.250	0.387	-6.657	9.441	9.755	2.417	2.728
-123	19.00	0.078	0.354	0.287	0.445	-4.879	8.594	10.049	3.318	4.765
-121	18.06	0.078	0.348	0.296	0.448	-4.975	8.173	9.681	2.808	4.308
-120	17.64	0.081	0.346	0.288	0.490	-4.357	7.931	9.507	3.192	4.760
-115	16.64	0.120	0.517	0.435	0.688	-4.302	10.504	14.251	5.636	9.365
-112	16.19	0.114	0.481	0.407	0.667	-4.383	10.606	14.139	5.692	9.208
-110	16.06	0.103	0.425	0.374	0.599	-1.733	6.723	9.738	4.552	7.561
-100	15.38	0.120	0.523	0.445	0.753	-2.036	9.120	13.455	6.539	10.862
-90	14.58	0.157	0.642	0.570	0.935	-2.009	11.001	16.814	8.323	14.121

Table 5.3: Thermal diffusion sensitivity and convective fractionation sensitivity. Thermal diffusion sensitivity values are for -50°C. [1]Grachev and Severinghaus (2003a). [2]Grachev and Severinghaus (2003b). [3]Kawamura et al. (2013).

gas pair x-y	Δm_{x-y}	$\Omega_{x-y}/\Delta m$ at -50°C	Γ_{x-y}
$^{29}N_2/^{28}N_2$	1	0.0140[1]	
$^{40}Ar/^{36}Ar$	4	0.0094[2]	-0.0175[3]
$^{86}Kr/^{82}Kr$	4	0.0028[3]	-0.0933[3]
$^{136}Xe/^{129}Xe$	7	0.0013[3]	-0.1259[3]

Table 5.4: Data input and results for least squares determination of fractionation partitioning. The first line represents the three equations, three unknowns (3x3) model using δ^{15}N, δ^{86}Kr, and δ^{136}Xe only. The second line is for the 3x4 model, including δ^{40}Ar.

$\delta^{15}N_{avg}$ (‰)	$\delta^{40}Ar_{avg}$ [‰]	$\delta^{86}Kr_{avg}$ [‰]	$\delta^{136}Xe_{avg}$ [‰]	ΔT [°C]	z_d [m]	z_c [m]
0.0764		0.0698	0.0635	-1.6	19	51
0.0764	0.0856	0.0698	0.0635	-3.3	23	85

Figure 5.1: Impressions from BID sampling. (left) Extracting a 24 cm diameter BID core from the core barrel. (center) Discarded BID cores from shallow depth. (right) The BID drilling setup on Taylor Glacier, including drillers Josh Gotez and Michael Jayred.

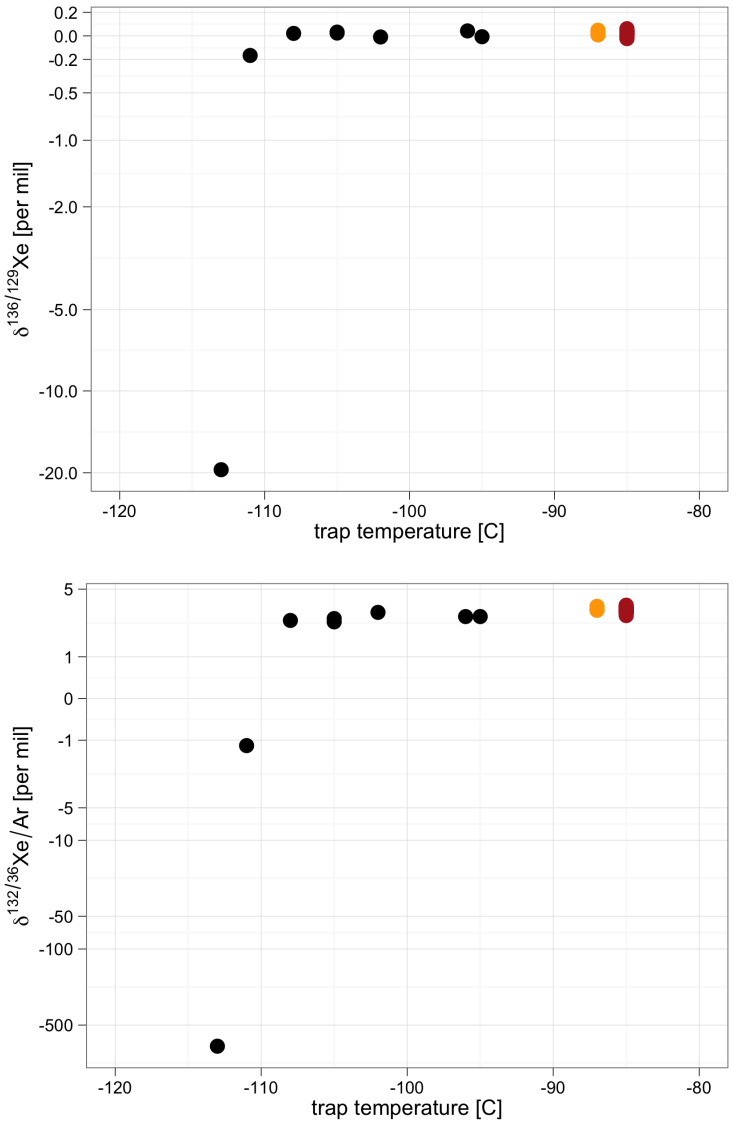

Figure 5.2: Xenon freeze test results. Top plot shows xenon isotopes vs trap temperature. Bottom plot is xenon/argon ratio vs trap temperature. Xenon is captured in the trap starting at approximately -100°C. Red points are measurements of aliquots of the same standard gas that was used for the freeze test, introduced directly into the mass spec. Orange points are also measurements of aliquots of the same standard gas, transferred through the gas handling line into a dip tube, and then measured on the mass spec. A quasi-logarithmic scale is used for the y-axis.

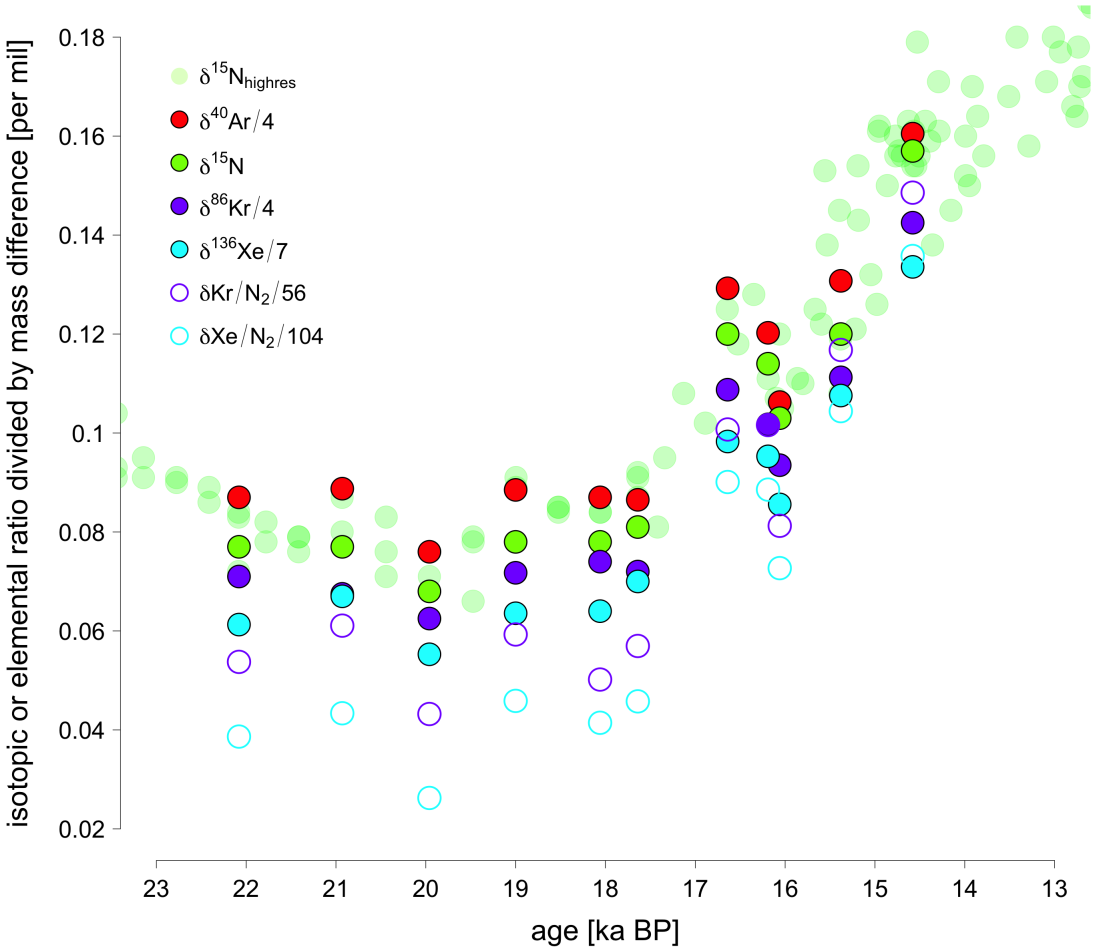

Figure 5.3: Isotopic and elemental ratios of inert gases from Taylor Glacier for the LGM and the beginning of the deglaciation. $\delta^{15}N_{highres}$ is high resolution gas data from small samples (15 g to 20 g), described in Chapter 2. All records on the Taylor Glacier gas age scale (also Chapter 2).

References

Bender, M., Sowers, T., and Lipenkov, V.: On the concentrations of O_2, N_2, and Ar in trapped gases from ice cores, Journal of Geophysical Research: Atmospheres, 100, 18 651–18 660, doi:10.1029/94JD02212, 1995.

Buizert, C., Cuffey, K. M., Severinghaus, J. P., Baggenstos, D., Fudge, T. J., Steig, E. J., Markle, B. R., Winstrup, M., Rhodes, R. H., Brook, E. J., Sowers, T. A., Clow, G. D., Cheng, H., Edwards, R. L., Sigl, M., McConnell, J. R., and Taylor, K. C.: The WAIS Divide deep ice core WD2014 chronology - Part 1: Methane synchronization (68-31 ka BP) and the gas age-ice age difference, Climate of the Past, 11, 153–173, doi:10.5194/cp-11-153-2015, 2015.

Caillon, N., Severinghaus, J. P., Barnola, J.-M., Chappellaz, J., Jouzel, J., and Parrenin, F.: Estimation of temperature change and of gas age-ice age difference, 108 kyr B.P., at Vostok, Antarctica, Journal of Geophysical Research: Atmospheres, 106, 31 893–31 901, doi:10.1029/2001JD900145, 2001.

Caillon, N., Severinghaus, J. P., Jouzel, J., Barnola, J. M., Kang, J. C., and Lipenkov, V. Y.: Timing of atmospheric CO2 and Antarctic temperature changes across termination III, Science, 299, 1728–1731, doi:10.1126/science.1078758, 2003.

Capron, E., Landais, A., Buiron, D., Cauquoin, A., Chappellaz, J., Debret, M., Jouzel, J., Leuenberger, M., Martinerie, P., Masson-Delmotte, V., Mulvaney, R., Parrenin, F., and Prié, F.: Glacial-interglacial dynamics of Antarctic firn columns: comparison between simulations and ice core air-δ^{15}N measurements, Climate of the Past, 9, 983–999, doi:10.5194/cp-9-983-2013, 2013.

Clow, G. D. and Waddington, E.: Acquisition of borehole temperature measurements from Taylor Dome and the Dry Valleys for paleoclimate reconstruction, Antarctic Journal of the United States, 31, 71–72, 1996.

Craig, H. and Wiens, R. C.: Gravitational Enrichment of $^{84}Kr/^{36}Ar$ Ratios in Polar Ice Caps: A Measure of Firn Thickness and Accumulation Temperature, Science, 271, pp. 1708–1710, URL http://www.jstor.org/stable/2890831, 1996.

Craig, H., Horibe, Y., and Sowers, T.: Gravitational Separation Of Gases And Isotopes In Polar Ice Caps, Science, 242, 1675–1678, doi:10.1126/science.242.4886.1675, 1988.

Freitag, J., Kipfstuhl, S., Laepple, T., and Wilhelms, F.: Impurity-controlled densification: a new model for stratified polar firn, Journal of Glaciology, 59, 1163–1169, doi:10.3189/2013JoG13J042, 2013.

Goujon, C., Barnola, J.-M., and Ritz, C.: Modeling the densification of polar

firn including heat diffusion: Application to close-off characteristics and gas isotopic fractionation for Antarctica and Greenland sites, Journal of Geophysical Research: Atmospheres, 108, 4792, doi:10.1029/2002JD003319, 2003.

Grachev, A. M. and Severinghaus, J. P.: Laboratory determination of thermal diffusion constants for $^{29}N_2/^{28}N_2$ in air at temperatures from -60 to 0°C for reconstruction of magnitudes of abrupt climate changes using the ice core fossil–air paleothermometer, Geochimica et Cosmochimica Acta, 67, 345–360, doi: 10.1016/S0016-7037(02)01115-8, 2003a.

Grachev, A. M. and Severinghaus, J. P.: Determining the Thermal Diffusion Factor for $^{40}Ar/^{36}Ar$ in Air To Aid Paleoreconstruction of Abrupt Climate Change, The Journal of Physical Chemistry A, 107, 4636–4642, doi:10.1021/jp027817u, 2003b.

Grew, K. and Ibbs, T.: Thermal diffusion in gases, Cambridge University Press, doi:10.1002/qj.49707934127, 1952.

Grootes, P. M., Steig, E. J., Stuiver, M., Waddington, E. D., and Morse, D. L.: The Taylor Dome Antarctic O-18 record and globally synchronous changes in climate, Quaternary Research, 56, 289–298, doi:10.1006/qres.2001.2276, 2001.

Headly, M. A.: Krypton and xenon in air trapped in polar ice cores: Paleo-atmospheric measurements for estimating past mean ocean temperature and summer snowmelt frequency, Ph.D. thesis, University of California, San Diego, URL http://search.proquest.com/docview/219988622, 2008.

Headly, M. A. and Severinghaus, J. P.: A method to measure Kr/N2 ratios in air bubbles trapped in ice cores and its application in reconstructing past mean ocean temperature, Journal of Geophysical Research: Atmospheres, 112, D19 105, doi:10.1029/2006JD008317, 2007.

Herron, M. and Langway, C. C.: Firn densification - an empirical-model, Journal of Glaciology, 25, 373–385, URL http://www.igsoc.org/journal/25/#part93, 1980.

Hörhold, M., Laepple, T., Freitag, J., Bigler, M., Fischer, H., and Kipfstuhl, S.: On the impact of impurities on the densification of polar firn, Earth and Planetary Science Letters, 325–326, 93–99, doi:10.1016/j.epsl.2011.12.022, 2012.

Ikeda-Fukazawa, T., Fukumizu, K., Kawamura, K., Aoki, S., Nakazawa, T., and Hondoh, T.: Effects of molecular diffusion on trapped gas composition in polar ice cores, Earth and Planetary Science Letters, 229, 183–192, doi:10.1016/j.epsl.2004.11.011, 2005.

Kawamura, K. and Severinghaus, J.: High-precision measurement of $^{86}Kr/^{82}Kr$ and $^{136}Xe/^{129}Xe$ in air to study convective mixing in polar firn, Geochimica et Cosmochimica Acta, 70, A309–A309, doi:10.1016/j.gca.2006.06.627, 2006.

Kawamura, K., Severinghaus, J. P., Ishidoya, S., Sugawara, S., Hashida, G., Motoyama, H., Fujii, Y., Aoki, S., and Nakazawa, T.: Convective mixing of air in firn at four polar sites, Earth and Planetary Science Letters, 244, 672–682, doi:10.1016/j.epsl.2006.02.017, 2006.

Kawamura, K., Severinghaus, J. P., Albert, M. R., Courville, Z. R., Fahnestock, M. A., Scambos, T., Shields, E., and Shuman, C. A.: Kinetic fractionation of gases by deep air convection in polar firn, Atmospheric Chemistry and Physics, 13, 11 141–11 155, doi:10.5194/acp-13-11141-2013, 2013.

Kobashi, T., Severinghaus, J. P., Brook, E. J., Barnola, J. M., and Grachev, A. M.: Precise timing and characterization of abrupt climate change 8200 years ago from air trapped in polar ice, Quaternary Science Reviews, 26, 1212–1222, doi:10.1016/j.quascirev.2007.01.009, 2007.

Kobashi, T., Severinghaus, J. P., and Kawamura, K.: Argon and nitrogen isotopes of trapped air in the GISP2 ice core during the Holocene epoch (0-11,500 B.P.): Methodology and implications for gas loss processes, Geochimica et Cosmochimica Acta, 72, 4675–4686, doi:10.1016/j.gca.2008.07.006, 2008.

Kuhl, T. W., Johnson, J. A., Shturmakov, A. J., Goetz, J. J., Gibson, C. J., and Lebar, D. A.: A new large-diameter ice-core drill: the Blue Ice Drill, Annals Of Glaciology, 55, 1–6, doi:10.3189/2014AoG68A009, 2014.

Landais, A., Caillon, N., Goujon, C., Grachev, A., Barnola, J., Chappellaz, J., Jouzel, J., Masson-Delmotte, V., and Leuenberger, M.: Quantification of rapid temperature change during DO event 12 and phasing with methane inferred from air isotopic measurements, Earth and Planetary Science Letters, 225, 221–232, doi:10.1016/j.epsl.2004.06.009, 2004.

Landais, A., Barnola, J., Kawamura, K., Caillon, N., Delmotte, M., Ommen, T. V., Dreyfus, G., Jouzel, J., Masson-Delmotte, V., Minster, B., Freitag, J., Leuenberger, M., Schwander, J., Huber, C., Etheridge, D., and Morgan, V.: Firn-air δ^{15}N in modern polar sites and glacial-interglacial ice: a model-data mismatch during glacial periods in Antarctica?, Quaternary Science Reviews, 25, 49–62, doi:10.1016/j.quascirev.2005.06.007, 2006.

Lott, D. E.: Improvements in noble gas separation methodology: A nude cryogenic trap, Geochemistry, Geophysics, Geosystems, 2, doi:10.1029/2001GC000202, 2001.

Loulergue, L., Parrenin, F., Blunier, T., Barnola, J.-M., Spahni, R., Schilt, A., Raisbeck, G., and Chappellaz, J.: New constraints on the gas age-ice age difference along the EPICA ice cores, 0–50 kyr, Climate of the Past, 3, 527–540, doi:10.5194/cp-3-527-2007, 2007.

Orsi, A.: Temperature reconstruction at the West Antarctic Ice Sheet Divide, for the last millennium, from the combination of borehole temperature and inert gas isotope measurements, Ph.D. thesis, University of California, San Diego, URL http://search.proquest.com/docview/1347671198, 2013.

Petrenko, V., Severinghaus, J., Brook, E., Reeh, N., and Schaefer, H.: Gas records from the West Greenland ice margin covering the Last Glacial Termination: a horizontal ice core, Quaternary Science Reviews, 25, 865–875, doi:10.1016/j.quascirev.2005.09.005, 2006.

Rasmussen, S. O., Abbott, P. M., Blunier, T., Bourne, A. J., Brook, E., Buchardt, S. L., Buizert, C., Chappellaz, J., Clausen, H. B., Cook, E., Dahl-Jensen, D., Davies, S. M., Guillevic, M., Kipfstuhl, S., Laepple, T., Seierstad, I. K., Severinghaus, J. P., Steffensen, J. P., Stowasser, C., Svensson, A., Vallelonga, P., Vinther, B. M., Wilhelms, F., and Winstrup, M.: A first chronology for the North Greenland Eemian Ice Drilling (NEEM) ice core, Climate of the Past, 9, 2713–2730, doi:10.5194/cp-9-2713-2013, 2013.

Ritz, S. P., Stocker, T. F., and Severinghaus, J. P.: Noble gases as proxies of mean ocean temperature: sensitivity studies using a climate model of reduced complexity, Quaternary Science Reviews, 30, 3728–3741, doi:10.1016/j.quascirev.2011.09.021, 2011.

Schwander, J., Stauffer, B., and Sigg, A.: Air mixing in firn and the age of the air at pore close-off, Annals of Glaciology, 10, 141–145, 1988.

Schwander, J., Sowers, T., Barnola, J.-M., Blunier, T., Fuchs, A., and Malaizé, B.: Age scale of the air in the summit ice: Implication for glacial-interglacial temperature change, Journal of Geophysical Research: Atmospheres, 102, 19 483–19 493, doi:10.1029/97JD01309, 1997.

Severinghaus, J. P. and Battle, M. O.: Fractionation of gases in polar ice during bubble close-off: New constraints from firn air Ne, Kr and Xe observations, Earth and Planetary Science Letters, 244, 474–500, doi:10.1016/j.epsl.2006.01.032, 2006.

Severinghaus, J. P. and Brook, E. J.: Abrupt Climate Change at the End of the Last Glacial Period Inferred from Trapped Air in Polar Ice, Science, 286, 930–934, doi:10.1126/science.286.5441.930, 1999.

Severinghaus, J. P., Sowers, T., Brook, E. J., Alley, R. B., and Bender, M. L.: Timing of abrupt climate change at the end of the Younger Dryas interval from thermally fractionated gases in polar ice, Nature, 391, 141–146, doi:10.1038/34346, 1998.

Severinghaus, J. P., Grachev, A., Luz, B., and Caillon, N.: A method for precise

measurement of argon 40/36 and krypton/argon ratios in trapped air in polar ice with applications to past firn thickness and abrupt climate change in Greenland and at Siple Dome, Antarctica, Geochimica et Cosmochimica Acta, 67, 325–343, doi:10.1016/S0016-7037(02)00965-1, 2003.

Severinghaus, J. P., Albert, M. R., Courville, Z. R., Fahnestock, M. A., Kawamura, K., Montzka, S. A., Mühle, J., Scambos, T. A., Shields, E., Shuman, C. A., Suwa, M., Tans, P., and Weiss, R. F.: Deep air convection in the firn at a zero-accumulation site, central Antarctica, Earth and Planetary Science Letters, 293, 359–367, doi:10.1016/j.epsl.2010.03.003, 2010.

Siddall, M., Milne, G. A., and Masson-Delmotte, V.: Uncertainties in elevation changes and their impact on Antarctic temperature records since the end of the last glacial period, Earth and Planetary Science Letters, 315-316, 12–23, doi:10.1016/j.epsl.2011.04.032, sea Level and Ice Sheet Evolution: A PALSEA Special Edition, 2012.

Sowers, T., Bender, M., and Raynaud, D.: Elemental and isotopic composition of occluded O_2 and N_2 in polar ice, Journal of Geophysical Research: Atmospheres, 94, 5137–5150, doi:10.1029/JD094iD04p05137, 1989.

Sowers, T., Bender, M., Raynaud, D., and Korotkevich, Y.: Delta-N-15 of N2 in air trapped in polar ice - a tracer of gas-transport in the firn and a possible constraint on ice age-gas age differences, Journal of Geophysical Research: Atmospheres, 97, 15 683–15 697, doi:10.1029/92JD01297, 1992.

Steig, E. J., Brook, E. J., White, J. W. C., Sucher, C. M., Bender, M. L., Lehman, S. J., Morse, D. L., Waddington, E. D., and Clow, G. D.: Synchronous climate changes in Antarctica and the North Atlantic, Science, 282, 92–95, doi:10.1126/science.282.5386.92, 1998.

Steig, E. J., Morse, D. L., Waddington, E. D., Stuiver, M., Grootes, P. M., Mayewski, P. A., Twickler, M. S., and Whitlow, S. I.: Wisconsinan and Holocene climate history from an ice core at Taylor Dome, western Ross Embayment, Antarctica, Geografiska Annaler Series A-Physical Geography, 82A, 213–235, doi:10.1111/j.0435-3676.2000.00122.x, 2000.